UNIVERSITÀ
DEGLI STUDI
DI PADOVA

DIPARTIMENTO
DI INGEGNERIA
DELL'INFORMAZIONE

UNIVERSITÀ DEGLI STUDI DI PADOVA

DEPARTMENT OF INFORMATION ENGINEERING
MASTER THESIS IN CONTROL SYSTEMS ENGINEERING

FAULT-TOLERANT ADAPTIVE SLIDING MODE CONTROL FOR WIND TURBINE HYDRAULIC PITCH SYSTEM

SUPERVISOR

PROF. ANGELO CENEDESE

DTU SUPERVISORS

PROF. DIMITRIOS PAPAGEORGIOU

PH.D. ALESSIO DALLABONA

MASTER CANDIDATE

ISABELLA CRESCENTE

ACADEMIC YEAR 2023/2024
OCTOBER 10, 2024

Preface

This thesis has been prepared over five months at the Section for Automation and Control, Department of Electrical and Photonics Engineering, at the Technical University of Denmark (DTU), as an exchange student from Università degli Studi di Padova (UNIPD), in partial fulfillment of the requirements for the Master's Degree in Control Systems Engineering.
The project was carried out from February 2024 to July 2024, under the supervision of Associate Professor Dimitrios Papageorgiou and PhD Student Alessio Dallabona.

Abstract

Wind energy is one of the most widespread renewable technologies, therefore, increasing wind turbine reliability is a crucial factor, especially nowadays when maintenance costs are high and climate change is a serious problem for the planet.
In this thesis, the utilization of a novel fault tolerant control architecture based on Super Twisting Sliding Mode Control (ST-SMC) is investigated for a conventional Wind Turbine (WT) Hydraulic Pitch System (HPS). The thesis offers a description of the mathematical model of the system dynamics with an overview of the most common faults that can affect it. This is followed by a review of Sliding Mode Control (SMC) and its variants, including the adaptive versions (Adaptive Sliding Mode Control, A-SMC). The latter are capable of adjusting themselves in order to reject disturbances and unknown dynamics in the system while maintaining the desired accuracy. Then, the design of the Super Twisting Sliding Mode Controller and the Adaptive Super Twisting Sliding Mode Controller is derived. In addition, the thesis analyses the performances of the proposed controllers in both nominal case and faulty scenarios, using evaluation metrics. The results show great adaptation capabilities for the adaptive techniques, which in some cases outperform the conventional controller. Lastly, potential future research directions related to the project are suggested.

Sommario

L'energia eolica è una delle tecnologie rinnovabili più diffuse, pertanto, l'aumento dell'affidabilità delle turbine eoliche è un fattore cruciale, soprattutto al giorno d'oggi con i costi di manutenzione elevati e le problematiche legate al cambiamento climatico che rappresentano una questione rilevante per il pianeta.
In questa tesi, viene studiato l'utilizzo di una nuova architettura di controllo a tolleranza di guasti basata sul Super Twisting Sliding Mode Control per un sistema idraulico di regolazione dell'angolo delle pale (Hydraulic Pitch System, HPS) convenzionale di una turbina eolica. La tesi offre una descrizione del modello matematico della dinamica del sistema con una panoramica dei guasti più frequenti che possono influenzarlo. Successivamente, viene presentato il concetto di Sliding Mode Control (SMC) e le sue varianti, comprese le versioni adattative (Adaptive Sliding Mode Control, A-SMC). Queste ultime sono in grado di adattarsi per respingere disturbi e dinamiche sconosciute del sistema, mantenendo allo stesso tempo l'accuratezza desiderata. In seguito, viene derivata la progettazione del Super Twisting Sliding Mode Controller e dell'Adaptive Super Twisting Sliding Mode Controller. Inoltre, vengono analizzate le prestazioni dei controllori proposti sia in condizioni nominali che in scenari con guasti utilizzando metriche di valutazione. I risultati mostrano grandi capacità di adattamento per le tecniche adattative, le quali in alcuni casi superano il controllore convenzionale. Infine, vengono suggerite le potenziali direzioni di ricerca futura per il progetto introdotto nella tesi.

Acknowledgements

I am profoundly grateful to my supervisors, Dimitrios Papageorgiou, Associate Professor and Alessio Dallabona, PhD Student at the Department of Electrical and Photonics Engineering in Automation and Control section at DTU, for their invaluable guidance, unwavering support, precious help and insightful feedback. Their suggestions have significantly improved the quality of this research.

I would like to express my appreciation to my local supervisor Prof. Cenedese for his willingness for the realization of my thesis.

My gratitude goes also to Prof. Valcher, even if she is not directly involved in this project, she always made herself available to help at any time during my university years.

Contents

List of Figures

List of Tables

Acronyms

A-SMC	. . . . . **A**daptive **S**liding **M**ode **C**ontrol
AG	. . . . . **A**daptive **G**ains
AG-ST-SMC	. . . . . **A**daptive **G**ains **S**uper **T**wisting **S**liding **M**ode **C**ontrol
BF	. . . . . **B**arrier **F**unction
BF-ST-SMC	. . . . . **B**arrier **F**unction **S**uper **T**wisting **S**liding **M**ode **C**ontrol
HO-SMC	. . . . . **H**igh **O**rder **S**liding **M**ode **C**ontrol
HPS	. . . . . **H**ydraulic **P**itch **S**ystem
N	. . . . . **N**ominal
PV	. . . . . **P**roportional **V**alve
SMC	. . . . . **S**liding **M**ode **C**ontrol
sqrtBF	. . . . . **sq**uare **r**oo**t** **B**arrier **F**unction
sqrtBF-ST-SMC	. . . . . **sq**uare **r**oo**t** **B**arrier **F**unction **S**uper **T**wisting **S**liding **M**ode **C**ontrol
ST-SMC	. . . . . **S**uper **T**wisting **S**liding **M**ode **C**ontrol
WT	. . . . . **W**ind **T**urbine

1

Introduction

1.1 Background and Motivation

Wind turbine production soared in 2021, surpassing all other renewable energy technologies. The total production in that year reached 1870 TWh, almost as much as all the others non-hydro renewable technologies combined. The push towards achieving Net Zero Emissions by 2050 is driving efforts to enhance turbine size and power, particularly focusing on offshore systems.

Minimizing downtime is priority for these systems. Besides maintenance costs, lost revenue due to energy production halts during repairs must also be considered. Offshore installations exacerbate maintenance challenges prolonging repair duration. Studies indicate that the primary source of wind turbine failures arises from the pitch regulation system. Implementing fault accommodation strategies can reduce hydraulic subsystem maintenance needs, significantly boosting turbine uptime. A passive approach to mitigate fault effects involves developing a robust control algorithm.

Sliding Mode Control (SMC), a robust nonlinear strategy characterized by high-frequency switching, reduces chattering through the adoption of the established Super-Twisting (ST)

algorithm. However, tuning such controllers often requires high gains, making the solution not feasible in practical applications. Therefore, ongoing research in the control community explores dynamically adaptive gain solutions.
This project aims to investigate adaptive approaches for the ST algorithm and assess their efficacy against prevalent faults affecting typical high-power wind turbine hydraulic pitch systems.

1.2 Scope of the Project

The goals of the thesis are:

1. Present the Hydraulic Pitch System in Wind Turbines and Fault-Tolerant Control algorithms: Super Twisting Sliding Mode Control (ST-SMC) and Adaptive Super Twisitng Sliding Mode Control (A-ST-SMC), in particular Adaptive Gains Super Twisitng Sliding Mode Control (AG-ST-SMC) and Barrier Function Super Twisitng Sliding Mode Control (BF-ST-SMC);
2. Design ST-SMC and A-ST-SMC solutions for the given model;
3. Perform controller simulations through MATLAB/Simulink environment under nominal conditions and faulty scenarios;
4. Compare the different methods.

1.3 Literature Review

In this section an overview of the state of art is presented.

1.3.1 Wind Turbine Hydraulic Pitch System and Faults

The model of the Wind Turbine Hydraulic Pitch System is based on studies conducted in [1] [2] [3]. In particular, in [1] the most significant faults occurring in a typical hydraulic pitch system in high-power turbines are reported.

1.3.2 Sliding Mode Control

Sliding Mode Control (SMC) is a sophisticated control strategy commonly used in control system implementations, particularly for dealing with systems that are subject to uncertainties and disturbances. It is characterized by its ability to force the system state to "slide" along a predetermined surface in the state space, known as the sliding surface, which ensures desired system behavior. The foundation of these controllers is a high-frequency switching control signal and this feature endows them with robustness against matched perturbations or disturbances and ensures finite-time convergence. However, this method leads to the phenomena of chattering, but it can be mitigated by implementing a continuous control function, such as the saturation function, as shown in [4]. The price to pay for this solution is a loss in performances. Subsequently, to overcome this problem, it was suggested to employ an High Order Sliding Mode Control (HO-SMC). In particular, the second-order Super Twisting Sliding Mode Control (ST-SMC) was introduced in [5]. Additionally, it was studied in [6] how to implement the Super Twisting strategy in arbitrary orders. Moreover, to improve the performance, literature has presented the adaptive control that self-tunes the controller parameters.

1.3.3 Adaptive Sliding Mode Control

Adaptive Sliding Mode Control is an advanced control technique that combines the adaptive control with SMC: the former adjusts controller parameters in real-time based on

system feedback, enhancing the performance and robustness of the control system, while the latter ensures that the system state trajectory remains on a predefined sliding surface. In fact, the controller drives the states of the system towards this sliding surface and then keeps them there despite uncertainties and disturbances.

In [7] an adaptive version of SMC was presented, where a robust Lyapunov function enabled the ST-SMC to counteract linearly increasing disturbances. Then, [8] introduced the concept of adaptive gains with ST-SMC. This led to the Adaptive Gain ST-SMC (AG-ST-SMC) introduction, which is capable to reject bounded disturbances with an unknown bounds as shown in [9]. The adaptive gain approach was also extended to arbitrary order SMC in [10] through the use of an adaptive continuous SMC. The AG-ST-SMC method was further explored in [11] [12] [13].

Another A-SMC method that has recently gained significant attention involves the use of Barrier Function (BF) to prevent the overestimation of gains. BF was initially applied in [14] with Lyapunov functions for nonlinear systems. Then, the first implementation of BF in SMC was demonstrated in [15], introducing BF-A-SMC for first-order SMC. Subsequently, in [16], the BF method was adapted for A-ST-SMC. Similarly, HO-SMCs were also modified to utilize this technique for controllers of arbitrary order, as shown in [17]. BF-ST-SMC technique was also employed in [18] [19] [20].

1.4 Thesis outline

The thesis in composed of six chapters:

- Chapter 1 contains an introduction to the thesis;
- in Chapter 2 the mathematical model of the Wind Turbine Hydraulic Pitch System is provided;
- Chapter 3 is dedicated to the theoretical explanation of Sliding Mode Control and its adaptive variants employed;

- Chapter 4 presents the design of each the controller;
- Chapter 5 reports the simulations and evaluates the results;
- Chapter 6 summarizes the analyses and hints future research directions.

2

System Model: Hydraulic Pitch System in Wind Turbine

This chapter provides an overview of the wind turbine structure and a detailed description of the mathematical model of the Hydraulic Pitch System (HPS).

2.1 Wind Turbine

Wind turbines are machines that convert the kinetic energy of the wind into electrical energy. This is possible due to the huge force of the wind that pushes the blades of these devices, causing them rotate. Nevertheless this may seem a simple task, designing a proper working and efficient structure requires an in-depth study of various disciplines, including mechanical, hydraulic, electrical and automation engineering. Figure 2.1 shows the architecture of a wind turbine.

It is important to remember that the objective of this thesis is to explore the turbine hub, which contains the pitch control unit and the pitch control system.

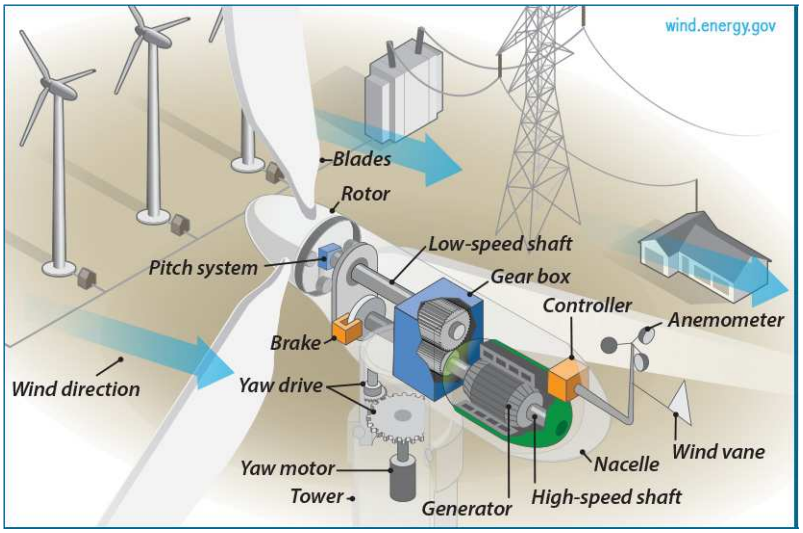

FIGURE 2.1: Structure of a wind turbine.

2.2 Hydraulic Pitch System

The structure consists of a wind turbine hydraulic pitch system that aims to control the angle of the turbine blades, namely the pitch angle β. The adjustment of the blades angle is important for multiple reasons, some of them are reported here:

- optimizing energy capture: by changing the pitch angle, it is possible to maximize the capture of the wind energy and thereby intensify the energy production;
- wind speed control: when weather conditions are critical, the adjustment of the blade angle allows the wind turbine to operate in safety conditions avoiding mechanical stress and potential damage to its components;
- fault detection and mitigation: hydraulic systems are equipped with sensors and monitoring systems to detect faults, namely if there is a deviation from expected readings, it indicates a potential fault. For instance, pressure sensors can detect leaks, while position sensors ensure that the blades are at the correct angle.

The HPS is mainly composed of a pump and an accumulator bank that supply three equivalent circuits. These circuits are connected to a proportional valve (PV) and to a hydraulic cylinder. The reference HPS is shown in Figure 2.2 during normal operation.

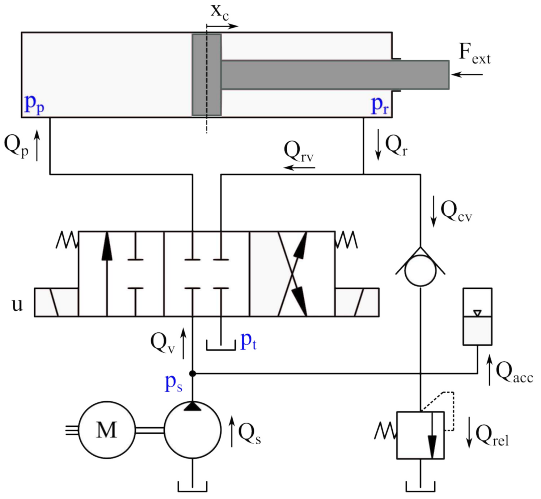

FIGURE 2.2: Reference Hydraulic Pitch System.

The main terms describing the system dynamics include the blade angle β and its velocity v_β, the position and velocity of the cylinder, denoted as x_c and v_c respectively, as well as the pressure of the piston side p_p and of the rod side p_r. Beside these, all the other variables and parameters employed in the following equations are collected in Table 2.1.

The study of the mathematical model can be split in four parts:

- hydraulic cylinder (Section 2.2.1);
- valves (Section 2.2.2);
- supply circuit (Section 2.2.3);
- sensors (Section 2.2.4).

Each element is presented in more detail in the next sections.

Variable/parameter	Description	Unit
β	pitch angle	rad
v_β	pitch angle velocity	rad/s
x_c	cylinder position	m
v_c	cylinder velocity	m/s
x_v	valve's pool position	m
M_{eq}	equivalent piston mass	kg
J_{tot}	inertia	$kg\,m^2$
A_p	area of piston	m^2
A_r	area of rod	m^2
p_p	piston side pressure	N/m^2
p_r	rod side pressure	N/m^2
p_s	supply pressure	N/m^2
p_t	tank pressure	N/m^2
β_e	effective bulk modulus	N/m^2
$B_v v_c$	viscous friction	N
$F_c \tanh\left(\frac{v_c}{\gamma}\right)$	Coulomb friction	N
F_{ext}	external force	N
$V_{0,p}$	initial volume of piston side chamber	m^3
$V_{0,r}$	initial volume of rod side chamber	m^3
Q_p	piston side flow	m^3/s
Q_r	rod side flow	m^3/s
Q_{rv}	flow from rod side chamber to the proportional valve	m^3/s
Q_{le}	leakage between cylinder inside and outside	m^3/s
Q_{li}	internal leakage between piston and rod side	m^3/s
Q_{cv}	check-valve flow	m^3/s
$K_v(\lvert x_v \rvert)$	nonlinear function of proportional valve spool dynamics with respect to spool position input	$m^3/(sPa)$
$H(\cdot)$	Heaviside step function	-
$sgn(\cdot)$	sign function	-
ϕ_v	piston and rod area ratio	-

TABLE 2.1: Variables and Parameters of the Hydraulic Pitch System.

2.2.1 Hydraulic Cylinder

The hydraulic cylinder is the part of the system responsible for the pitching of the blades, namely it makes sure that the desired pitch angle β is applied to the blades with a force generated by the pressure difference, which varies the cylinder position x_c. Its dynamics

is represented by the Newton's second law that states:

$$M_{eq}\dot{v}_c = A_p p_p - A_r p_r - B_v v_c - F_c \tanh\left(\frac{v_c}{\gamma}\right) + f_{Fr,c} - F_{ext} \tag{2.1}$$

where $F_{Fr,c} = B_v v_c + F_c \tanh(\frac{v_c}{\gamma})$ is the friction, $f_{Fr,c}$ is a fault due to increased friction and F_{ext} is the external force that acts against the control purpose as a disturbance.

The hydraulic cylinder consists of two chambers: the piston side one and the rod side one. On the hand, the piston side is where the piston head is located. The piston moves in one direction when there is a pressure difference (Δp) between the two chambers and, as a consequence, it exerts force on the piston. On the other hand, the rod side chamber is placed in the opposite part of the cylinder with respect to the piston side one. The rod is connected to the piston and extends out of the cylinder. When pressure is applied to the piston side, it moves the piston and, consequently, the rod in the opposite direction.

The expressions for the pressure dynamics inside the piston side and rod side chambers are:

$$\dot{p}_p = \frac{\beta_{e,p}}{V_{0,p} + A_p x_c}(Q_p - A_p v_c - Q_{le,p} - Q_{li}) \tag{2.2}$$

$$\dot{p}_r = \frac{\beta_{e,r}}{V_{0,p} + A_r(x_{c,max} - x_c)}(-Q_r - A_r v_c - Q_{le,r} + Q_{li}) \tag{2.3}$$

where $Q_{le,p}$, $Q_{le,r}$ and Q_{li} are elements related to the leakage faults in the system. In the nominal case, these terms are considered to be zero.

$\beta_{e,i}$ is the effective bulk modulus of the oil for the respective chamber. The bulk modulus of a fluid represents its resistance to uniform compression, i.e. quantifies the amount of pressure needed to change the volume of the material and it depends on the type of oil, pressure and temperature.

The relation for the bulk modulus is given by:

$$\beta_e = \frac{1}{\frac{1}{\beta_{oil}} + \epsilon_a(p)\left(\frac{1}{c_{adP}} - \frac{1}{\beta_{oil}}\right)} + f_{B,e} \tag{2.4}$$

where

$$\epsilon_a(p) = \frac{1}{\frac{1-\epsilon_{a,0}}{\epsilon_{a,0}} \left(\frac{p_{atm}}{p}\right)^{\frac{-1}{c_{ad}}} + 1} \tag{2.5}$$

The fault $f_{B,e}$ is related to oil degradation.

Furthermore, it is important to define the flow rate entering and the flow rate exiting from the chambers ($Q_{le,p}$ and $Q_{le,r}$) and the leakage flows (Q_{li}):

$$Q_{le,p} = C_{le,p}(p_p - p_{atm}) + f_{Q_{le,p}} \tag{2.6}$$

$$Q_{le,r} = C_{le,r}(p_r - p_{atm}) + f_{Q_{le,r}} \tag{2.7}$$

$$Q_{li} = C_{li}(p_p - p_r) + f_{Q_{li}} \tag{2.8}$$

where $f_{Q_{le,p}}$, $f_{Q_{le,r}}$ and $f_{Q_{li}}$ are faults regarding flows leakage.

2.2.2 Valves

The Proportional Valve (PV) is the component of the system that allows for the control of the cylinder position. A PV is a type of valve used in fluid control systems to regulate the flow rate or pressure of a fluid based on an input signal, in this case by changing the valve's spool position x_v. It is different from the standard on/off valve that has merely two states (fully open or fully close), in fact the proportional valve gives a continuous and precise control over the fluid flow or pressure by varying the valve opening proportionally to the input signal. The introduction of a PV enables the system to work in a regenerative way.

The following equations express the flows with respect to the valve's spool position x_v:

$$Q_p = K_v(x_v)\left[\sqrt{|p_s - p_p|}sgn(p_s - p_p)H(x_v) - \sqrt{|p_p - p_t|}sgn(p_p - p_t)H(-x_v)\right] + f_{Q_p} \tag{2.9}$$

$$Q_{rv} = -K_v(x_v)\phi_v\left[\sqrt{|p_s - p_r|}sgn(p_s - p_r)H(x_v)H(-x_v)\right] + f_{Q_{rv}} \tag{2.10}$$

where f_{Q_p} and $f_{Q_{rv}}$ are other faults related to the flow.
It is important to recall that $H(x)$ is the Heaviside step function, defined as:

$$H(x) = \begin{cases} 1, & x \geq 0 \\ 0, & x < 0 \end{cases} \tag{2.11}$$

and $sign(x)$ is:

$$sgn(x) = \begin{cases} 1, & x > 0 \\ 0, & x = 0 \\ -1, & x < 0 \end{cases} \tag{2.12}$$

In Equation 2.10, the flow across the PV is defined, which is generally different than the flow to/from rod side chamber, given by

$$Q_r = Q_{rv} + Q_{cv} \tag{2.13}$$

where Q_{cv} represents the flow through the check valve used for operating the circuit in regenerative mode, for reducing the size of the supply circuit. The equation for the flow in the check valve is given by

$$Q_{cv} = K_{cv}(p_r - p_s - p_{cv,c})H(p_r + p_{cv,c} - p_s) + f_{Q_{cv}} \tag{2.14}$$

$f_{Q_{cv}}$ was included as a possible fault manifesting a flow perturbation.

2.2.3 Supply Circuit

The pump station in a wind turbine's hydraulic pitch system serves as the control center for adjusting the angle of the turbine blades. The pump station consists of hydraulic pumps, valves, and other hydraulic components. When the wind conditions change or

when the turbine needs to be shut down for maintenance or safety reasons, the pump station activates to adjust the pitch angle of the blades accordingly.

2.2.4 Sensors

In this project it is assumed that the sensors provide the measurements of key system states, specifically β, x_c, p_p and p_r. Instead, v_c is not detected directly, but obtained by deriving x_c.

2.3 Full Hydraulic Pitch System

In a HPS for a WT the pitch angle β of the blades is controlled by the position of the hydraulic cylinder x_c. The hydraulic cylinder's linear motion x_c is converted into rotary motion of the blade β through mechanical linkages or a crank mechanism. From Figure 2.3 it is possible to see that the blade base is attached to the hub through the bearing, which acts as a rotating mechanism. The latter is fixed to the hydraulic cylinder that provides the movement of it via the pressure system, namely the HPS.

Reconsidering the equation for the dynamics of x_c without faults:

$$\begin{aligned} M\dot{v}_c &= A_p p_p - A_r p_r - F_{Fr,c} - F_{ext} \\ \dot{x}_c &= v_c \end{aligned} \tag{2.15}$$

then, angular dynamics of the blade is described by:

$$\begin{aligned} J_{tot}\dot{v}_\beta &= \left(A_p p_p - A_r p_r\right) r \sin\left(\psi\left(x_c\right)\right) - M_{fric} - M_{ext} \\ \dot{\beta} &= v_\beta \end{aligned} \tag{2.16}$$

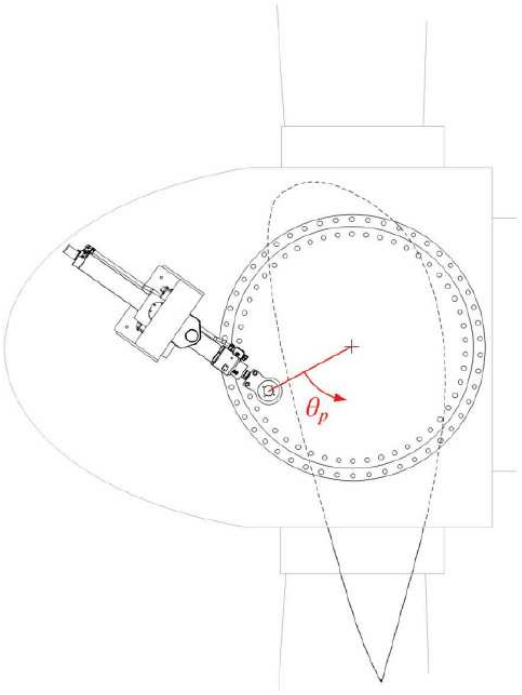

FIGURE 2.3: Cross section scheme with pitch hydraulic cylinder.

It can be observed that the equations correspond to the dynamics of the cylinder as outlined in Equation 2.15, except for the inclusion of a variable momentum arm. This variable is assumed to remain relatively constant for the system under consideration. Consequently, the control design focuses on tracking the angle, while the cylinder dynamics exhibit stable internal behavior, assuming a fully rigid mechanical connection between the cylinder and the blade bearing. Thus, there exists a static relationship transforming x_c to β.

Let us apply some simplification for simplifying the reading:

$$Vol_p = V_{0,p} + A_p x_c \tag{2.17}$$

$$Vol_r = V_{0,p} + A_r(x_{c,max} - x_c) \tag{2.18}$$

$$J_{tot} = I \tag{2.19}$$

The dynamics of the full system is given by:

$$\begin{cases} \dot{\beta} & = v_\beta \\ \dot{v}_\beta & = \frac{1}{I}[-M_{fric} - M_{ext} + r\sin(\psi_p(x_c))(A_p p_p - A_r p_r)] \\ \dot{x}_c & = v_c \\ \dot{v}_c & = \frac{1}{M_{eq}}(A_p p_p - A_r p_r - F_{Fr} - F_{ext}) \\ \dot{p}_p & = \frac{\beta_e}{Vol_p}[-A_p v_c + K_{Qp} u] \\ \dot{p}_r & = \frac{\beta_e}{Vol_r}(A_r v_c - K_{Qrv} u - Q_{cv}) \end{cases} \tag{2.20}$$

2.4 Fault description

Based on the work in [1], the faults are inserted in the system as additive terms noted with blue characters. They will be introduced into the system one at time because in real applications it is unlikely that they will occur simultaneously and studying of this would increase the complexity of the project.
Let us assume that the perturbations are much lower than the main signal.

Table 2.2 describes in detail the faults that may occur in the system where a ranking is given (high, medium and low) to underline the severity on how each fault propagates through the structure.

Fault Name	Fault Model	Description	Severity
$f_{Fr,c}$	$\Delta B_c v_c + \Delta_{F_c} \tanh(v_c/\gamma)$	Increased friction in the cylinder because of sludge formation. Not critical under a certain threshold, but it can cause the cylinder to get stuck. In the initial phase it appears as a variation of friction coefficients.	High
$f_{B,e}$	$\Delta_{B,e}$	Fault related to oil contamination, difficult to model differently than a generic variation with respect to the nominal value.	Medium
$Q_{le,p}$, $Q_{le,r}$	$\Delta_{Q_{le,i}}(p_i - p_{atm})$	Oil leakage between a cylinder chamber and the outside. It can be slow or abrupt, according to wear. Even with small values the turbine will be shut down. From a control point of view, leakage does, however, act to increase the damping in the system.	High
Q_{li}	$\Delta_{Q_{li}}(p_p - p_r)$	Oil leakage between the two chambers in the cylinder. Same characteristics as the external one, it just increases damping in the pitching.	Low
Q_p, Q_{rv}	$\Delta_{K_e}[\cdot]$	Variation in the proportionality coefficient due to mechanical wear of the valve, or by incorrect valve command. As long as the valve is able to operate the severity is low.	Low
Q_{cv}	$\Delta_{Q_{cv}}$	It is usually a discrete-time nature fault leading to the valve getting stuck, more than leakages or a variation in the proportional flow coefficient.	High
f_{y,p_s}, f_{y,p_p} f_{y,p_r}	Δ_{y,p_i}	Wrong measurement in the related pressure sensor.	Low
f_{y,x_c}	Δ_{y,x_c}	Wrong measurement in the cylinder position sensor. Position measurements are the only signals used in the control loop. Hence, their importance.	High

TABLE 2.2: Faults description ranked by their severity.

3

Sliding Mode Control

This Chapter firstly addresses a review on Sliding Mode Control (SMC) and secondly on Adaptive Sliding Mode Control (A-SMC).

3.1 Sliding Mode Control (SMC)

3.1.1 Standard Sliding Mode Control (SMC)

Sliding Mode Control is a sophisticated control method and one of the best choices for nonlinear control systems when high accuracy and robust response are required. It can be employed in both linear and nonlinear dynamical systems, directly considering robustness problems as part of the design process. Specifically, SMC includes the uncertainty as part of the design process, providing additional robustness property compared to traditional feedback control techniques. Nevertheless, SMC presents one main issue: chattering phenomenon. It occurs due to the switching property of the sliding mode control law, but there exist strategies able to reduce chattering, which will be faced afterwards in the next sections.

To explore more in detail SMC, let us consider the following two-dimensional system:

$$\begin{cases} \dot{x}_1 = x_2 \\ \dot{x}_2 = u + f \end{cases} \tag{3.1}$$

where f is a disturbance function.

The aim is to design u ensuring that both states converge to zero.

Let us start with a simple controller, for instance the following full state feedback controller:

$$u = -k_1 x_1 - k_2 x_2 \tag{3.2}$$

If there are no disturbances, i.e. $f = 0$, the controller perfectly works (see Figure 3.1), otherwise, if for example $f = \sin(2t)$, it does not properly react to the perturbation (see Figure 3.3). Figure 3.2 and 3.4 illustrate their relative Simulink schemes.

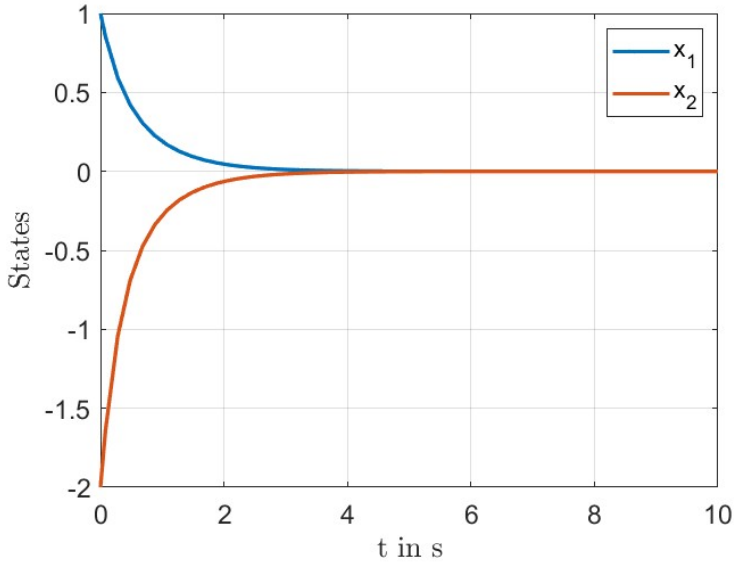

FIGURE 3.1: Plot of the states x_1 and x_2 with full state feedback control action. Parameters: $x_1(0) = 1$, $x_2(0) = -2$, $f = 0$, $k_1 = 5$, $k_2 = 5$.

To overcome this issue, a Sliding Mode Controller can be employed.

Let us define the so-called sliding variable s:

$$s = cx_1 + \dot{x}_1 \tag{3.3}$$

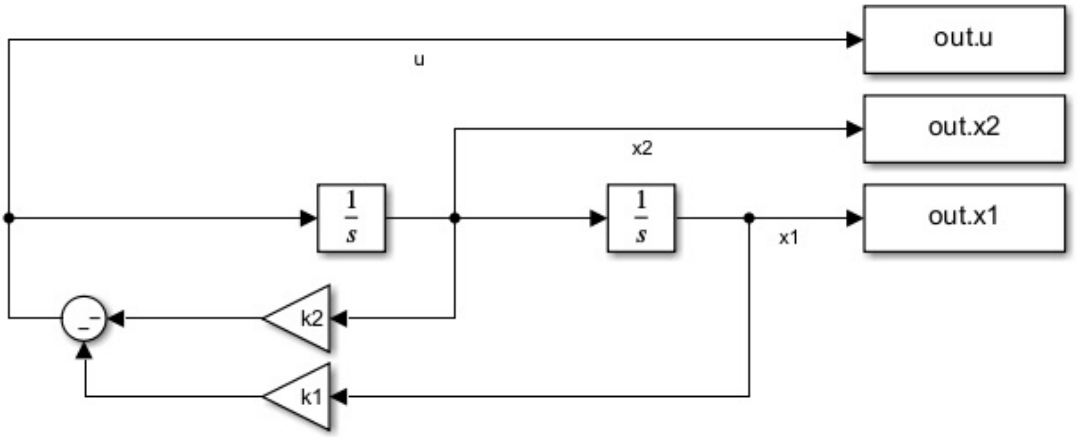

FIGURE 3.2: Simulink scheme of the full state feedback controller with no disturbance, i.e. $f = 0$.

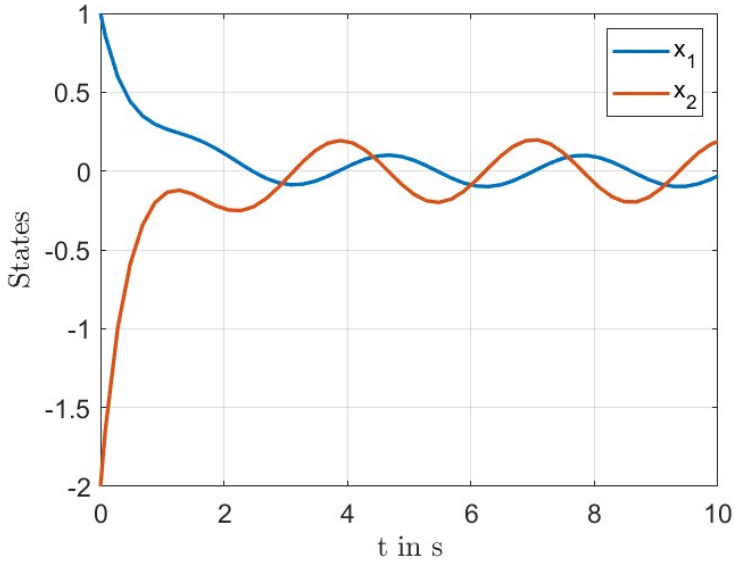

FIGURE 3.3: Plot of the states x_1 and x_2 with full state feedback control action. Parameters: $x_1(0) = 1$, $x_2(0) = -2$, $f = \sin(2t)$, $k_1 = 5$, $k_2 = 5$.

where $c > 0$ is the state convergence rate when $s = 0$ holds (there is no fixed formula for defining sliding surface, but there are some guidelines: $s = 0$ and u must appear in some derivative of s, the degree of the derivative corresponds to the relative degree).

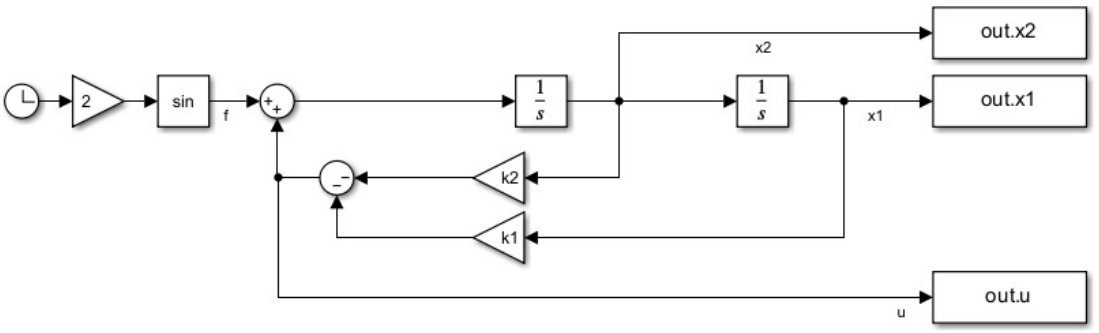

FIGURE 3.4: Simulink scheme of the full state feedback controller with disturbance, $f = \sin(2t)$.

Then impose it equal to zero:

$$\begin{aligned} s &= 0 \\ 0 &= cx_1 + \dot{x}_1 \\ \dot{x}_1 &= -cx_1 \end{aligned} \tag{3.4}$$

The relation that represents the sliding surface is a straight line passing through the origin. As it can be seen from Figure 3.5, the red point goes towards the line and then slides along it reaching the origin. The system is asymptotically stable since the states converge first to the sliding surface $s = 0$ in finite time and then there is exponential convergence in the origin.

The solution is:

$$x_1 = x_{1,0}\, e^{-ct} \tag{3.5}$$

Now let us search for the control input u. As first step, compute the dynamics of s:

$$\begin{aligned} \dot{s} &= c\dot{x}_1 + \ddot{x}_1 \\ &= cx_2 + \dot{x}_2 \\ &= cx_2 + u + f \end{aligned} \tag{3.6}$$

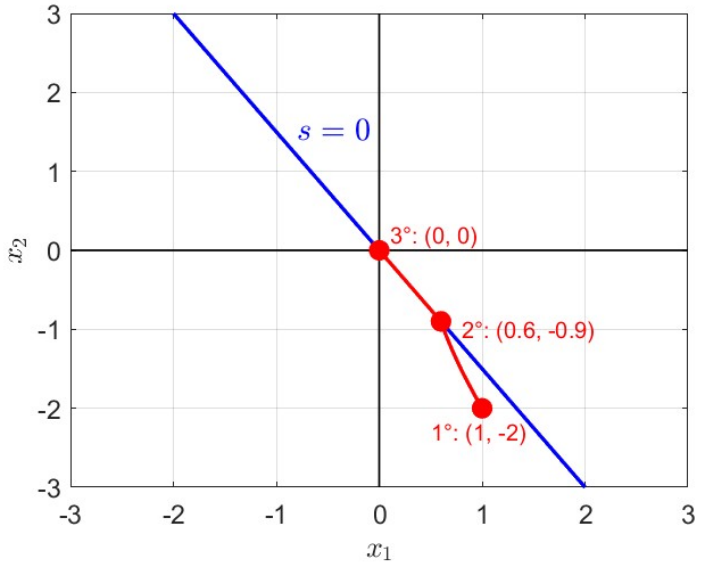

FIGURE 3.5: Convergence towards the origin of both states with sliding surface $s = 0$. Parameters: $x_1(0) = 1, x_2(0) = -2$.

Assume that the disturbance bounds are known:

$$|f| \leq L \tag{3.7}$$

Let us express u such that $\dot{s} = 0$, i.e. select u in such a way cancels out some known terms:

$$\begin{aligned} \dot{s} &= cx_2 + u + f \\ 0 &= cx_2 + u + f \\ u_{eq} &= -cx_2 \end{aligned} \tag{3.8}$$

Design u_{SMC} as the SMC action to counteract the disturbance:

$$u_{SMC} = k\, sgn(s) \tag{3.9}$$

with $k > L$ in order to obtain finite time stability. It is important to recall that u_{SMC} represents the unknown, but at least the bound L gives some information on the disturbance.

So, the total control law is given by the sum of both controllers:

$$u = -cx_2 - k\, sgn(s) \tag{3.10}$$

From Figure 3.6 it can be noticed that the controller u chatters, but the sliding variable s reaches zero in short time, (see Figure 3.7) and the states plotted with $f = \sin(2t)$ now they converge to zero (see Figure 3.8).

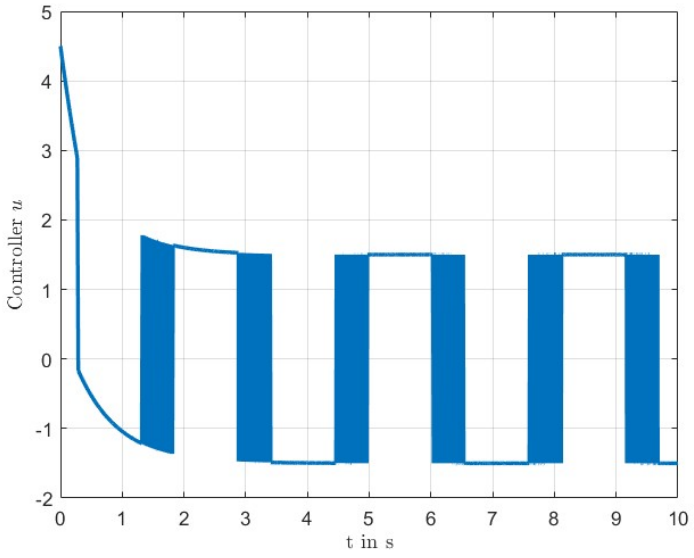

FIGURE 3.6: Control input u with Sliding Mode Control action. Parameters: $x_1(0) = 1$, $x_2(0) = -2$, $f = \sin(2t)$, $c = 1.5$, $\rho = 1.5$.

3.1.2 Super-Twisting Sliding Mode Control (ST-SMC)

As stated before, standard Sliding Mode Control leads the system to chattering phenomenon because of its discontinuous input. Therefore, various solutions have been studied in the literature to address this issue. The fist attempt can be made by substituting the $sign(x)$ function with a continuous and smoother function like $atan$, $atanh$, $sigmoid$, etc. However, the trade-off for implementing this strategy is a loss in performance when the value x is close to the origin.

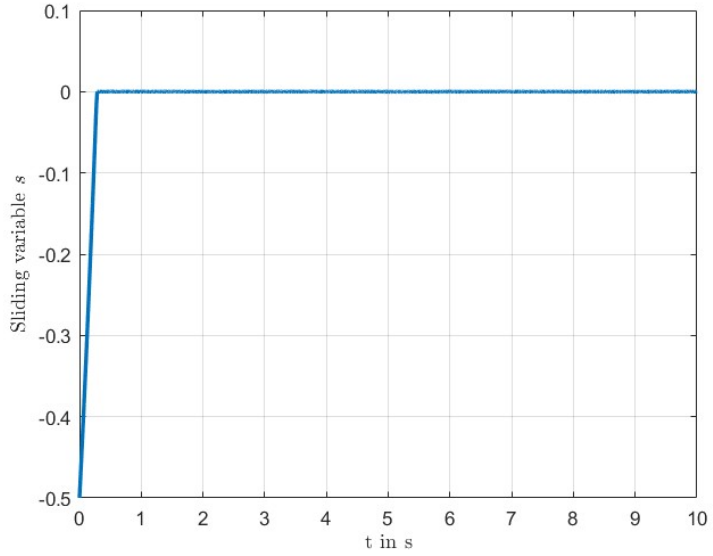

FIGURE 3.7: Plot of sliding variable s with Sliding Mode Control action. Parameters: $x_1(0) = 1$, $x_2(0) = -2$, $f = \sin(2t)$, $c = 1.5$, $\rho = 1.5$.

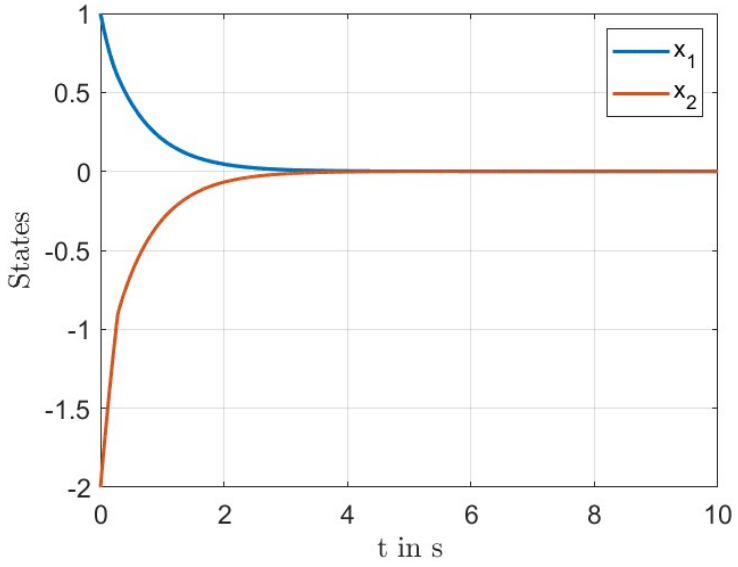

FIGURE 3.8: Plot of the states x_1 and x_2 with Sliding Mode Control action. Parameters: $x_1(0) = 1$, $x_2(0) = -2$, $f = \sin(2t)$, $c = 1.5$, $\rho = 1.5$.

Hence, exploit a High-Order Sliding Mode Control (HO-SMC) with a continuous input improves the performance. In general, this method has a main drawback: it requires knowledge of the sliding variable's derivative.

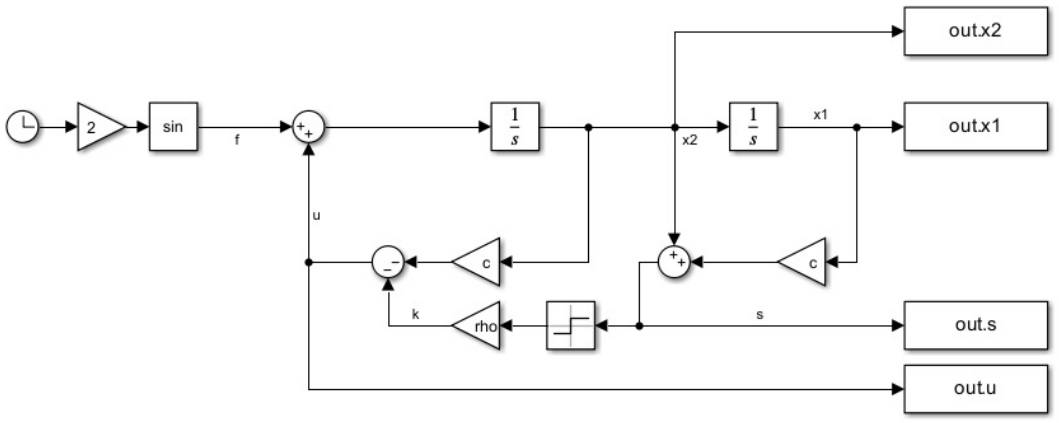

FIGURE 3.9: Simulink scheme of the Sliding Mode Controller with disturbance, $f = \sin(2t)$.

In literature particular attention has been given to the second-order Super Twisting Sliding Mode Control (ST-SMC) because it does not require any information about the time derivative of the sliding variable, only the measurement of the sliding variable itself. Furthermore, it ensures a robust control solution.

Let us define the output tracking error as:

$$e = y - r \tag{3.11}$$

and consider the following sliding variable:

$$s = \dot{e} + \lambda e \text{ with } \lambda > 0 \tag{3.12}$$

In order to drive the sliding variable to zero ($s = 0$) in finite time, one can use the continuous super twisting controller:

$$\begin{cases} u_{ST-SMC} & = -k_1 |s|^{\frac{1}{2}} sgn(s) + v, \qquad k_1 > 1.8\sqrt{k_2 + L} \\ \dot{v} & = -k_2 \, sgn(s), \qquad\qquad\qquad k_2 > L > |\dot{d}| \end{cases} \tag{3.13}$$

The ST-SMC is a second-order SMC since it drives both s and $\dot{s}$ to zero in finite time.

With this strategy, as said above, it is possible to partially solve the chattering problem. However, the gains k_1 and k_2 are set as constants and they can be easily overestimated. To overcome this issue, it is possible to exploit an adaptive law that allows to vary the gains with the most appropriate value depending on the conditions.
In the next sections, some of these approaches will be studied in detail: Adaptive Gains ST-SMC and Barrier Function ST-SMC.

3.2 Adaptive Super Twisting Sliding Mode Control (A-ST-SMC)

To sum up what it has been explained so far, the standard SMC is affected by the chattering problem due to its discontinuous input.
Therefore, a first attempt is to use a continuous saturation function instead of the $sign(x)$ function, but this has a negative impact on the performance.
Hence, it was suggested to use a HO-SMC, in particular the second order ST-SMC, which provides a continuous input and better results. The disadvantages of this approach is that it requires information on the sliding variable derivative and the gains may be bigger than necessary since they are set as constants.
Thus, an adaptive law is a better solution because it allows to change the gains, ensures a good performance and handles very well the chattering problem.
In this project Adaptive Gains and Barrier Function algorithm are explored.

3.2.1 Adaptive Gains Super Twisting Sliding mode control (AG-ST-SMC)

Adaptive Gains Super Twisting Sliding Mode Control (AG-ST-SMC) is a technique that combines two approaches to reduce the chattering: a higher-order of SMC (Super Twisting strategy) and adaptive gains. The main benefit of the Super Twisting element, in addition to attenuating chattering, is that it does not require any information on the boundaries of the disturbance, but only of its gradient. In many applications this value is not known, it is only assumed that the perturbations are bounded. A common problem that one can meet is the overestimation of this value, that leads to unnecessarily high gains. Therefore, another advantage of the method is its ability to adapt the gains, which can improve the elimination of chattering.

Hence, the new problem is formulated as:

$$\begin{cases} u_{AG-ST-SMC} & = -\alpha|s|^{\frac{1}{2}}sgn(s) + v \\ \dot{v} & = -\frac{\beta}{2}sgn(s) \end{cases} \tag{3.14}$$

where α and β are the adaptive gains and they correspond to the previous gains k_1 and k_2 respectively. These two new gains are adjusted via the following formulas:

$$\dot{\alpha} = \begin{cases} \omega\sqrt{\frac{\gamma}{2}}sgn(|s| - \mu) & \text{if } \alpha > \alpha_m \\ \eta & \text{if } \alpha \leq \alpha_m \end{cases} \tag{3.15}$$

$$\beta = 2\epsilon\alpha \tag{3.16}$$

The parameters ω, γ, μ, η, α_m and ϵ are all positive constants. The best value for them has to be found by trial and error procedure.

Let us see in detail the meaning of each term as done in [21]:

- ω and γ both govern how quickly α increases or decreases once α exceeds a set value of α_m. They are split into two separate parameters for more convenient tuning.

- μ is the threshold of the sliding variable. In an ideal SMC this value would be $\mu = 0$, but this is not the case in practical implementation. The lower this parameter is chosen, the closer the ideal SMC will be achieved. However, the lowest achievable value can not be known beforehand and the addition of disturbances will likely increase this reachable threshold.

- η corresponds the slope of the increasing rate of α when it goes below α_m. It is usually chosen as a low value.

- α_m represents a value of α at which point it starts constantly growing to ensure that α is not reduced past a certain value.

- ϵ_{AG} is a constant of proportionality between α and β.

3.2.2 Barrier Function Super Twisting Sliding Mode Control (BF-ST-SMC)

Another strategy studied in modern literature is the Barrier Function based algorithm. Similar to the AG-ST-SMC, the Barrier Function Super Twisting Sliding Mode Control (BF-ST-SMC) aims to avoid chattering while ensuring the convergence of the sliding variable and of its derivative to the neighborhood of zero, without requiring knowledge of the perturbation bounds or their derivatives. It is based on dynamically adapting the gains in order to not overestimate them. In this case, the variable gain is indicated as $L(t, s)$ and the new problem formulation is as follows:

$$\begin{cases} u(t)_{BF-ST-SMC} & = -L(t,s)|s|^{\frac{1}{2}} sgn(s) + v \\ \dot{v} & = -L^2(t,s)\, sgn(s) \end{cases} \tag{3.17}$$

namely $L(t, s)$ and $L^2(t, s)$ are related to the former k_1 and k_2 respectively.
The procedure of the BF-ST-SMC algorithm is split in two phases:

- First, linearly increase the variable gain $L(t, s)$ until the sliding variable s reaches for the first time the neighborhood of zero $|s| \leq \epsilon/2$ at the time instant $\bar{t}$, with $\epsilon > 0$.

$$l(t) = L_1 t + L_0 \quad \text{with} \quad t \geq 0 \tag{3.18}$$

- Then, the variable gain $L(t, s)$ switches to the barrier function and the sliding variable is ensured to stay inside the neighborhood of zero never escaping: $|s(t)| < \epsilon$.

$$L_b(s) = \frac{\epsilon \cdot K}{\epsilon - |s|} \quad \text{with} \quad s \in (-\epsilon, \epsilon) \tag{3.19}$$

  In Figure 3.10 is illustrated the plot of the Barrier Function. The more s approaches to the boundaries of ϵ, the more the gain $L_b(s)$ will increase its value. If $s = 0$, the Barrier Function will assume the starting gain value, i.e. K. The advantage of this approach is that s never escapes from the boundaries thanks to the really high value that $L_b(s)$ will take if the parameters are well tuned.

Therefore, the law that rules the adaptive gain is:

$$L(t, s) = \begin{cases} l(t) & \text{if } 0 \leq t \leq \bar{t}(s) \\ L_b(s(t)) & \text{if } t > \bar{t}(s) \end{cases} \tag{3.20}$$

The adaptation, therefore, ensures that the gains are not overestimated. Now let us explain each parameter of the adaptation law and its role as reported in [21]:

- L_0 is the initial value of the gain at time $t = 0$;
- L_1 indicates the rate of growth of the gain when the sliding variable has not yet reached the threshold to switch to the barrier function;
- ϵ corresponds the threshold of the sliding variable and is the parameter that determines the maximum error of the system;

- K is the minimum value of the gain that can be taken inside the barrier function, this value is assigned to L_b when the sliding variable is equal to zero: $L_b(s = 0) = K$.

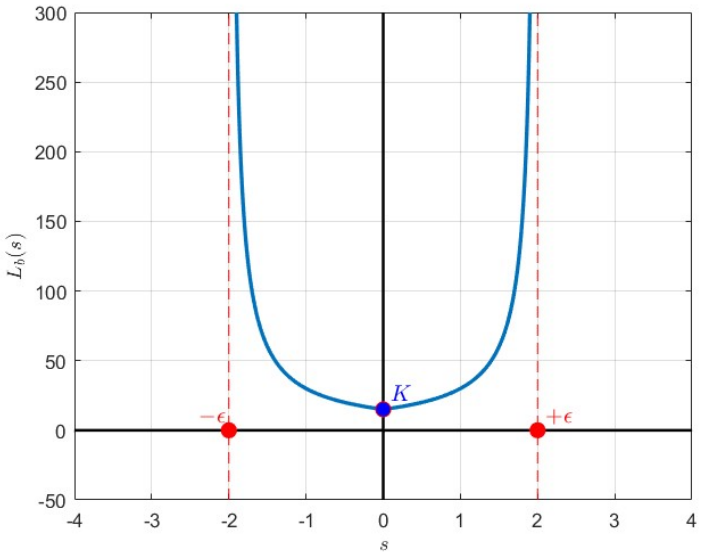

FIGURE 3.10: Barrier function plot. Parameters: $K = 15$ and $\epsilon = 2$.

3.2.3 square root Barrier Function Super Twisting Sliding Mode Control (sqrtBF-ST-SMC)

It has been presented another version of the Barrier Function in [16] that makes use of the square root:

$$L_b(s) = \frac{\sqrt{\epsilon} \cdot K}{\sqrt{\epsilon - |s|}} \quad \text{with} \quad s \in (-\epsilon, \epsilon) \tag{3.21}$$

In this thesis it is referred as as square root Barrier Function Super Twisting Sliding Mode Control (sqrtBF-ST-SMC).

4

Controllers Design

In this Chapter, the design of the controllers developed in the MATLAB/Simulink environment for the Wind Turbine Pitch Hydraulic System will be explained. At the beginning the standard Super Twisting Sliding Mode Control algorithm will be discussed, and then the Adaptive versions of it.

4.1 Sliding Mode Controller Design

Before going into details with the controller design, let us explain some variables that will be recurrently mentioned:

- Blade angle amplitude error:

$$e = \beta - r \tag{4.1}$$

- Blade angle velocity error:

$$\dot{e} = \dot{\beta} - \dot{r} = v_\beta - \dot{r} \tag{4.2}$$

- Blade angle acceleration error:

$$\ddot{e} = \ddot{\beta} - \ddot{r} = \dot{v}_\beta - \ddot{r} = \frac{M_{fric} + M_{ext}}{I} + \frac{r}{I}\sin(\psi_p(x_c))(A_p p_p - A_r p_r) - \ddot{r} \quad (4.3)$$

It is necessary to derive the error until the input term u does not appear in the expression to match the relative degree, therefore it is required to differentiate it one more time:

$$\begin{aligned} e^{(3)} =& \frac{r A_p \beta_e}{I\ Vol_p} Q_p(u)\sin(\psi_p(x_c)) + \frac{r A_r \beta_e}{I\ Vol_r} Q_{xv}(u)\sin(\psi_p(x_c)) \\ & - \frac{r A_p^2 \beta_e}{I\ Vol_p} v_c \sin(\psi_p(x_c)) - \frac{r A_r^2 \beta_e}{I\ Vol_r} v_c \sin(\psi_p(x_c)) \\ & + \frac{r A_r \beta_e}{I\ Vol_r} Q_{cv}\sin(\psi_p(x_c)) \\ & + \underbrace{\frac{r}{I} F_h \cos(\psi_p(x_c)) \frac{d\psi_p}{dx_c} v_c}_{\xi} - \frac{\dot{M}_{fric} + \dot{M}_{ext}}{I} - r^{(3)} \end{aligned} \quad (4.4)$$

To design a Sliding Mode Controller, the sliding surface needs to be defined. Since the direct pitch angle orientation system is of relative degree 3 and the ST-SMC is of order 2, the sliding surface requires the derivatives of the blade angle amplitude error. In particular, the surface is chosen as a second-order linear system of the blade angle amplitude error as follows:

$$\begin{aligned} s &= \left(\frac{d}{dt} + c_1\right)\left(\frac{d}{dt} + c_2\right) e \\ &= \ddot{e} + (c_1 + c_2)\dot{e} + c_1 c_2 e \\ &= \ddot{e} + \lambda_2 \dot{e} + \lambda_1 e \end{aligned} \quad (4.5)$$

where $\lambda_1 = c_1 c_2 > 0$ and $\lambda_2 = (c_1 + c_2) > 0$. They are the error convergence rates when the system is in sliding mode, i.e. when the conditions $s = 0$ holds.

By substituting the error and its derivatives in the Equation 4.5, s becomes:

$$s = \frac{r}{I}\sin(\psi_p(x_c))(A_p p_p - A_r p_r) - \frac{M_{fric} + M_{ext}}{I} + \lambda_2 v_\beta + \lambda_1 \beta - \ddot{r} - \lambda_2 \dot{r} - \lambda_1 r \quad (4.6)$$

The sliding surface dynamics is computed in order to obtain an expression depending on u and to derive the equivalent controller:

$$\begin{aligned}
\dot{s} =& e^{(3)} + \lambda_2 \ddot{e} + \lambda_1 \dot{e} \\
=& \frac{r A_p \beta_e}{I \ Vol_p} Q_p(u) \sin(\psi_p(x_c)) + \frac{r A_r \beta_e}{I \ Vol_r} Q_{xv}(u) \sin(\psi_p(x_c)) \\
& - \frac{r A_p^2 \beta_e}{I \ Vol_p} v_c \sin(\psi_p(x_c)) - \frac{r A_r^2 \beta_e}{I \ Vol_r} v_c \sin(\psi_p(x_c)) \\
& + \frac{r A_r \beta_e}{I \ Vol_r} Q_{cv} \sin(\psi_p(x_c)) + \xi - \frac{\dot{M}_{fric} + \dot{M}_{ext}}{I} \\
& - r^{(3)} + \lambda_2 \left(\frac{r}{I} \sin(\psi_p(x_c)) F_h - \frac{M_{fric} + M_{ext}}{I} - \ddot{r} \right) + \lambda_1 (v_\beta - \dot{r})
\end{aligned} \tag{4.7}$$

Let us apply the following simplifications:

$$Q_p(u) = K_{Q_p} u \tag{4.8}$$

$$Q_{x_v}(u) = K_{Q_{rv}} u \tag{4.9}$$

For the sake of simplicity, one can define:

$$g = \frac{r A_p \beta_e}{I Vol_p} K_{Q_p} \sin(\psi_p(x_c)) + \frac{r A_r \beta_e}{I Vol_r} K_{Q_{rv}} \sin(\psi_p(x_c)) \tag{4.10}$$

and

$$\begin{aligned}
f =& \frac{r A_p^2 \beta_e}{I Vol_p} v_c \sin(\psi_p(x_c)) - \frac{r A_r^2 \beta_e}{I Vol_r} v_c \sin(\psi_p(x_c)) \\
& - \frac{r A_p^2 \beta_e}{I Vol_p} v_c \sin(\psi_p(x_c)) + \frac{r A_r^2 \beta_e}{I Vol_r} v_c \sin(\psi_p(x_c)) \\
& + r^{(3)} - \lambda_2 \left(\frac{r}{I} \sin(\psi_p(x_c)) F_h - \frac{\hat{r}_d}{I} - \ddot{r} \right) \\
& - \lambda_1 (v_\beta - \dot{r})
\end{aligned} \tag{4.11}$$

Hence, the dynamics of s can be represented as:

$$\dot{s} = gu + f \tag{4.12}$$

Imposing $\dot{s} = 0$ and isolating u, it can be obtained the equivalent controller such that cancels the original dynamics:

$$u_{eq} = -\frac{1}{g} f \tag{4.13}$$

Then, the Sliding Mode Control action has to be introduced because, even if $\dot{s}$ is ideally in zero with u_{eq} action, actually there is still present a disturbance $d(t)$. Therefore, let us define u_{SMC} as the control action of the first order SMC:

$$u_{SMC} = -k \; sgn(s) \tag{4.14}$$

and the disturbance to win is:

$$d(t) = \xi - \frac{M_{fric} + M_{ext}}{I} - \lambda_2 \left(\frac{M_{fric} + M_{ext} - \hat{r}_d}{I} \right) \tag{4.15}$$

Thus, the global control law is expressed as the sum of both controls:

$$\begin{aligned}
u &= u_{eq} + \frac{1}{g} u_{SMC} \\
&= \frac{1}{g}(-f - k \, sgn(s)) \\
&= \frac{1}{\frac{rA_p\beta_e}{IVol_p} K_{Q_p} \sin(\psi_p(x_c)) + \frac{rA_r\beta_e}{IVol_r} K_{Q_r} \sin(\psi_p(x_c))} \\
&\quad \times \left[\frac{rA_p^2\beta_e}{IVol_p} v_c \sin(\psi_p(x_c)) - \frac{rA_r^2\beta_e}{IVol_r} v_c \sin(\psi_p(x_c)) - \frac{rA_p^2\beta_e}{IVol_p} v_c \sin(\psi_p(x_c)) \right. \\
&\qquad + \frac{rA_r^2\beta_e}{IVol_r} v_c \sin(\psi_p(x_c)) + r^{(3)} - \lambda_2 \left(\frac{r}{I} \sin(\psi_p(x_c)) F_h - \frac{\hat{r}_d}{I} - \ddot{r} \right) \\
&\qquad \left. - \lambda_1(v_\beta - \dot{r}) - k \, sgn(s) \right]
\end{aligned} \tag{4.16}$$

Due to chattering problems already discussed, to implement the previous controller, it is necessary to substitute the $sign(x)$ function with a smoother function.

In this thesis project the following approximation is chosen:

$$sgn(x) \approx \frac{2}{\pi} atan(kx) \tag{4.17}$$

where k is a positive constant that gives the steepness. The more it is big, the better the approximation will be.

4.1.1 Super Twisting Sliding Mode Controller Design

A better attempt is to explore an High Order of SMC, in particular a second order version, the Super Twisting Sliding Mode Control. It is defined as follows:

$$\begin{cases} u_{ST-SMC} & = -k_1 |s|^{\frac{1}{2}} sgn(s) + v, \qquad k_1 > 1.8\sqrt{k_2 + L} \\ \dot{v} & = -k_2 sgn(s), \qquad\qquad\qquad k_2 > L > |\dot{d}| \end{cases} \tag{4.18}$$

where the final control law becomes:

$$u = u_{eq} + \frac{1}{g} u_{ST-SMC} \tag{4.19}$$

which is given to the system as input.

The gains k_1 and k_2 are chosen as positive constants. However, as previously stated, this is a static law that can not further adjust itself, it is required the knowledge of the derivative of the disturbance bounds $\dot{d}$ that in practice usually is unlikely to be known and the chattering is just reduced, not eliminated. Therefore, to improve the performance, the gains k_1 and k_2 require an adaptation law.

4.2 Adaptive Gain Super Twisting Sliding Mode Controller Design

The AG-ST-SMC is one of the Adaptive SMC that adapts the gains and it is formulated as follows:

$$\begin{cases} u_{AG-ST-SMC} & = -\alpha |s|^{\frac{1}{2}} sgn(s) + v \\ \dot{v} & = -\frac{\beta}{2} sgn(s) \end{cases} \tag{4.20}$$

and u is the new control law:

$$u = u_{eq} + \frac{1}{g} u_{AG-ST-SMC} \tag{4.21}$$

In this new formulation of the problem, α corresponds to the previous gain k_1 and β to k_2. These two new gains are adapted via the following formulas:

$$\dot{\alpha} = \begin{cases} \omega \sqrt{\frac{\gamma}{2}} sgn(|s| - \mu) & \text{if } \alpha > \alpha_m \\ \eta & \text{if } \alpha \leq \alpha_m \end{cases} \tag{4.22}$$

$$\beta = 2\epsilon\alpha \tag{4.23}$$

4.3 Barrier Function Super Twisting Sliding Mode Controller Design

The other method explored is the BF-ST-SMC. The previous method AG-ST-SMC ensures that the sliding variable converges in finite-time to a zone close to zero, but the size of the zone close to zero depends on the upper bound of the disturbance. Therefore, these values can not be known beforehand and there is no proof that the sliding variable will not escape from this neighbourhood of zero. In order to circumvent these limitations, the use of BF

is introduced. The BF control action is given by:

$$\begin{cases} u_{BF-ST-SMC}(t) & = -L(t,s)|s|^{1/2} sgn(s) + v \\ \dot{v} & = -L^2(t,s)\, sgn(s) \end{cases} \tag{4.24}$$

where the formulas that rule the adaptive gain are:

$$L(t,s) = \begin{cases} l(t) = L_1 t + L_0 & \text{if } 0 \leq t \leq \bar{t}(s) \\ L_b(s) = \frac{\epsilon K}{\epsilon - |s|} & \text{if } t > \bar{t}(s) \end{cases} \tag{4.25}$$

The global law is given by the sum of both controls:

$$u = u_{eq} + \frac{1}{g} u_{BF-ST-SMC} \tag{4.26}$$

4.4 square root Barrier Function Sliding Mode Controller Design

Same formulation as before except for the new $L_b(s)$ which is:

$$L_b(s) = \frac{\sqrt{\epsilon} \cdot K}{\sqrt{\epsilon - |s|}} \quad \text{with } s \in (-\epsilon, \epsilon) \tag{4.27}$$

5

Simulation Results

In this chapter the controllers designed in the previous one are tested with a high-fidelity simulator to analyze their performances and then the results are discussed. The simulations were conducted in the MATLAB/Simulink environment.

5.1 Test Scenarios

As a first step, control goal has to be set. The purpose is to have a satisfactory tracking of the reference, a reasonable error and a realistic input, namely avoiding saturation and excessive chattering. Another task is to keep the gains as small as possible meeting the previous requests.
It is considered a good performance when the error is inside the range $[-0.005, 0.005]rad$ for β. Furthermore, the maximum absolute value that the input can assume in this system is $1m$.

The controllers have been tested with simulation time of $250s$ and by leveraging the openFAST simulator by NREL to obtain realistic pitch angle reference and external load.

Figure 5.1 shows the Simulink block scheme of openFAST simulator, namely the entire wind turbine system. Figure 5.2 instead, displays the Simulink block scheme of the Hydraulic Pitch System.

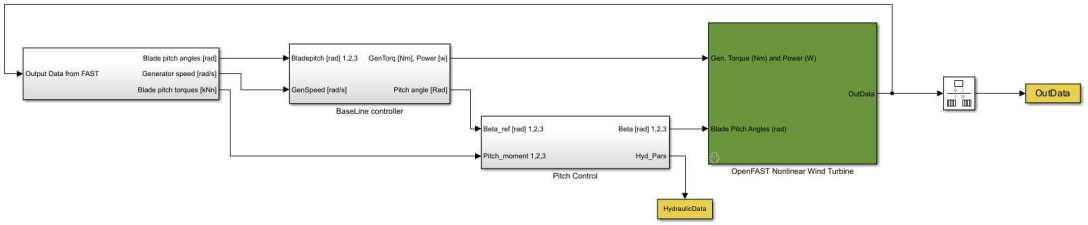

FIGURE 5.1: Simulink block scheme of openFAST simulator.

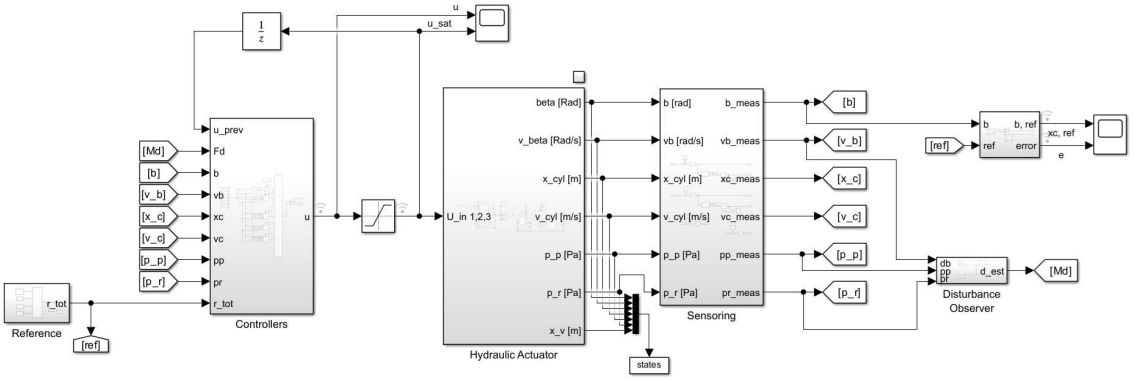

FIGURE 5.2: Simulink block scheme of the HPS.

The system is tested both under nominal conditions, namely without the presence of faults, and under several faulty scenarios.

The performance criteria used to compare the different solutions are:

- Normalized Maximum Absolute Error (MAX($|e|$));
- Normalized Mean Square Root of the Error (RMS(e));
- Normalized Mean Square Root of the Input Signal (RMS($u_{sat} - \bar{u}_{sat}$)), where its moving average is subtracted in order to obtain an indication of chattering.

To have more valid outcomes, the initial samples are discarded, since they are related to the initialization of the controllers. For the nominal case it was assumed to consider

samples from time instant $t = 5s$ and for the faults case from $t = 30s$, namely when the fault is introduced in the system.
Metrics are normalized because they can be more easily interpreted, especially when the original scales of the data are different. This helps the visualization and understanding the relationships between the methods employed.

The tests are organized in two sections:

- Pitch angle β as output in nominal case (Section 5.2);
- Pitch angle β as output in fault case (Section 5.3).

For the sake of simplicity, N is employed to indicate the nominal (standard or baseline) control (ST-SMC), AG for invoking AG-ST-SMC, BF refers to BF-ST-SMC and lastly sqrtBF is used to mention sqrtBF-ST-SMC.

5.2 Pitch angle β as output in nominal case

In this Section the controllers are tested in the system with β as output in the nominal case and the simulation time is $250s$.

5.2.1 BF-ST-SMC

In Figure 5.3 the performances of the Barrier Function controller with fixed values chosen for K (8, 10, 12, 16, 20) and with their relative ϵ found by trial and error (respectively 39, 26.5, 29.5, 19, 18) are plotted. Every ϵ reported is the limit case for which the controller properly works. If that parameter is decreased, the sliding variable s escapes from the boundaries $[-\epsilon, \epsilon]$ and the tracking of the reference is lost. For practical reasons, the parameters for the linear function are set $L_0 = K$ and $L_1 = 0$ and the switching to the barrier function is imposed after $5s$. In Table 5.1 the simulations are discussed.

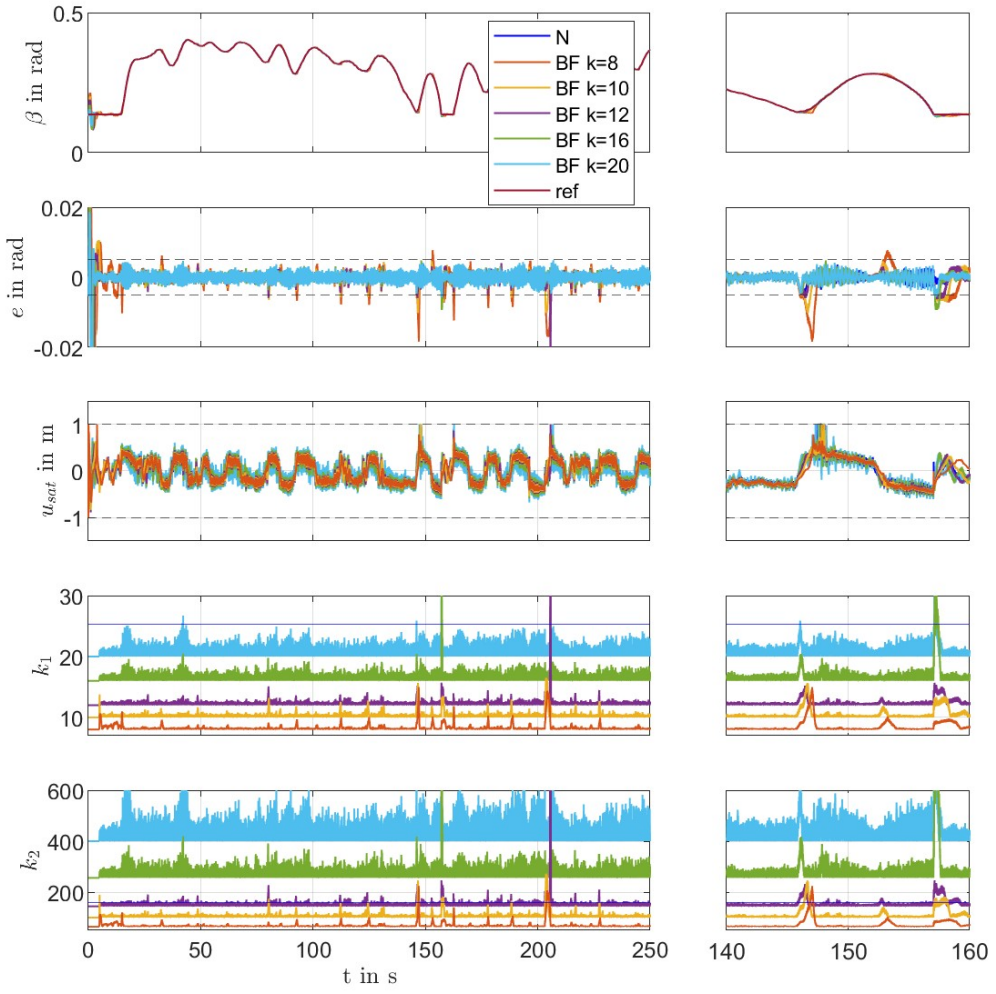

FIGURE 5.3: Plot of output β, error e, saturated input u_{sat}, gains k_1 and k_2 with BF-ST-SMC strategy and simulation time $250s$ in nominal case. Parameters: fixed K (8, 10, 12, 16, 20) and various ϵ (respectively 39, 26.5, 29.5, 19, 18). On the right, a zoom from time instant $t = 140s$ to $t = 160s$.

It can be noticed that for $K = 10$ the ϵ value 26.5 corresponds to a case of outlier since it differs from the other values, it should be inside the range $[29.5, 39]$, namely the ϵ used for the next K and the previous one.

Examining the results, some noteworthy details have been noticed. If the goal is to decrease K, in order to keep a satisfying tracking of the reference, it is required to increase ϵ and vice versa. To obtain a smaller error and more accuracy, it is needed on the hand to

reduce ϵ, but on the other hand to raise K that provokes more oscillations in the control input, therefore more chattering. Otherwise, if it is preferable have less oscillations in the control input, K needs to be diminished and ϵ enlarged, causing a bigger error and less accuracy.
$K = 12$ appears to be a good tradeoff between parameters because the input does not oscillate as much as for higher values of K, the error is well bounded in the tolerance range and finally the gains values are similar or below respect to the standard ones. Another reason why this value is chosen, it is because it mimics the gains used in the standard ST-SMC ($k_{1,N} = 25.2228$, $k_{2,N} = 160$). Considering that the relation of BF gains is $k_{2,BF} = k_{1,BF}^2$, by calculating $\sqrt{k_{2,N}}$ one gets $\sqrt{160} \approx 12.65$.

In Figure 5.4 the performances of the Barrier Function controller with the chosen value $K = 12$ and varying ϵ are presented. The starting ϵ is the limit case 39, then this value is increased from 10% to 50% with step of 10%, i.e. 42.9, 46.8, 50.7, 54.6, 58.5 and finally the value that will be used for the faults analysis, that is 2500.

For what concern the output β, the error e and the saturated input u_{sat}, the performances are more or less the same with different values of ϵ. Instead, regarding the gains, it can be noticed that for $\epsilon = 2500$ the gains are not really adapted and they emulate the standard controller gains that are constants, but the performance still holds the requirements. This occurs because the width of the band is very big. Hence, the more ϵ is small (within the limit case), the more the gains are adjusted.

5.2.2 sqrtBF-ST-SMC

In Figure 5.5 and Table 5.2 the performances of the square root Barrier Function controller with the fixed values chosen for K (8, 10, 12, 16, 20) and with their relative ϵ found by trial and error (respectively 22, 15.5, 22, 12, 10) are reported and discussed. Every ϵ is the limit case in which the controller properly works, otherwise, if that parameters is diminished, the sliding variable s goes out from the boundaries $[-\epsilon, \epsilon]$ and the tracking of the reference is not followed anymore. For practical reasons, the parameters for the linear

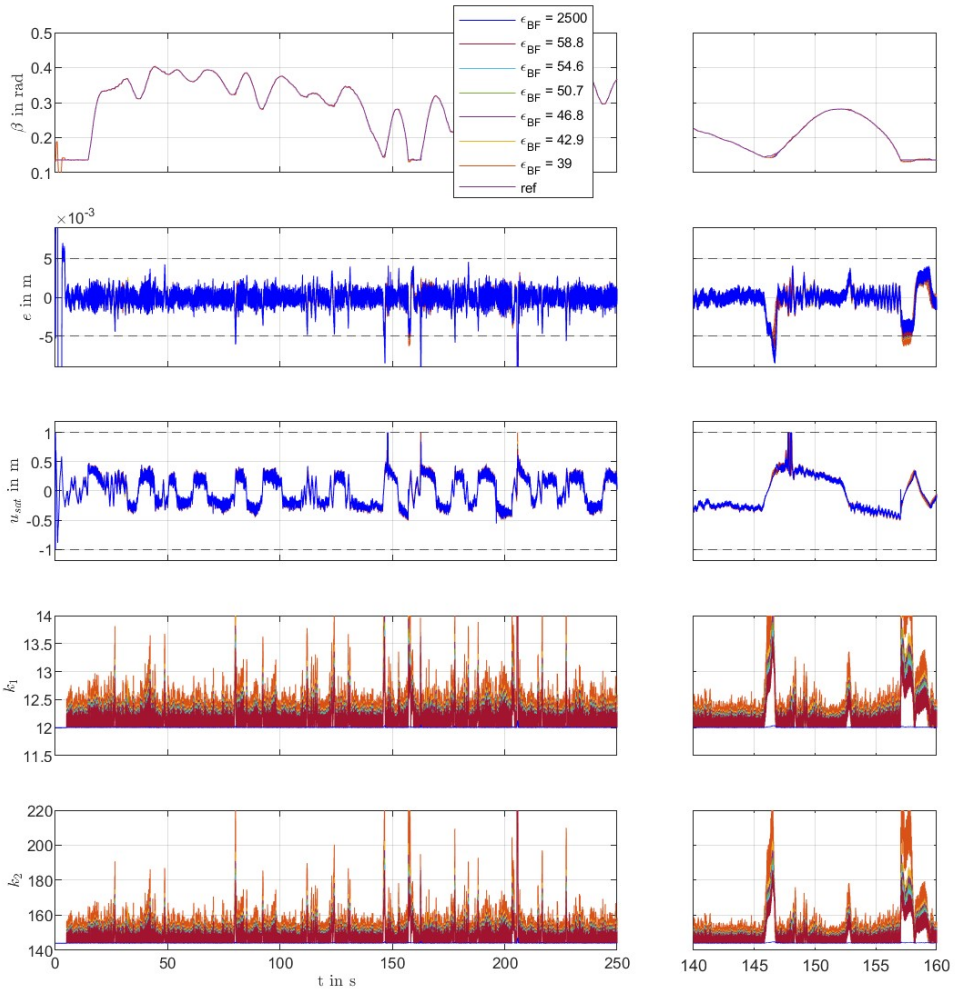

FIGURE 5.4: Plot of output β, error e, saturated input u_{sat}, gains k_1 and k_2 with BF-ST-SMC strategy and simulation time $250s$ in nominal case. Parameters: $K = 12$ and various ϵ (39, 42.9, 46.8, 50.7, 54.6, 58.5 and 2500). On the right, a zoom from time instant $t = 140s$ to $t = 160s$.

function are set $L_0 = K$ and $L_1 = 0$ and the switching to the barrier function is imposed after $5s$.

Notice that for $K = 10$ the ϵ value 15.5 corresponds to a case of outlier since it differs from the other values, where the ϵ used for the next K and the previous one is in both cases 22.

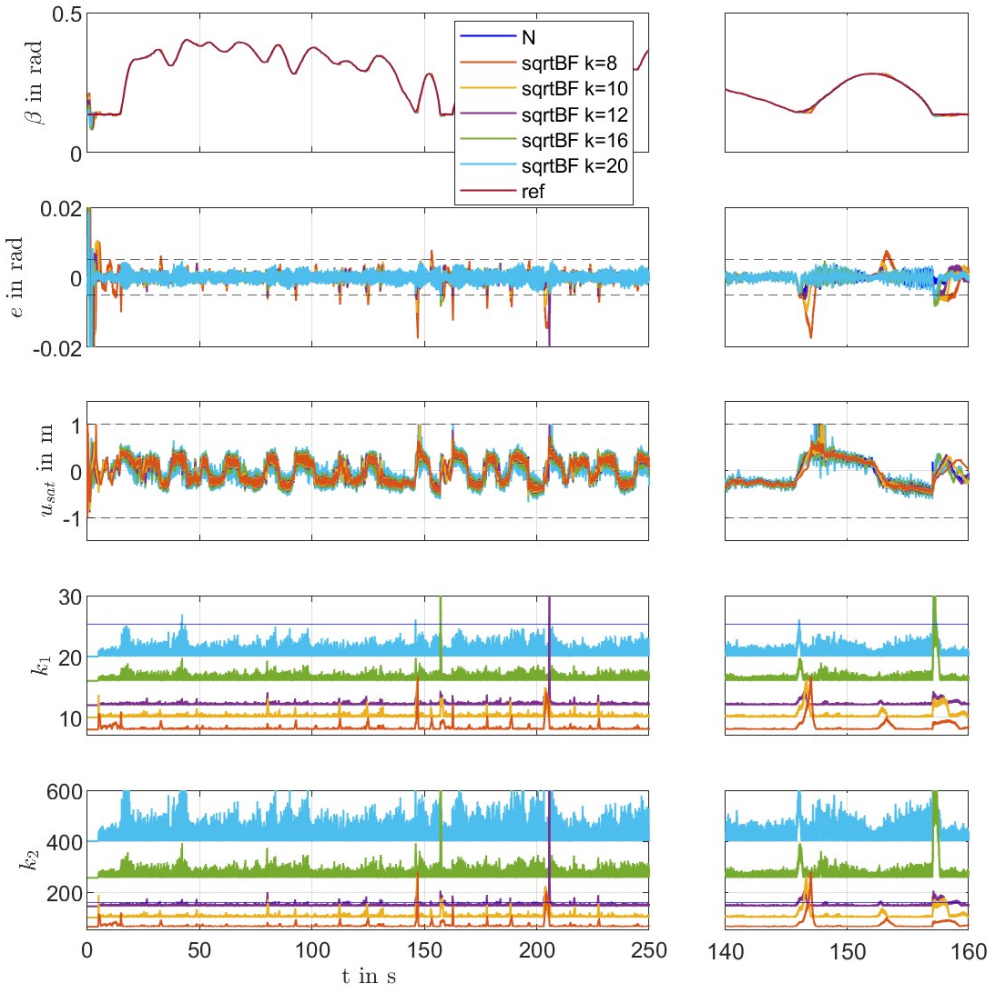

FIGURE 5.5: Plot of output β, error e, saturated input u_{sat}, gains k_1 and k_2 with sqrtBF-ST-SMC strategy and simulation time $250s$ in nominal case. Parameters: fixed K (8, 10, 12, 16, 20) and various ϵ (respectively 22, 15.5, 22, 12, 10). On the right, a zoom from time instant $t = 140s$ to $t = 160s$.

Observing the results, same conclusions as in the BF-ST-SMC case can be extracted, therefore $K = 12$ seems to be an adequate tradeoff between parameters: the input does not oscillate as much as higher values of K, the error is well bounded in the tolerance range, the gains values are similar or below respect to the standard ones and emulate the values of standard ST-SMC gains.

In Figure 5.6 the performances of the square root Barrier Function controller with the

selected $K = 12$ and changing ϵ are presented. The initial ϵ is the limit case 22, then this value is enlarged from 10% to 50% with step of 10%, i.e. 24.2, 26.4, 28.6, 30.8, 33.0 and finally the value that will be used for the faults analysis, namely 1500.

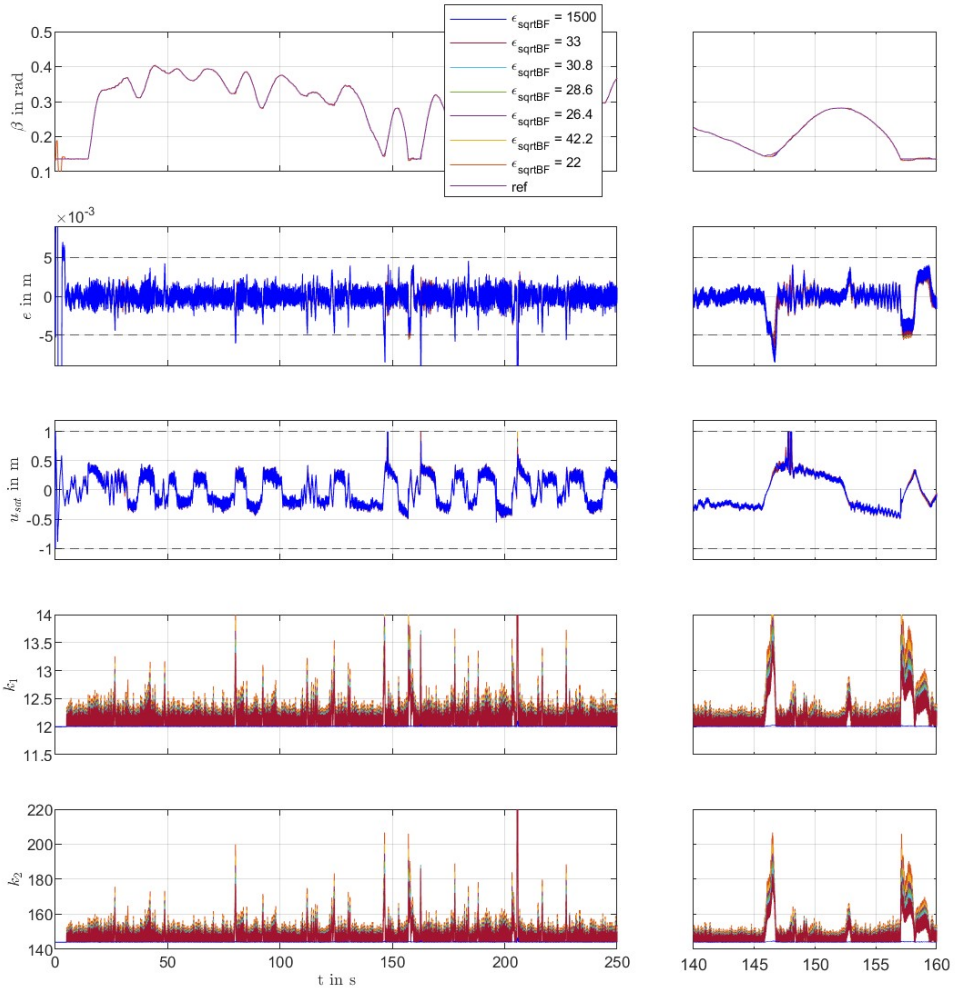

FIGURE 5.6: Plot of output β, error e, saturated input u_{sat}, gains k_1 and k_2 with sqrtBF-ST-SMC strategy and simulation time $250s$ in nominal case. Parameters: $K = 12$ and various ϵ (22, 24.2, 26.4, 28.6, 30.8, 33.0 and 1500). On the right, a zoom from time instant $t = 140s$ to $t = 160s$.

By looking at the tests, similar interpretations done in the BF-ST-SMC case can be done. Therefore, for what regards the output β, the error e and the saturated input u_{sat}, the performances are really close to each other with different values of ϵ. Instead, it can

be observed that for $\epsilon = 1500$ the gains are not actually dynamically adjusted and they emulate the standard controller behaviour that has constants, but anyway the performance is still satisfying the requests. This happens because the bandwidth is very large. As stated before, the more ϵ is small (within the limit case), the more the gains are adapted.

5.2.3 AG-ST-SMC

The tuning for this method is more challenging since a lot of parameters are involved. In Table 5.3 few tuning solutions are listed and in Figure 5.7 their behaviours is presented.

The parameter ϵ_{AG} is fixed because the idea is to mimic the proportional relation between the standard ST-SMC gains: $k_{2,N} = x \cdot k_{1,N}$, therefore $x = \frac{k_{2,N}}{k_{1,N}} = \frac{160}{25.2228} \approx 6$. Since $k_{2,AG} = 2 \cdot \epsilon_{AG} \cdot k_{1,AG}$, hence $\epsilon_{AG} = \frac{1}{2}\frac{k_{2,AG}}{k_{1,AG}} \approx 3$.
The value of α_m was chosen considering that it should be a lower value than $k_{1,N}$ due to the control goal and in order to let adapt $k_{1,AG}$ just when it is needed. The others parameters were found by trial and error.

Simulation Number	α_m	ω	γ	μ	η	ϵ_{AG}
1	5	50	50	5	50	3
2	10	50	50	5	50	3
3	10	25	25	5	25	3
4	5	25	25	5	25	3

TABLE 5.3: Simulation parameters for AG-ST-SMC in nominal case.

The simulations have similar performances. The third solution is selected for the faulty scenarios because of the best tracking performance and less chattering in the input.

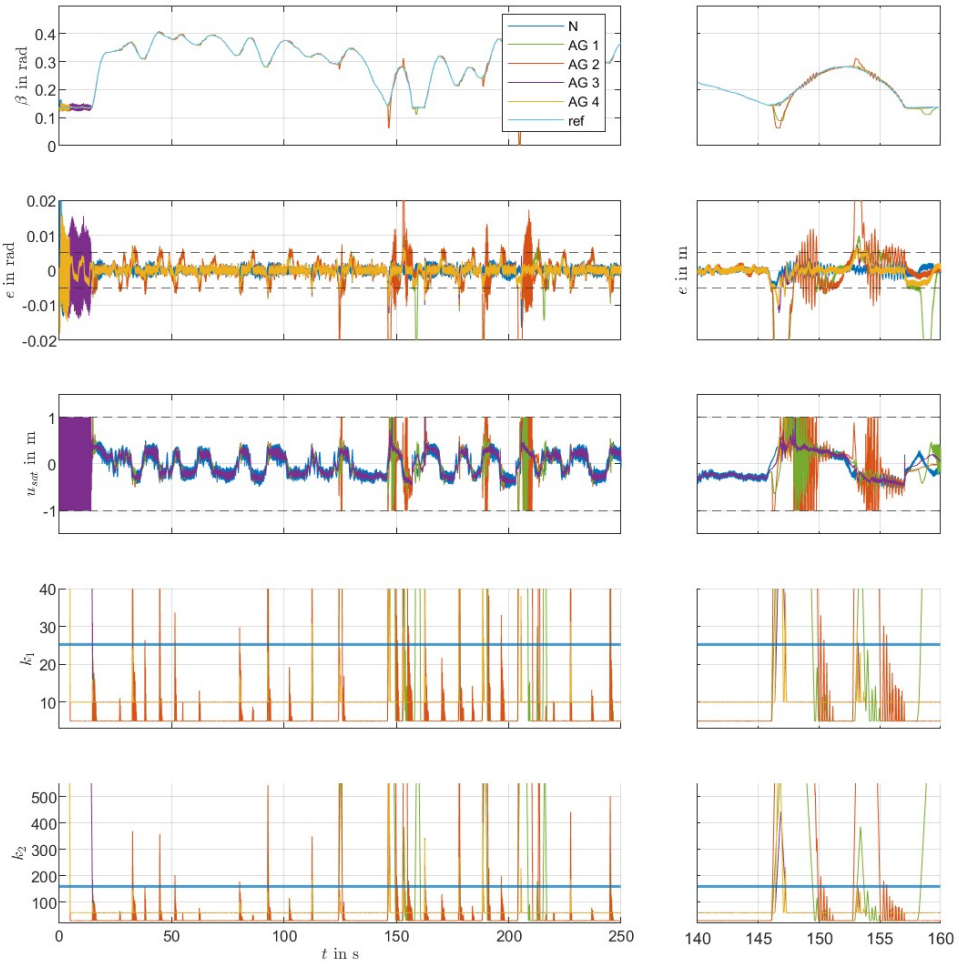

FIGURE 5.7: Plot of output β, error e, saturated input u_{sat}, gains k_1 and k_2 with AG-ST-SMC strategy and simulation time $250s$ in nominal case. Parameters are listed in Table 5.3. On the right, a zoom from time instant $t = 140s$ to $t = 160s$.

5.2.4 Comparison and Conclusions nominal case

Figure 5.8 presents a comparison between of all the controllers and Figure 5.9 analyses them in detail through the defined metrics.

It is possible to see that all the controllers have suitable performances since all the requirements are satisfied.

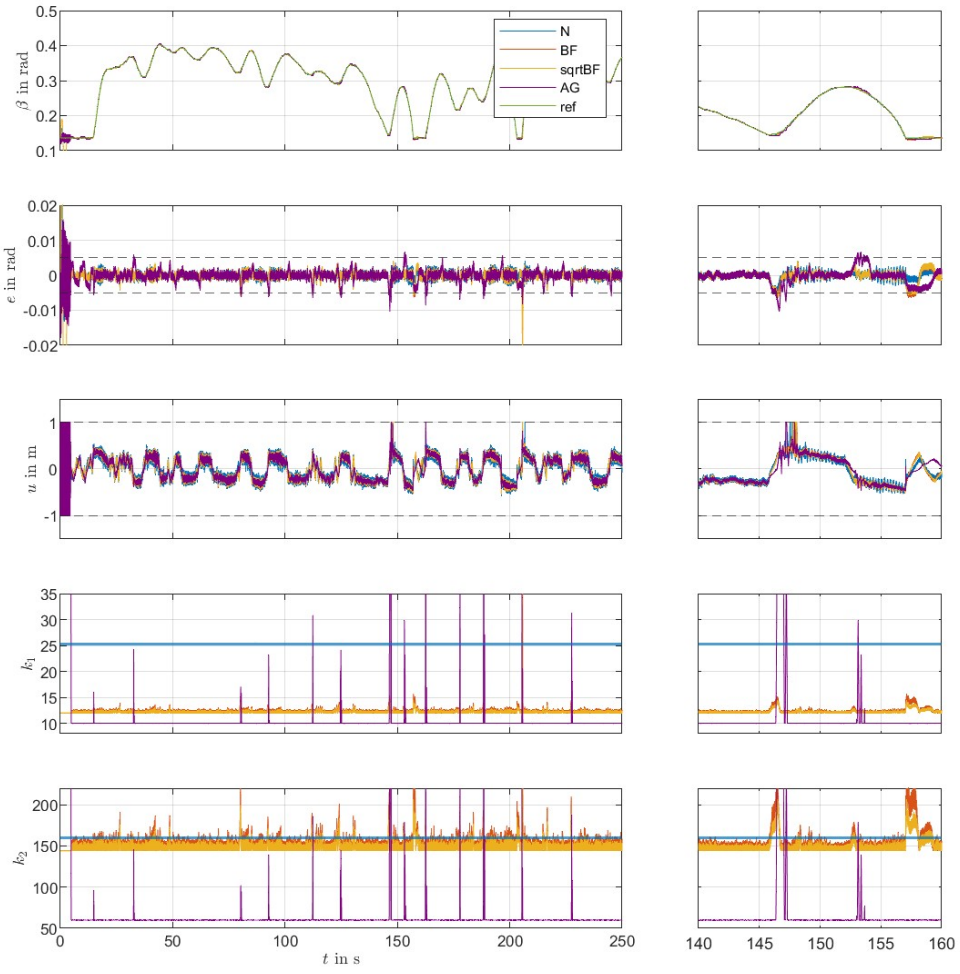

FIGURE 5.8: Plot of output β, error e, saturated input u_{sat}, gains k_1 and k_2, with simulation time $250s$ in nominal case with four controllers. On the right, a zoom from time instant $t = 140s$ to $t = 160s$.

5.3 Pitch angle β as output in fault case

In this section the controllers are tested with the introduction of faults. In Table 5.4 the values of all the simulated faults are listed. In each simulation there is just one fault activated and it starts to affect the system at the time instant $t = 30s$.

Some values of the controllers parameters are different compared to the ones used in

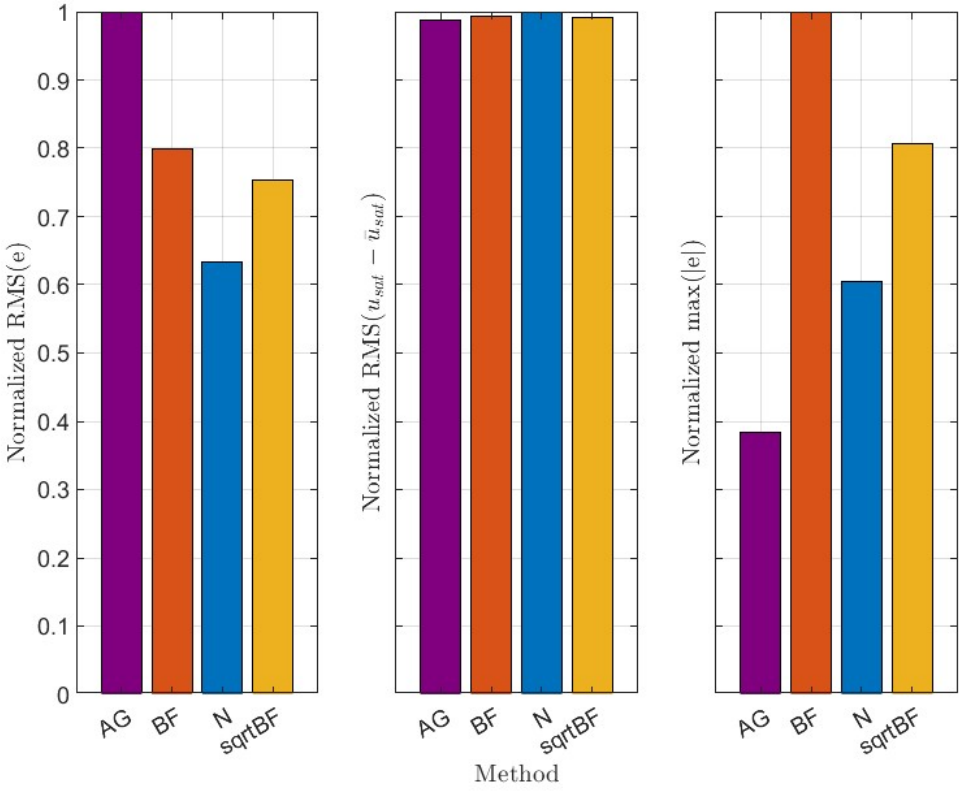

FIGURE 5.9: Metrics for the four controllers in nominal case: Normalized RMS(e), Normalized RMS($u_{sat} - \bar{u}_{sat}$) and Normalized MAX($|e|$).

the nominal case. To handle the faults, it was needed a new tuning that brought to the following values:

- BF-ST-SMC: $K_{BF} = 12$, $\epsilon_{BF} = 2500$, $L_{0,BF} = 12$, $L_{1,BF} = 0$;
- sqrtBF-ST-SMC: $K_{sqrtBF} = 12$, $\epsilon_{sqrtBF} = 1500$, $L_{0,sqrtBF} = 12$, $L_{1,sqrtBF} = 0$;
- AG-ST-SMC: $\omega = 25$, $\gamma = 25$, $\mu = 5$, $\eta = 25$, $\alpha_m = 10$ and $\epsilon_{AG} = 3$.

As seen in the previous section, namely in the nominal case, when BF and sqrtBF mechanisms are implemented, increasing the ϵ parameter does not affect the overall performance, except for exceeding the limit case found in order to not have the sliding variable s escaping from the boundaries. With the injection of faults in the system, it was needful to enlarge a lot ϵ to have s inside the range $[-\epsilon, \epsilon]$, therefore $\epsilon_{BF} = 2500$ and $\epsilon_{sqrtBF} = 1500$

are used. For what concern the AG strategy, it was not indispensable to change any parameters. Moreover, also in this tests the parameters for the linear function of BF and sqrtBF strategy are implemented as $L_0 = K$ and $L_1 = 0$ and the switching to the barrier function occurs at $5s$.

In the following, from Figure 5.10 to 5.44, the simulations of the faults and the metric analysis are reported with the four controllers all together to let us do a comparison between the performances of the different methods.

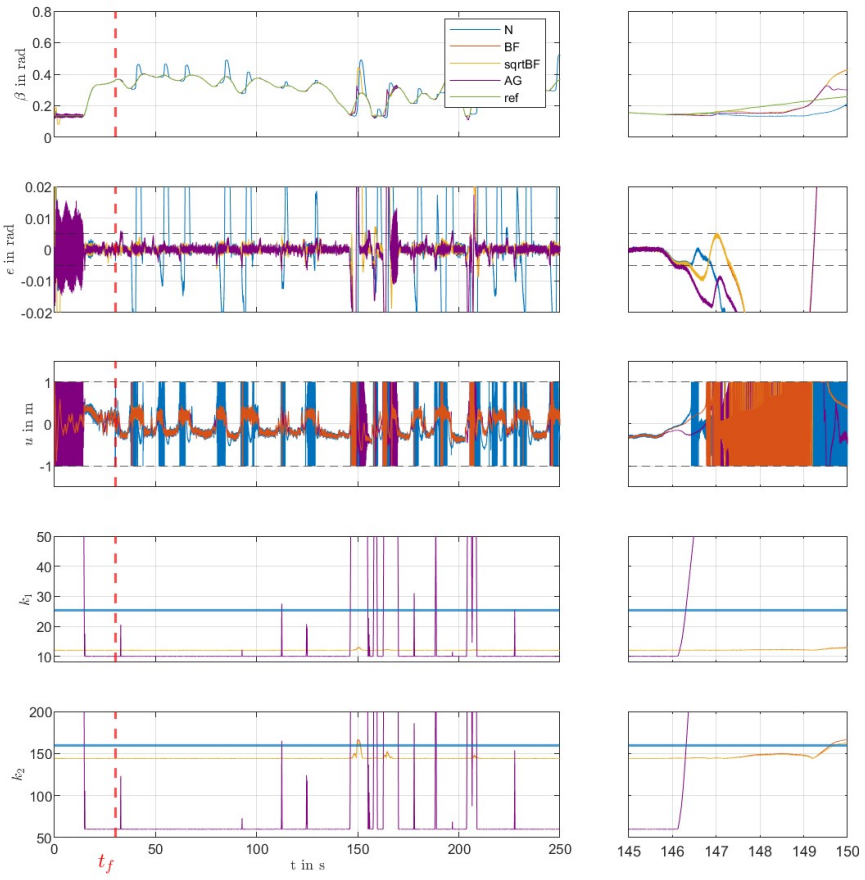

(A) Plot of the output β, error e, input u, and gains k_1, k_2. Simulation time $250s$, fault injection at $t_f = 30s$. On the right, a zoom from time instant $t = 145s$ to $t = 150s$.

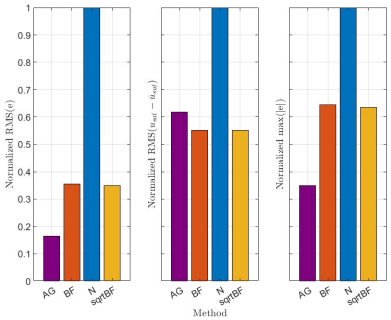

(B) Metrics in faulty case: Normalized RMS(e), normalized RMS($u_{sat} - \bar{u}_{sat}$) and normalized MAX($|e|$).

FIGURE 5.10: Fault 1 - Simulation results and metrics.

Parameters	Observations
$K = 8, \epsilon = 39$	• k_1 and k_2 are adapted; • The average value of k_1 and k_2 are decreased with respect to the standard ST-SMC values ($k_1 = 25.2228$, $k_2 = 160$); • The control input is always between $[-1, 1]m$, except for the beginning; • The system is able to track the reference; • The $\|e\|$ crosses the tolerance $[-0.005, 0.005]rad$ because the controller is not strong enough, the gains are too low.
$K = 10, \epsilon = 26.5$	• k_1 and k_2 are adapted; • The average value of k_1 and k_2 are decreased with respect to the standard ST-SMC values ($k_1 = 25.2228$, $k_2 = 160$); • The control input is always between $[-1, 1]m$, except for the beginning and around time instant $150s$; • The system is able to track the reference; • The $\|e\|$ crosses the tolerance $[-0.005, 0.005]rad$ because the controller is not strong enough, the gains are too low.
$K = 12, \epsilon = 29.5$	• k_1 and k_2 are adapted; • The average value of k_1 is decreased with respect to the standard ST-SMC values ($k_1 = 25.2228$) and the average value of k_2 is slightly increased with respect to the standard ST-SMC values ($k_2 = 160$); • The control input is always between $[-1, 1]m$, except for the beginning and around $150s$; • The system is able to track the reference; • The $\|e\|$ almost never crosses the tolerance $[-0.005, 0.005]rad$.
$K = 16, \epsilon = 19$	• k_1 and k_2 are adapted; • The average value of k_1 is decreased with respect to the standard ST-SMC values ($k_1 = 25.2228$) and the average value of k_2 is increased with respect to the standard ST-SMC values ($k_2 = 160$); • The control input is always between $[-1, 1]m$, except for the beginning and around time instant $150s$; • The system is able to track the reference; • The $\|e\|$ almost never crosses the tolerance $[-0.005, 0.005]rad$.
$K = 20, \epsilon = 18$	• k_1 and k_2 are adapted; • The average value of k_1 is decreased with respect to the standard ST-SMC values ($k_1 = 25.2228$) and the average value of k_2 is increased with respect to the standard ST-SMC values ($k_2 = 160$); • The control input is always between $[-1, 1]m$, except for the beginning and around time instant $150s$, furthermore there are more oscillations; • The system is able to track the reference; • The $\|e\|$ never crosses the tolerance $[-0.005, 0.005]rad$, except for the beginning.

TABLE 5.1: Summary of controller parameters and observations for BF method in nominal case.

Parameters	Observations
$K = 8$, $\epsilon = 22$	• k_1 and k_2 are adapted; • The average value of k_1 and k_2 are decreased with respect to the standard ST-SMC values ($k_1 = 25.2228$, $k_2 = 160$); • The control input is always between $[-1, 1]m$, except for the beginning; • The system is able to track the reference; • The $\|e\|$ crosses the tolerance $[-0.005, 0.005]rad$ because the controller is not strong enough, the gains are too low.
$K = 10$, $\epsilon = 15.5$	• k_1 and k_2 are adapted; • The average value of k_1 and k_2 are decreased with respect to the standard ST-SMC values ($k_1 = 25.2228$, $k_2 = 160$); • The control input is always between $[-1, 1]m$, except for the beginning and around time instant $150s$; • The system is able to track the reference; • The $\|e\|$ crosses the tolerance $[-0.005, 0.005]rad$ because the controller is not strong enough, the gains are too low.
$K = 12$, $\epsilon = 22$	• k_1 and k_2 are adapted; • The average value of k_1 and k_2 are decreased with respect to the standard ST-SMC values ($k_1 = 25.2228$, $k_2 = 160$); • The control input is always between $[-1, 1]m$, except for the beginning and around $150s$; • The system is able to track the reference; • The $\|e\|$ almost never crosses the tolerance $[-0.005, 0.005]rad$.
$K = 16$, $\epsilon = 12$	• k_1 and k_2 are adapted; • The average value of k_1 is decreased with respect to the standard ST-SMC values ($k_1 = 25.2228$) and the average value of k_2 is increased with respect to the standard ST-SMC values ($k_2 = 160$); • The control input is always between $[-1, 1]m$, except for the beginning and around time instant $150s$; • The system is able to track the reference; • The $\|e\|$ almost never crosses the tolerance $[-0.005, 0.005]rad$, except for the beginning.
$K = 20$, $\epsilon = 10$	• k_1 and k_2 are adapted; • The average value of k_1 is decreased with respect to the standard ST-SMC values ($k_1 = 25.2228$) and the average value of k_2 is increased with respect to the standard ST-SMC values ($k_2 = 160$); • The control input is always between $[-1, 1]m$, except for the beginning and around time instant $150s$, furthermore there are more oscillations; • The system is able to track the reference; • The $\|e\|$ never crosses the tolerance $[-0.005, 0.005]rad$, except for the beginning.

TABLE 5.2: Summary of controller parameters and observations for sqrtBF method in nominal case.

Number fault	Name	Value
1	Piston Pressure p_p Sensor - Bias	5.0×10^6 Pa
2	Piston Pressure p_p Sensor - Gain	1.125
3	Piston Pressure p_p Sensor - Drift	1.0×10^5 Pa
4	Piston Pressure p_p Sensor - Precision, Noise Increase	12.5% of nominal var
5	Piston Pressure p_p Sensor - Activation fault 4	1
6	Piston Pressure p_p Sensor - Stuck	1.25×10^7 Pa
7	Piston Pressure p_p Sensor - Activation fault 6	1
8	Rod Pressure p_r Sensor - Bias	1.5×10^7 Pa
9	Rod Pressure p_r Sensor - Gain	1.0
10	Rod Pressure p_r Sensor - Drift	7.5×10^4 Pa
11	Rod Pressure p_r Sensor - Precision, Noise Increase	12.5% of nominal var
12	Rod Pressure p_r Sensor - Activation fault 11	1
13	Rod Pressure p_r Sensor - Stuck	1.25×10^7 Pa
14	Rod Pressure p_r Sensor - Activation fault 13	1
15	Cylinder Position x_c Sensor - Bias	-0.2
16	Cylinder Position x_c Sensor - Gain	0.875
17	Cylinder Position x_c Sensor - Drift	-0.005
18	Cylinder Position x_c Sensor - Precision, Noise Increase	12.5% of nominal var
19	Cylinder Position x_c Sensor - Activation fault 18	1
20	Cylinder Position x_c Sensor - Stuck	0.375
21	Cylinder Position x_c Sensor - Activation fault 20	1
22	Pitch Angle β Sensor - Bias	-0.25
23	Pitch Angle β Sensor - Gain	0.875
24	Pitch Angle β Sensor - Drift	-0.005
25	Pitch Angle β Sensor - Precision, Noise Increase	10% of nominal var
26	Pitch Angle β Sensor - Activation fault 25	1
27	Pitch Angle β Sensor - Stuck	0.15
28	Pitch Angle β Sensor - Activation fault 27	1
29	Friction for x_c - Viscous Friction	100
30	Friction for x_c - Coulomb Friction	125
31	Friction for β - Viscous Friction	100
32	Friction for β - Coulomb Friction	100
33	Bulk Modulus	-1.0625
34	Leakages - $Q_{le,p}$	2.0×10^{-10} m^3/s
35	Leakages - $Q_{le,r}$	5.0×10^{-10} m^3/s
36	Leakages - Q_{li}	3.0×10^{-10} m^3/s
37	Valve Flows - Q_{cv}	12.5×10^{-10} m^3/s
38	Valve Flows - Q_p	1.2×10^{-6} m^3/s
39	Valve Flows - Q_{rv}	1.8×10^{-6} m^3/s
40	Valve - Increased csi	6.25
41	Valve - Decreased w_0	312.5 rad/s
42	Supply Pressure p_s Sensor - Bias	1.25×10^7 Pa
43	Supply Pressure p_s Sensor - Drift	4.0×10^4 Pa

TABLE 5.4: Faults values for various sensors and components in faulty scenarios.

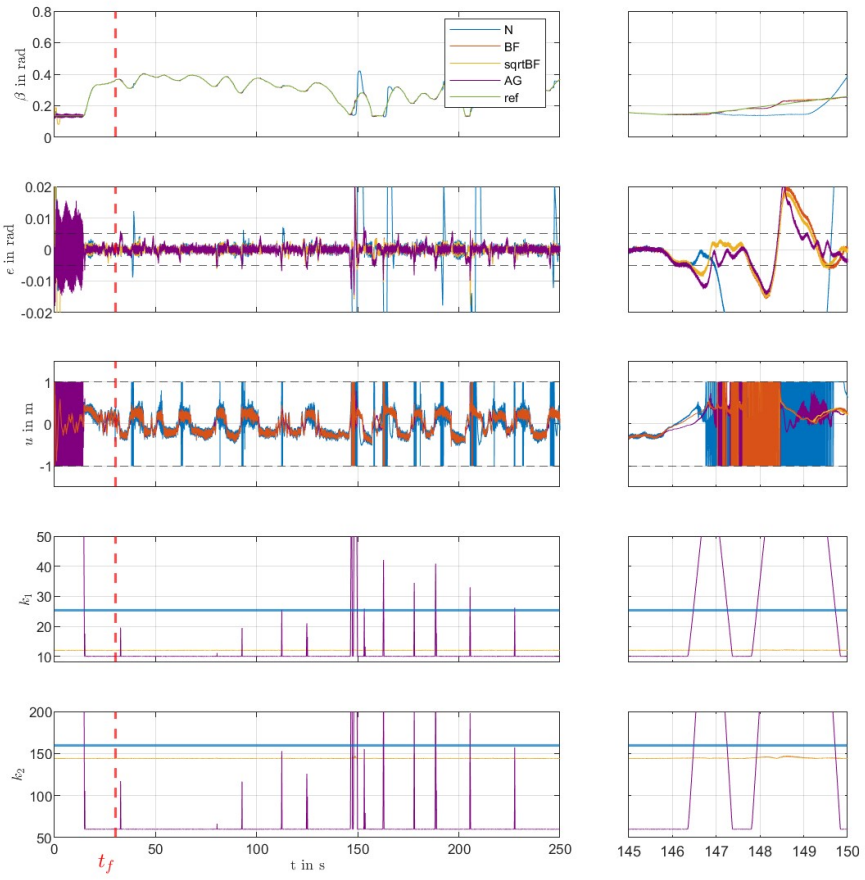

(A) Plot of the output β, error e, input u, and gains k_1, k_2. Simulation time $250s$, fault injection at $t_f = 30s$. On the right, a zoom from time instant $t = 145s$ to $t = 150s$.

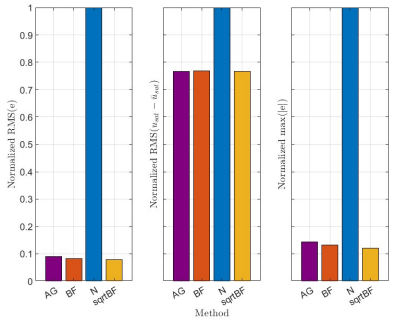

(B) Metrics in faulty case: Normalized RMS(e), normalized RMS($u_{sat} - \bar{u}_{sat}$) and normalized MAX($|e|$).

FIGURE 5.11: Fault 2 - Simulation results and metrics.

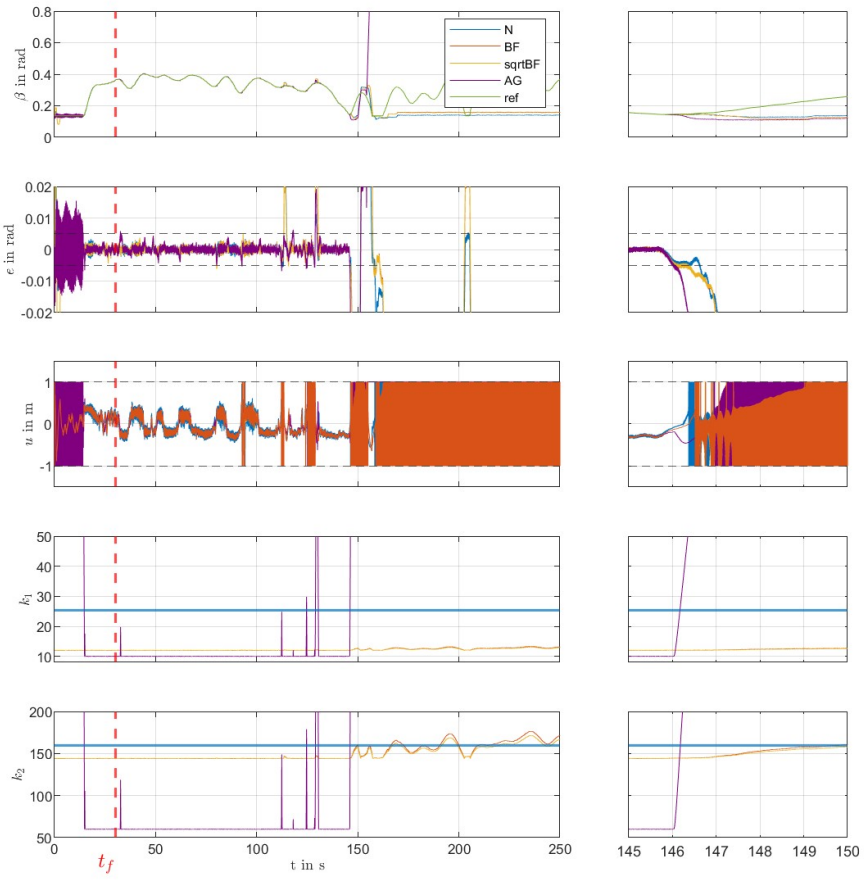

(A) Plot of the output β, error e, input u, and gains k_1, k_2. Simulation time $250s$, fault injection at $t_f = 30s$. On the right, a zoom from time instant $t = 145s$ to $t = 150s$.

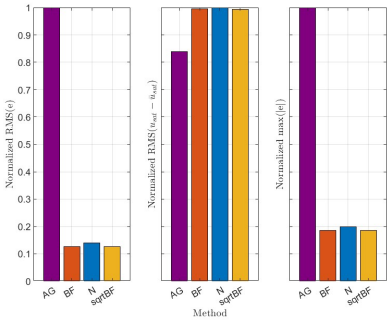

(B) Metrics in faulty case: Normalized RMS(e), normalized RMS($u_{sat} - \bar{u}_{sat}$) and normalized MAX($|e|$).

FIGURE 5.12: Fault 3 - Simulation results and metrics.

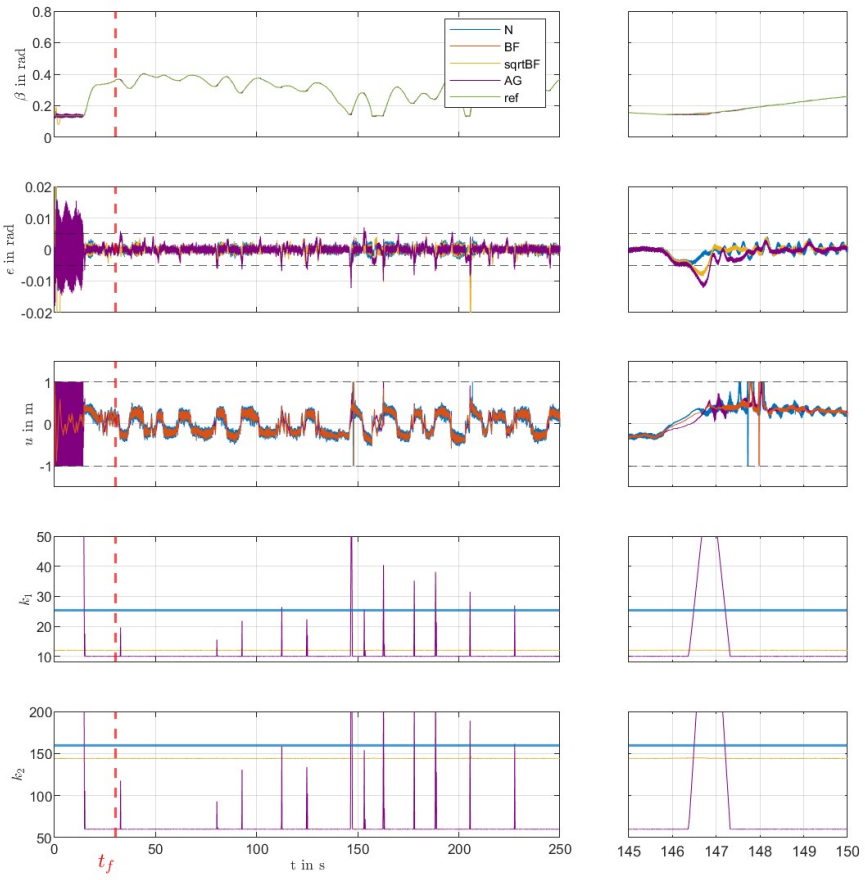

(A) Plot of the output β, error e, input u, and gains k_1, k_2. Simulation time $250s$, fault injection at $t_f = 30s$. On the right, a zoom from time instant $t = 145s$ to $t = 150s$.

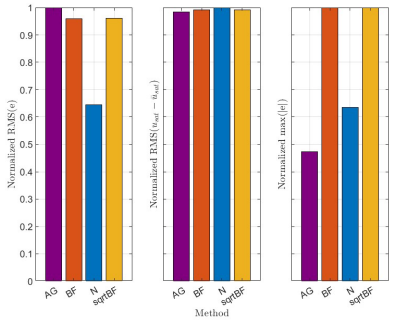

(B) Metrics in faulty case: Normalized RMS(e), normalized RMS($u_{sat} - \bar{u}_{sat}$) and normalized MAX($|e|$).

FIGURE 5.13: Fault 4 - Simulation results and metrics.

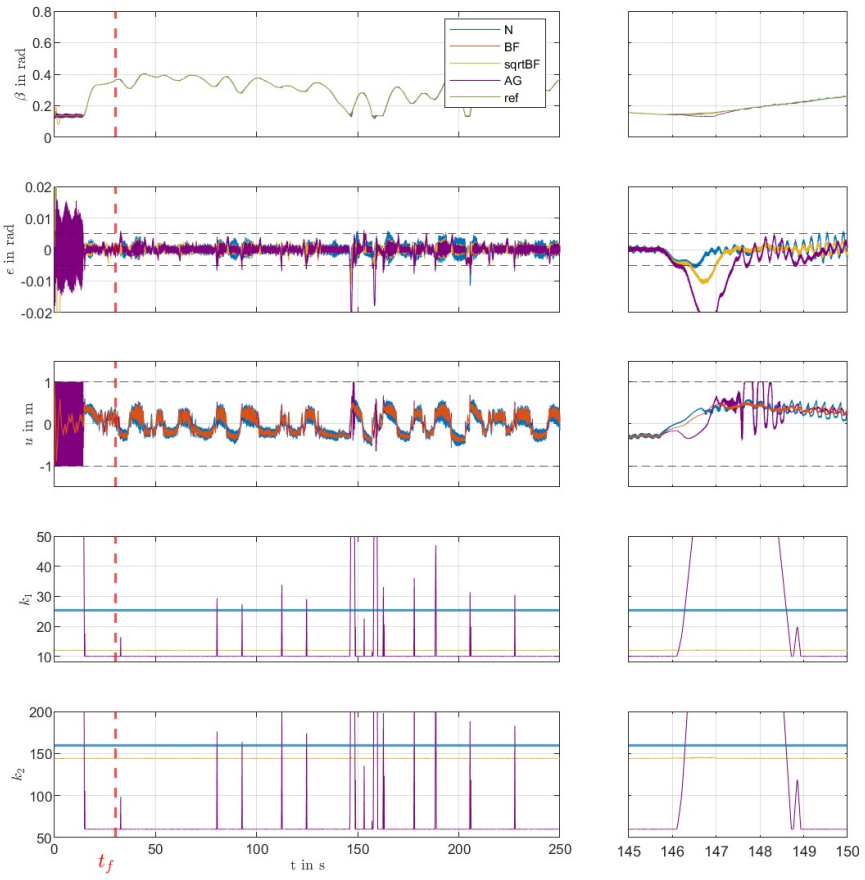

(A) Plot of the output β, error e, input u, and gains k_1, k_2. Simulation time $250s$, fault injection at $t_f = 30s$. On the right, a zoom from time instant $t = 145s$ to $t = 150s$.

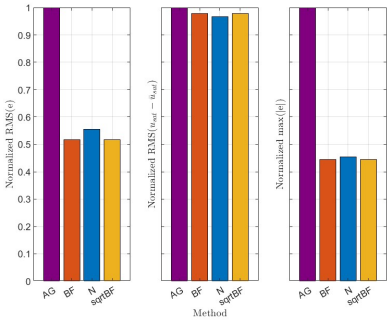

(B) Metrics in faulty case: Normalized RMS(e), normalized RMS($u_{sat} - \bar{u}_{sat}$) and normalized MAX($|e|$).

FIGURE 5.14: Fault 6 - Simulation results and metrics.

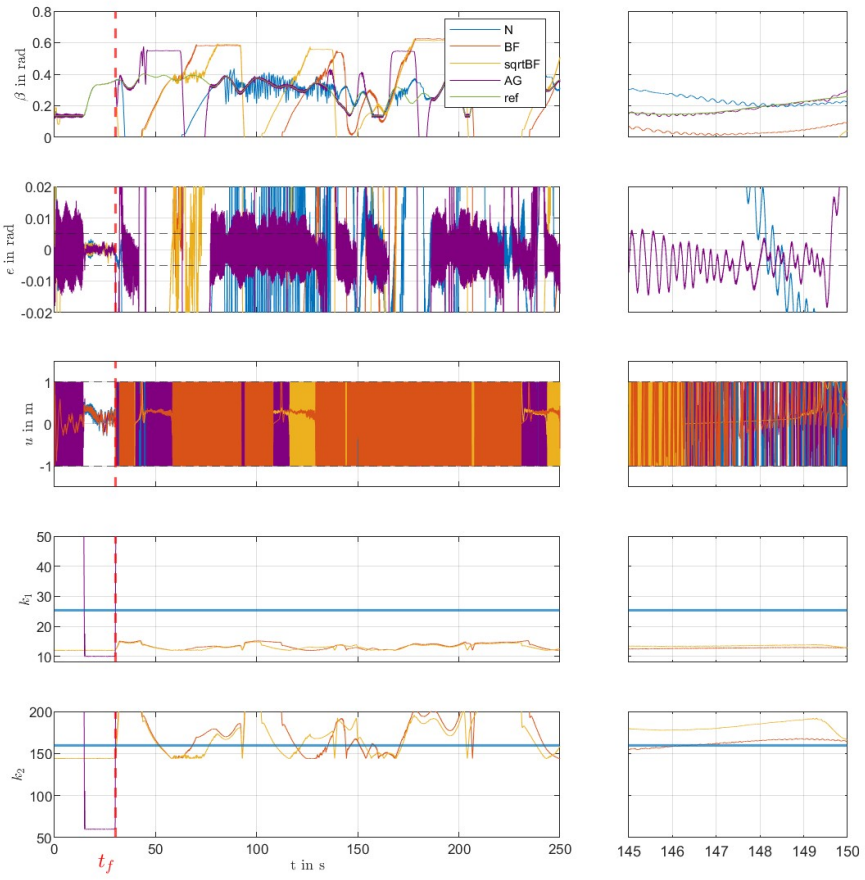

(A) Plot of the output β, error e, input u, and gains k_1, k_2. Simulation time $250s$, fault injection at $t_f = 30s$. On the right, a zoom from time instant $t = 145s$ to $t = 150s$.

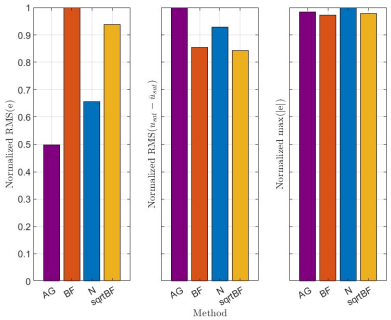

(B) Metrics in faulty case: Normalized RMS(e), normalized RMS($u_{sat} - \bar{u}_{sat}$) and normalized MAX($|e|$).

FIGURE 5.15: Fault 8 - Simulation results and metrics.

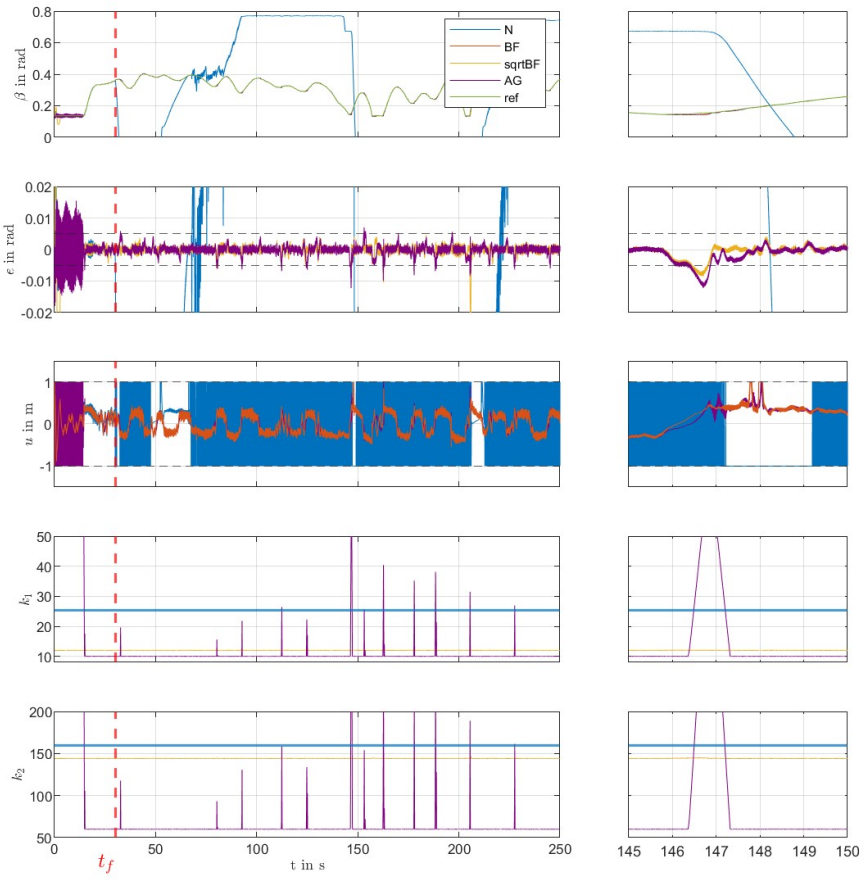

(A) Plot of the output β, error e, input u, and gains k_1, k_2. Simulation time $250s$, fault injection at $t_f = 30s$. On the right, a zoom from time instant $t = 145s$ to $t = 150s$.

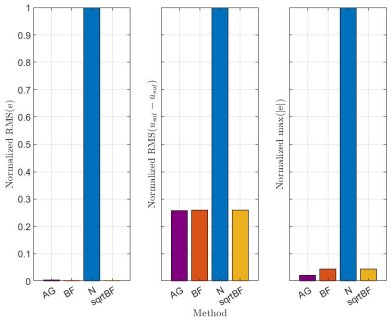

(B) Metrics in faulty case: Normalized RMS(e), normalized RMS($u_{sat} - \bar{u}_{sat}$) and normalized MAX($|e|$).

FIGURE 5.16: Fault 9 - Simulation results and metrics.

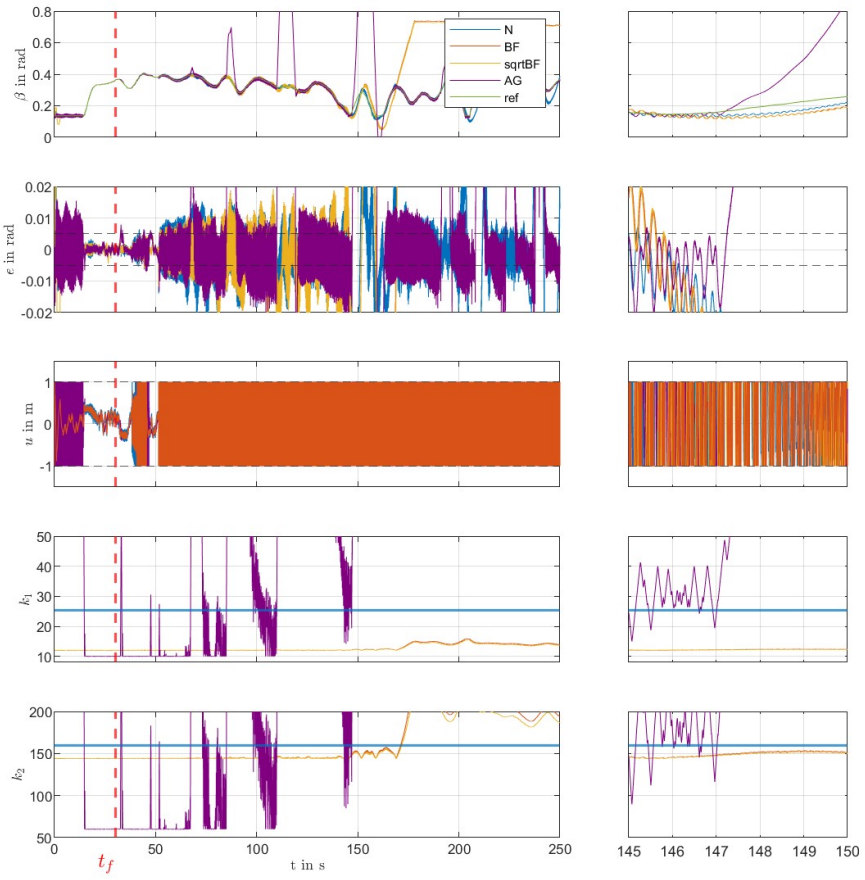

(A) Plot of the output β, error e, input u, and gains k_1, k_2. Simulation time $250s$, fault injection at $t_f = 30s$. On the right, a zoom from time instant $t = 145s$ to $t = 150s$.

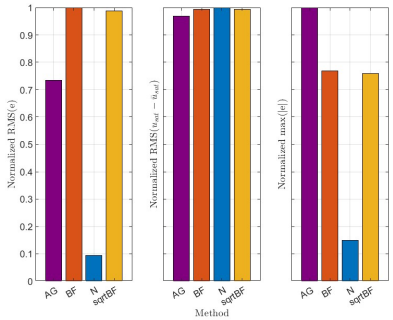

(B) Metrics in faulty case: Normalized RMS(e), normalized RMS($u_{sat} - \bar{u}_{sat}$) and normalized MAX($|e|$).

FIGURE 5.17: Fault 10 - Simulation results and metrics.

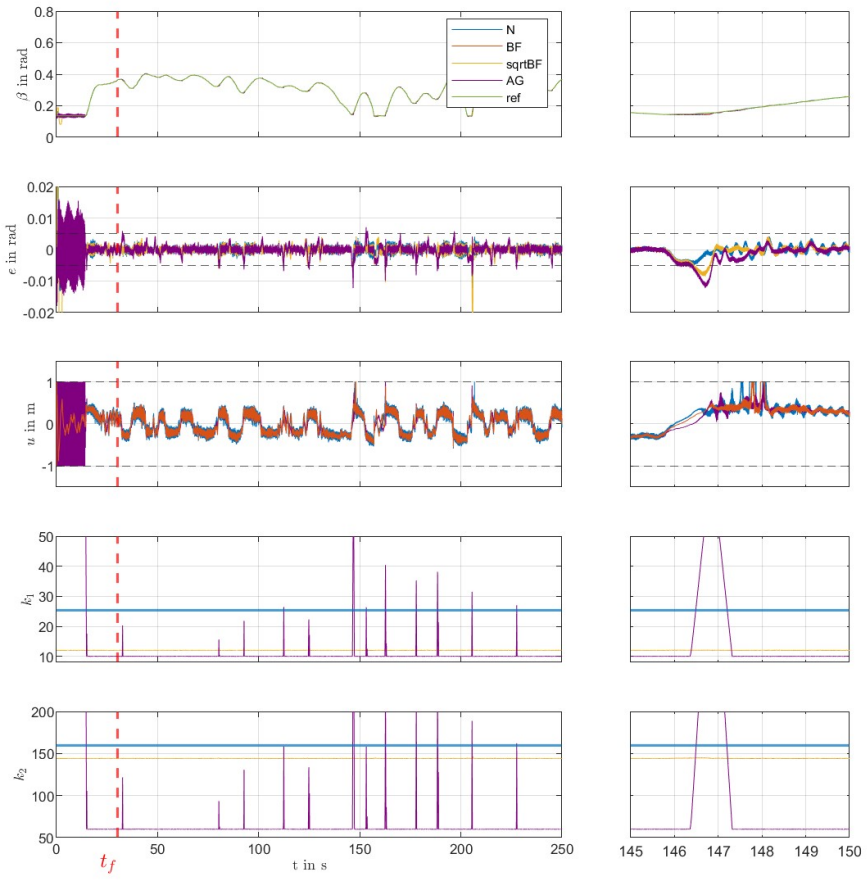

(A) Plot of the output β, error e, input u, and gains k_1, k_2. Simulation time $250s$, fault injection at $t_f = 30s$. On the right, a zoom from time instant $t = 145s$ to $t = 150s$.

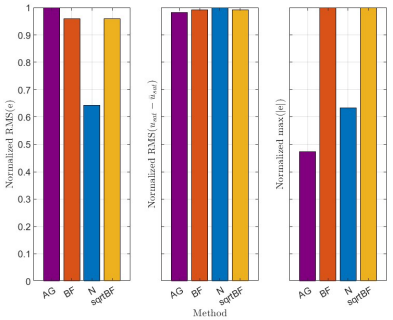

(B) Metrics in faulty case: Normalized RMS(e), normalized RMS($u_{sat} - \bar{u}_{sat}$) and normalized MAX($|e|$).

FIGURE 5.18: Fault 11 - Simulation results and metrics.

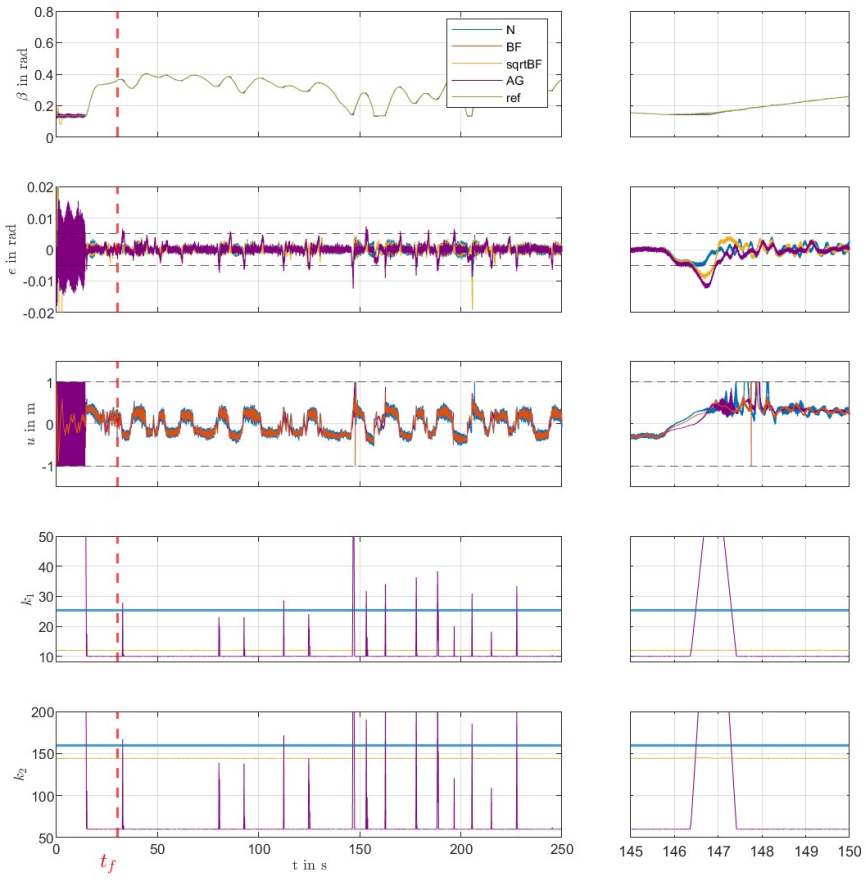

(A) Plot of the output β, error e, input u, and gains k_1, k_2. Simulation time $250s$, fault injection at $t_f = 30s$. On the right, a zoom from time instant $t = 145s$ to $t = 150s$.

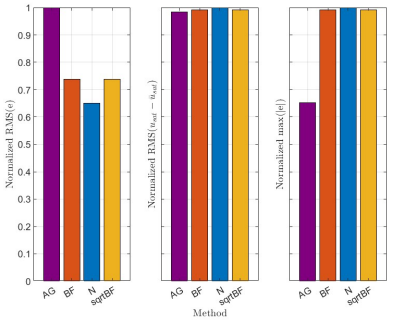

(B) Metrics in faulty case: Normalized RMS(e), normalized RMS($u_{sat} - \bar{u}_{sat}$) and normalized MAX($|e|$).

FIGURE 5.19: Fault 13 - Simulation results and metrics.

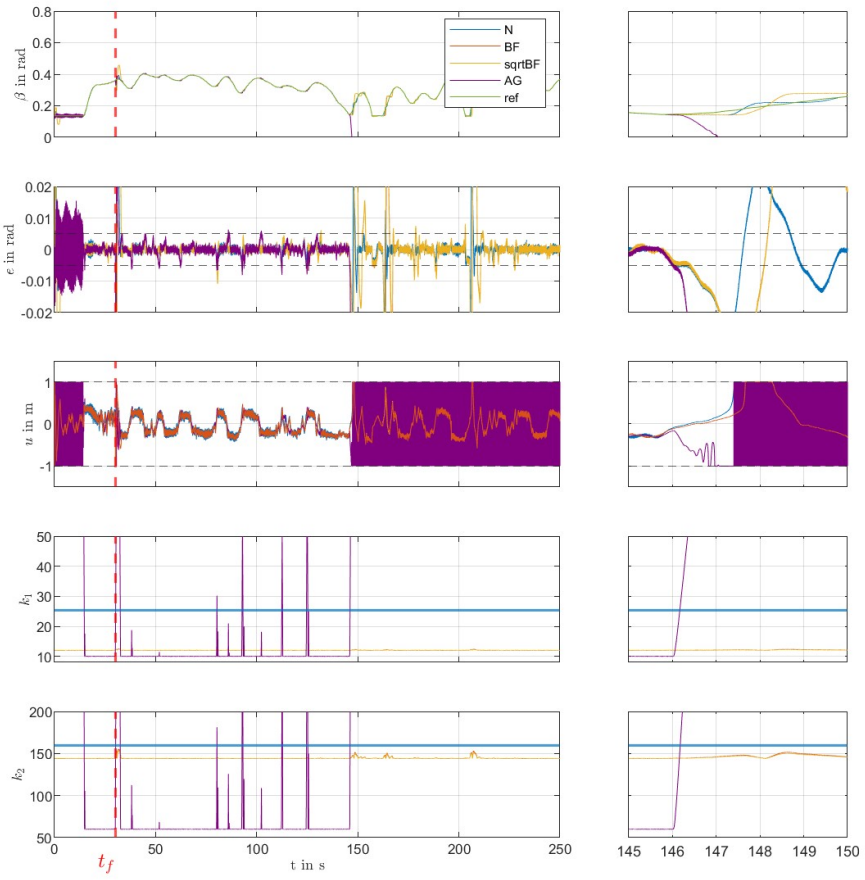

(A) Plot of the output β, error e, input u, and gains k_1, k_2. Simulation time $250s$, fault injection at $t_f = 30s$. On the right, a zoom from time instant $t = 145s$ to $t = 150s$.

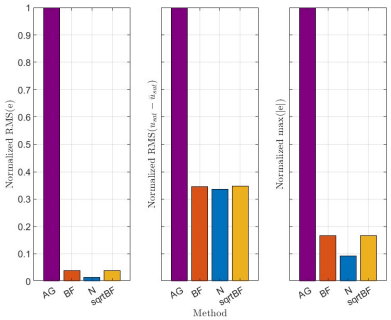

(B) Metrics in faulty case: Normalized RMS(e), normalized RMS($u_{sat} - \bar{u}_{sat}$) and normalized MAX($|e|$).

FIGURE 5.20: Fault 15 - Simulation results and metrics.

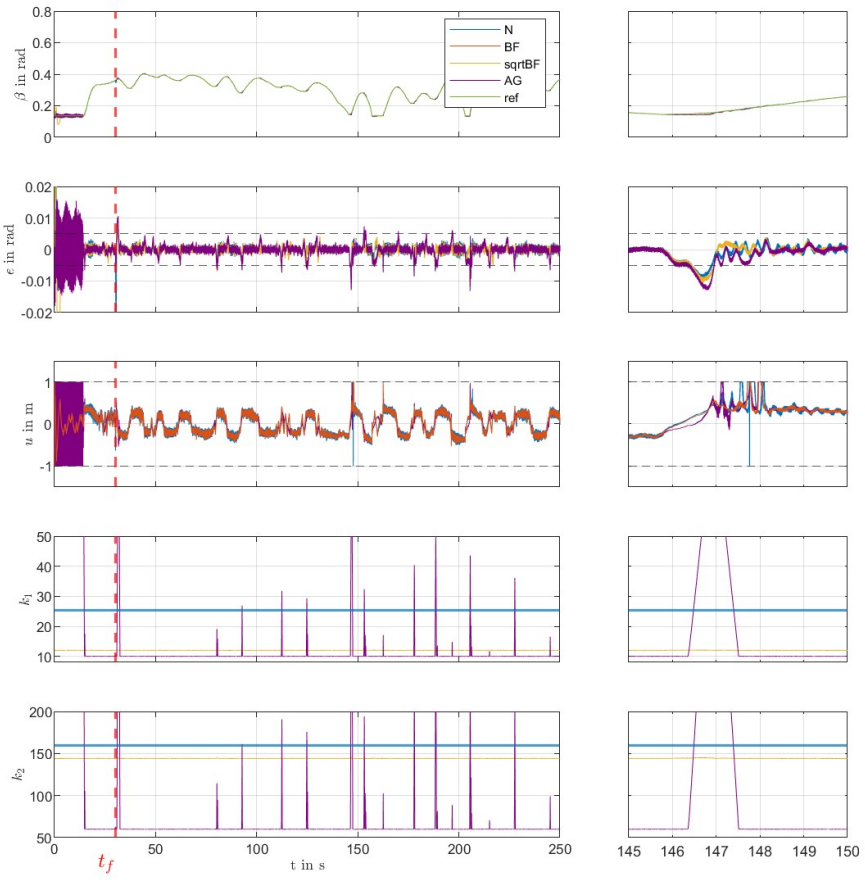

(A) Plot of the output β, error e, input u, and gains k_1, k_2. Simulation time $250s$, fault injection at $t_f = 30s$. On the right, a zoom from time instant $t = 145s$ to $t = 150s$.

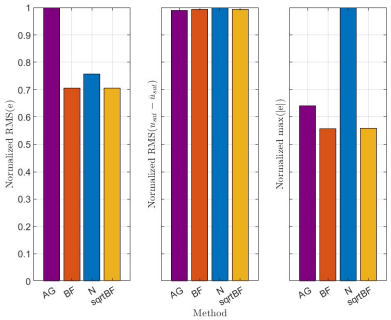

(B) Metrics in faulty case: Normalized RMS(e), normalized RMS($u_{sat} - \bar{u}_{sat}$) and normalized MAX($|e|$).

FIGURE 5.21: Fault 16 - Simulation results and metrics.

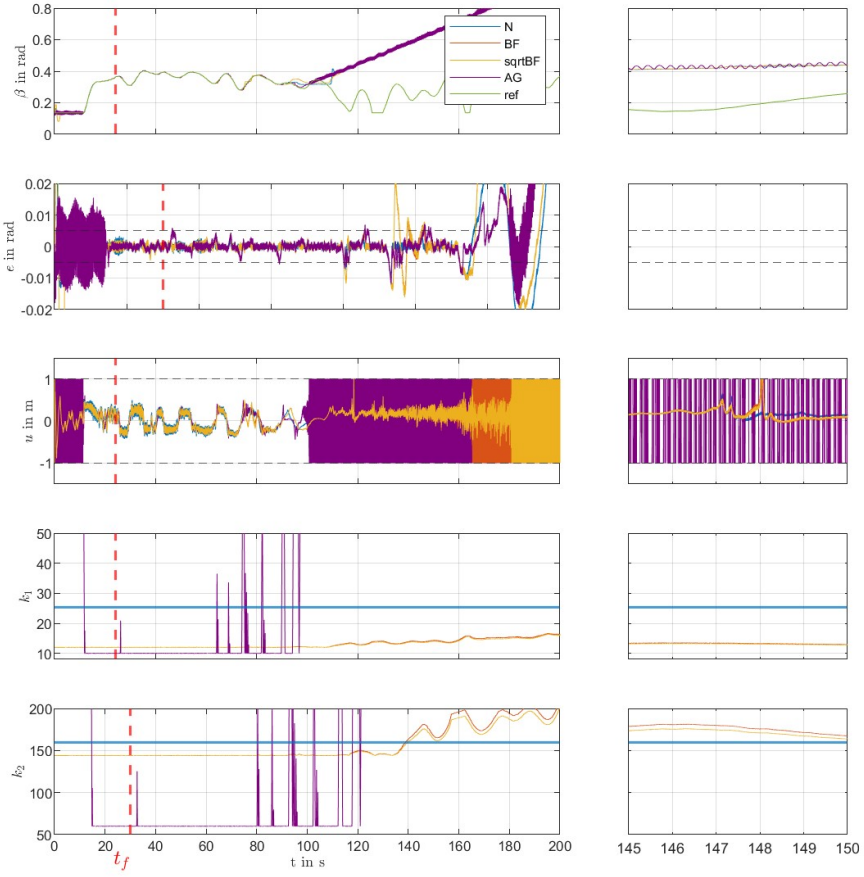

(A) Plot of the output β, error e, input u, and gains k_1, k_2. Simulation time $250s$, fault injection at $t_f = 30s$. On the right, a zoom from time instant $t = 145s$ to $t = 150s$.

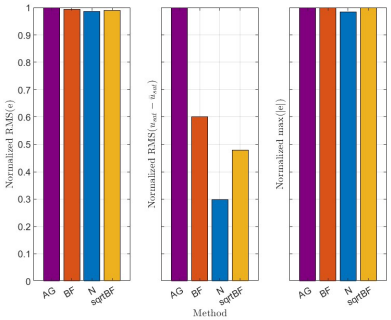

(B) Metrics in faulty case: Normalized RMS(e), normalized RMS($u_{sat} - \bar{u}_{sat}$) and normalized MAX($|e|$).

FIGURE 5.22: Fault 17 - Simulation results and metrics.

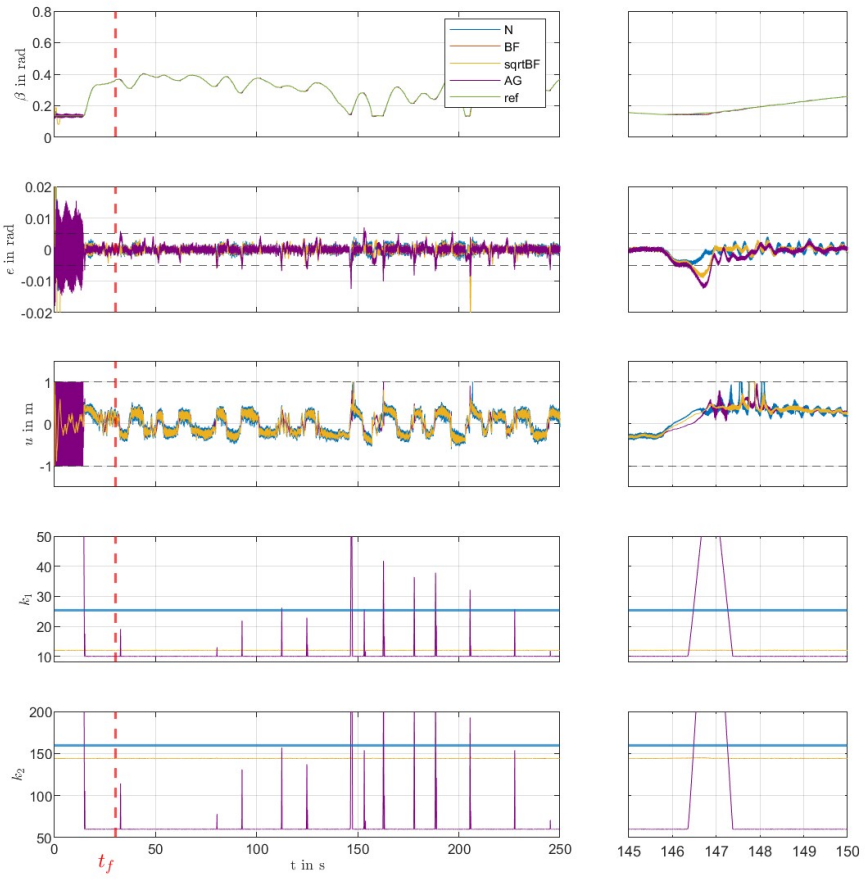

(A) Plot of the output β, error e, input u, and gains k_1, k_2. Simulation time $250s$, fault injection at $t_f = 30s$. On the right, a zoom from time instant $t = 145s$ to $t = 150s$.

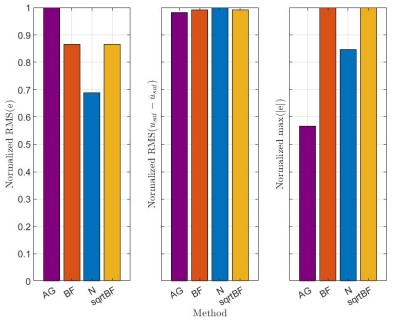

(B) Metrics in faulty case: Normalized RMS(e), normalized RMS($u_{sat} - \bar{u}_{sat}$) and normalized MAX($|e|$).

FIGURE 5.23: Fault 18 - Simulation results and metrics.

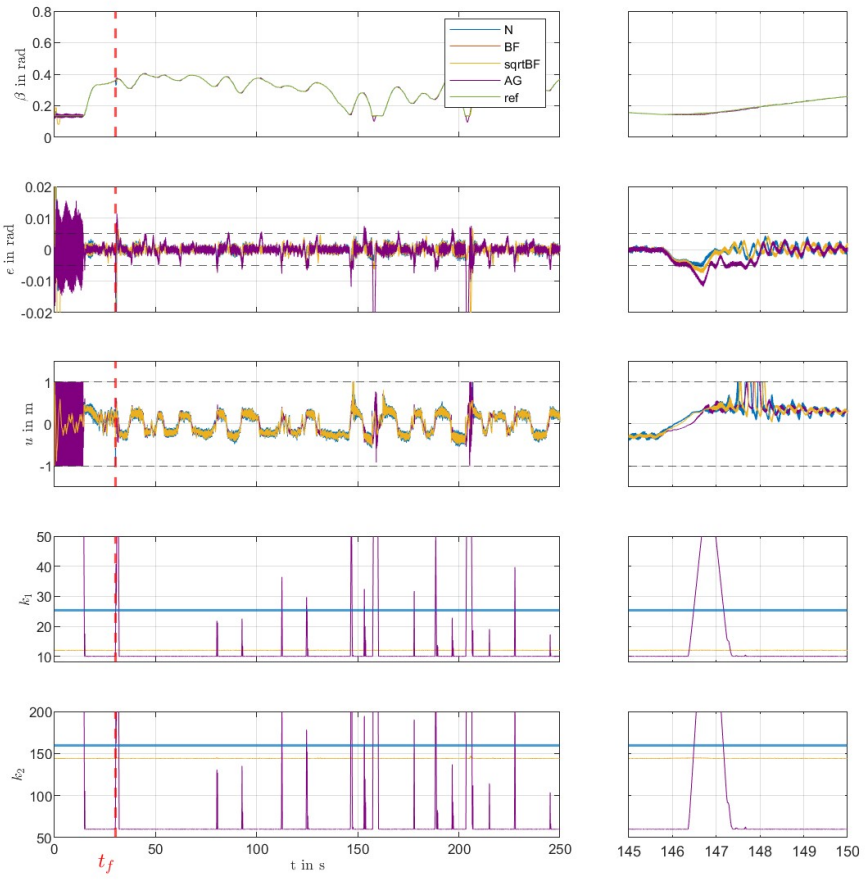

(A) Plot of the output β, error e, input u, and gains k_1, k_2. Simulation time $250s$, fault injection at $t_f = 30s$. On the right, a zoom from time instant $t = 145s$ to $t = 150s$.

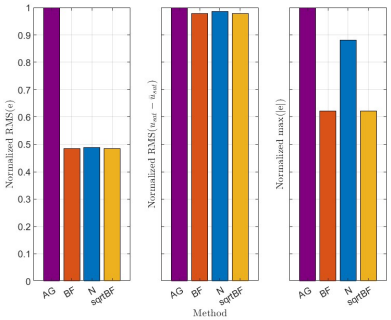

(B) Metrics in faulty case: Normalized RMS(e), normalized RMS($u_{sat} - \bar{u}_{sat}$) and normalized MAX($|e|$).

FIGURE 5.24: Fault 20 - Simulation results and metrics.

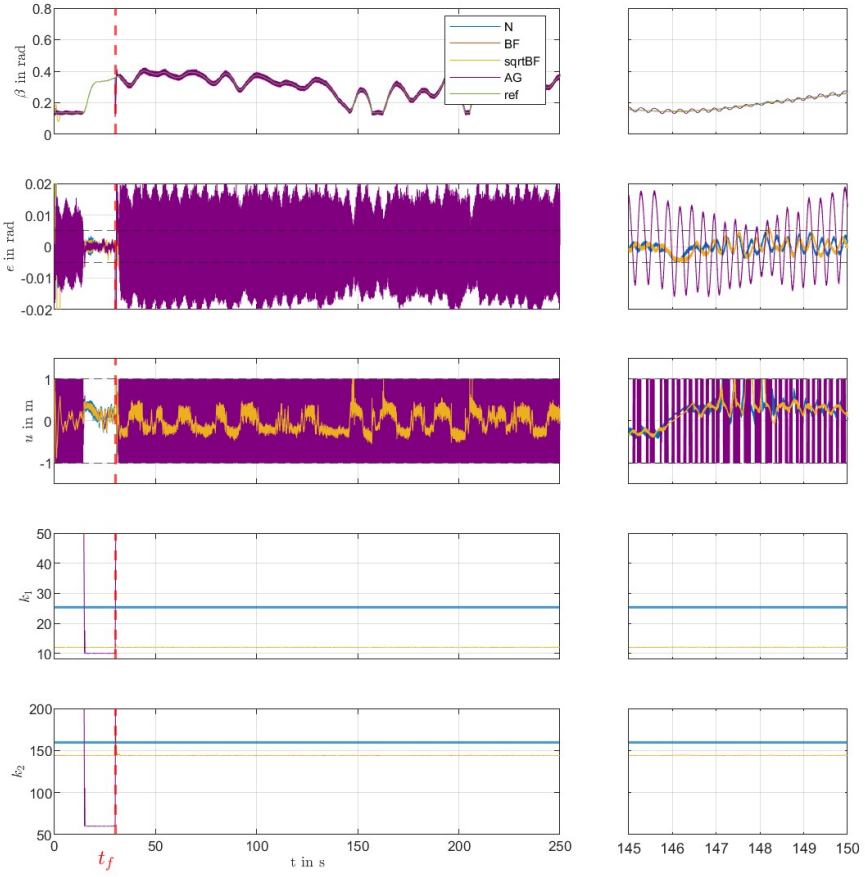

(A) Plot of the output β, error e, input u, and gains k_1, k_2. Simulation time $250s$, fault injection at $t_f = 30s$. On the right, a zoom from time instant $t = 145s$ to $t = 150s$.

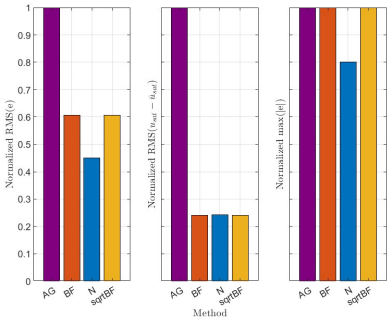

(B) Metrics in faulty case: Normalized RMS(e), normalized RMS($u_{sat} - \bar{u}_{sat}$) and normalized MAX($|e|$).

FIGURE 5.25: Fault 22 - Simulation results and metrics.

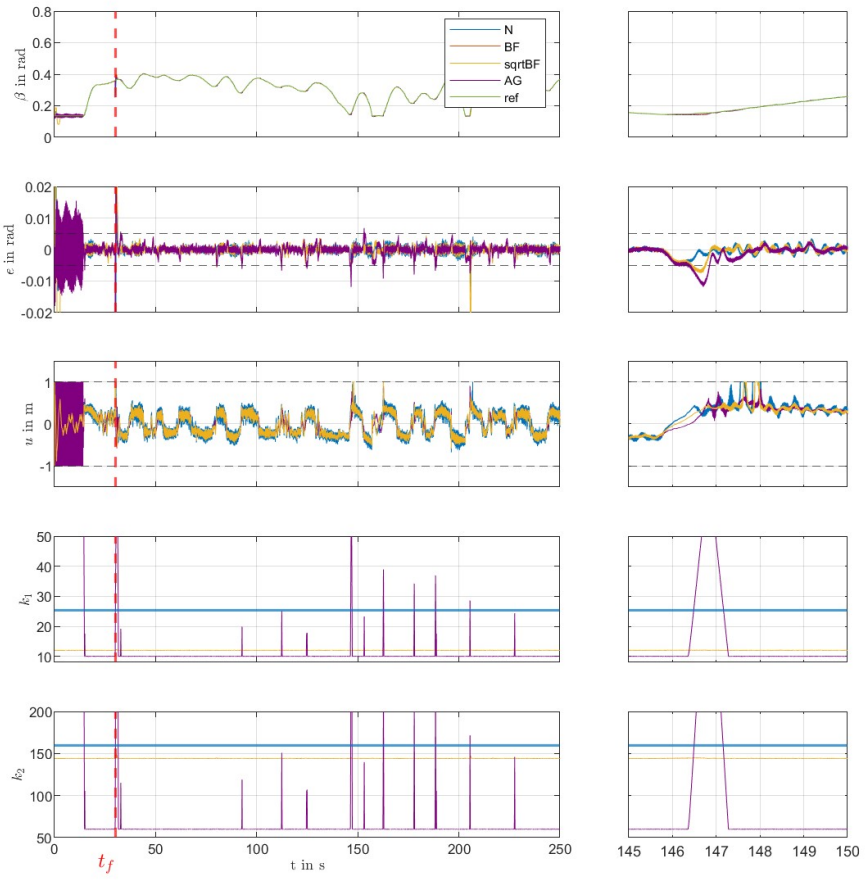

(A) Plot of the output β, error e, input u, and gains k_1, k_2. Simulation time $250s$, fault injection at $t_f = 30s$. On the right, a zoom from time instant $t = 145s$ to $t = 150s$.

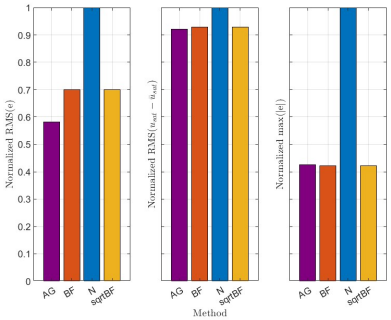

(B) Metrics in faulty case: Normalized RMS(e), normalized RMS($u_{sat} - \bar{u}_{sat}$) and normalized MAX($|e|$).

FIGURE 5.26: Fault 23 - Simulation results and metrics.

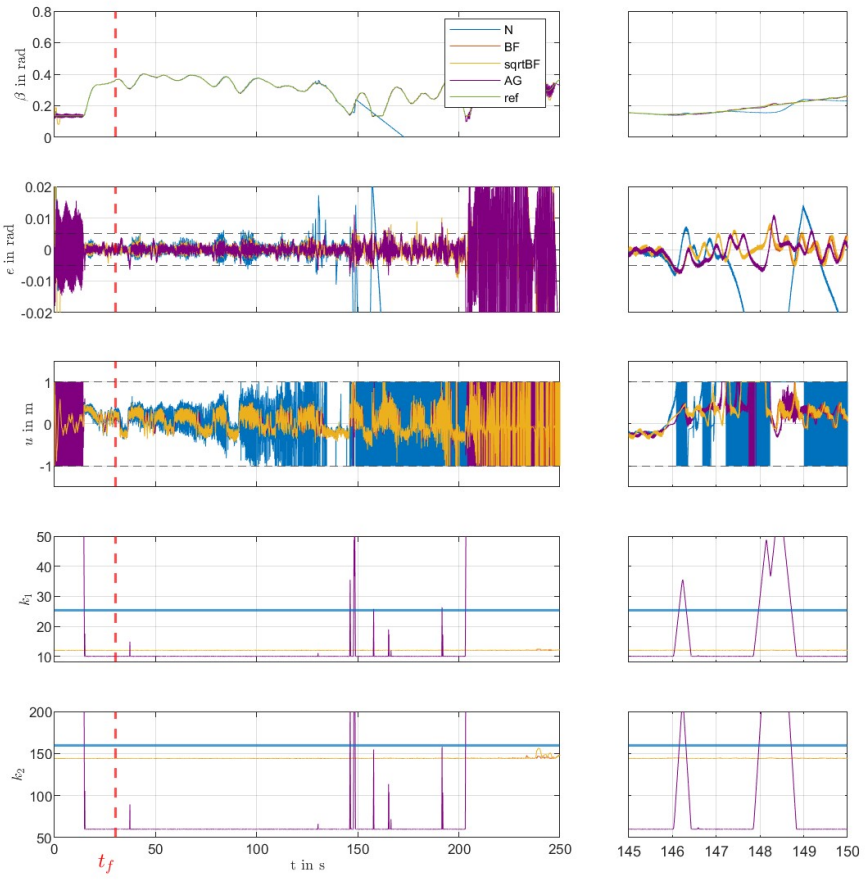

(A) Plot of the output β, error e, input u, and gains k_1, k_2. Simulation time $250s$, fault injection at $t_f = 30s$. On the right, a zoom from time instant $t = 145s$ to $t = 150s$.

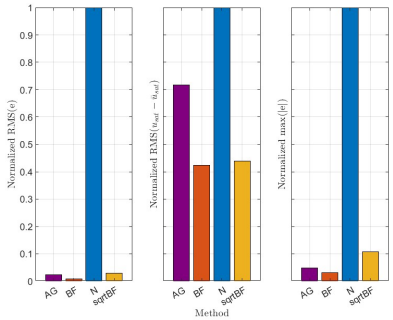

(B) Metrics in faulty case: Normalized RMS(e), normalized RMS($u_{sat} - \bar{u}_{sat}$) and normalized MAX($|e|$).

FIGURE 5.27: Fault 24 - Simulation results and metrics.

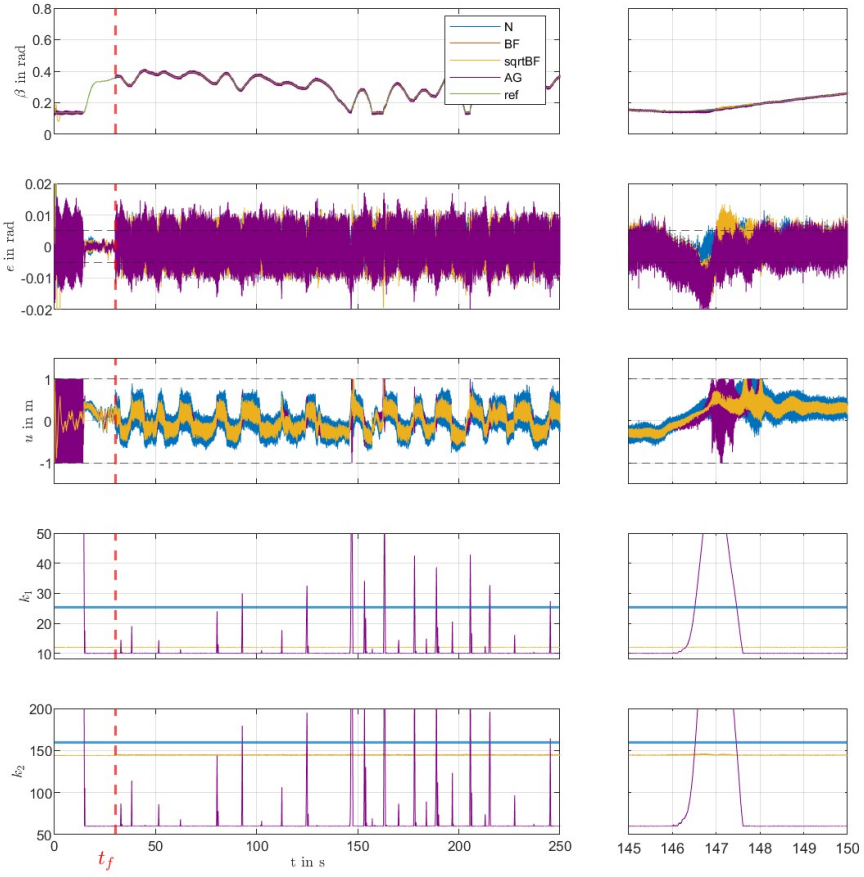

(A) Plot of the output β, error e, input u, and gains k_1, k_2. Simulation time $250s$, fault injection at $t_f = 30s$. On the right, a zoom from time instant $t = 145s$ to $t = 150s$.

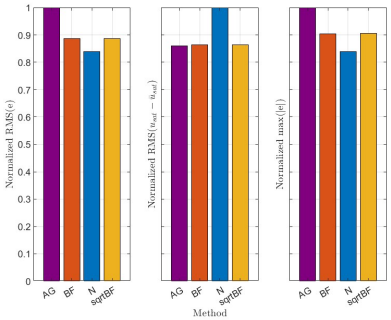

(B) Metrics in faulty case: Normalized RMS(e), normalized RMS($u_{sat} - \bar{u}_{sat}$) and normalized MAX($|e|$).

FIGURE 5.28: Fault 25 - Simulation results and metrics.

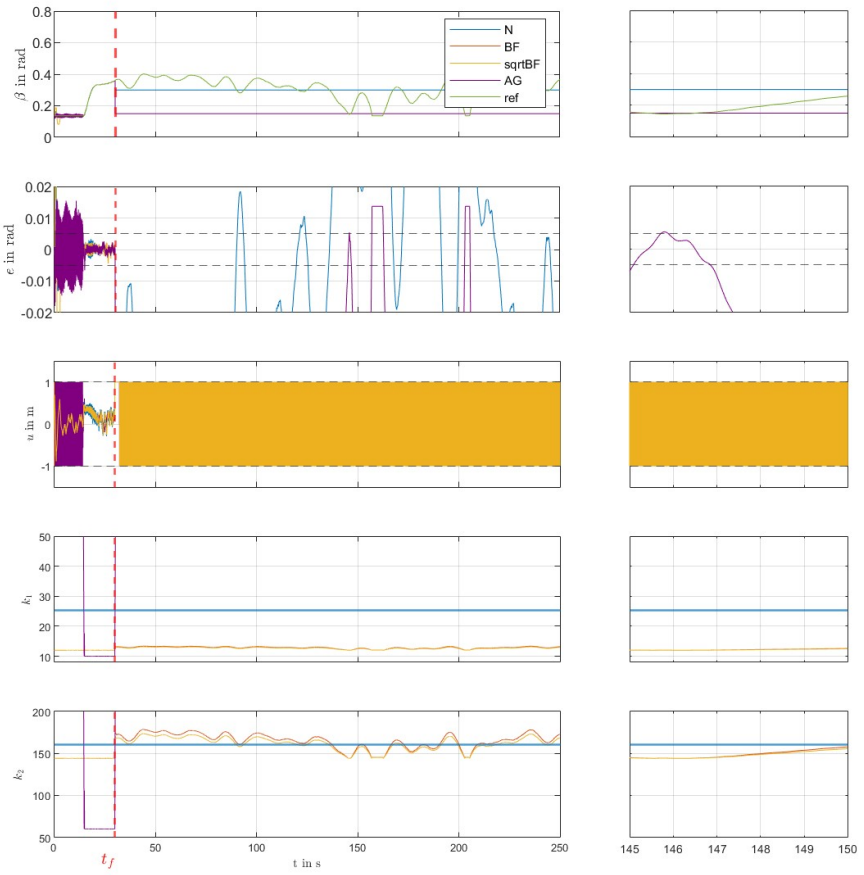

(A) Plot of the output β, error e, input u, and gains k_1, k_2. Simulation time $250s$, fault injection at $t_f = 30s$. On the right, a zoom from time instant $t = 145s$ to $t = 150s$.

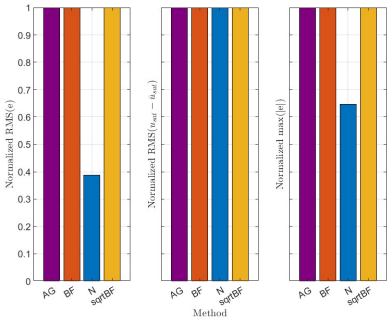

(B) Metrics in faulty case: Normalized RMS(e), normalized RMS($u_{sat} - \bar{u}_{sat}$) and normalized MAX($|e|$).

FIGURE 5.29: Fault 27 - Simulation results and metrics.

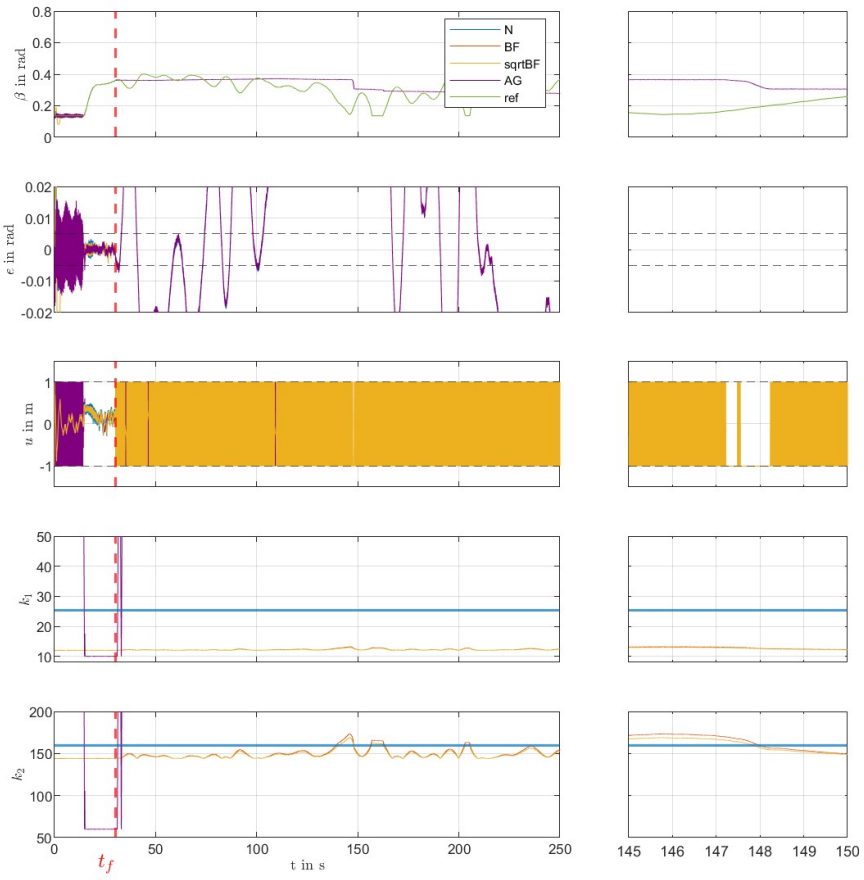

(A) Plot of the output β, error e, input u, and gains k_1, k_2. Simulation time $250s$, fault injection at $t_f = 30s$. On the right, a zoom from time instant $t = 145s$ to $t = 150s$.

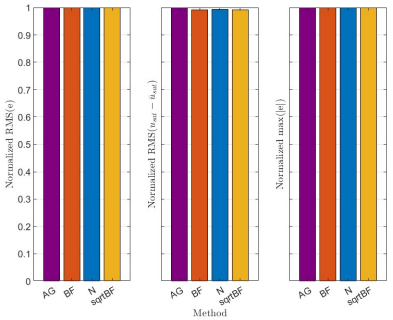

(B) Metrics in faulty case: Normalized RMS(e), normalized RMS($u_{sat} - \bar{u}_{sat}$) and normalized MAX($|e|$).

FIGURE 5.30: Fault 29 - Simulation results and metrics.

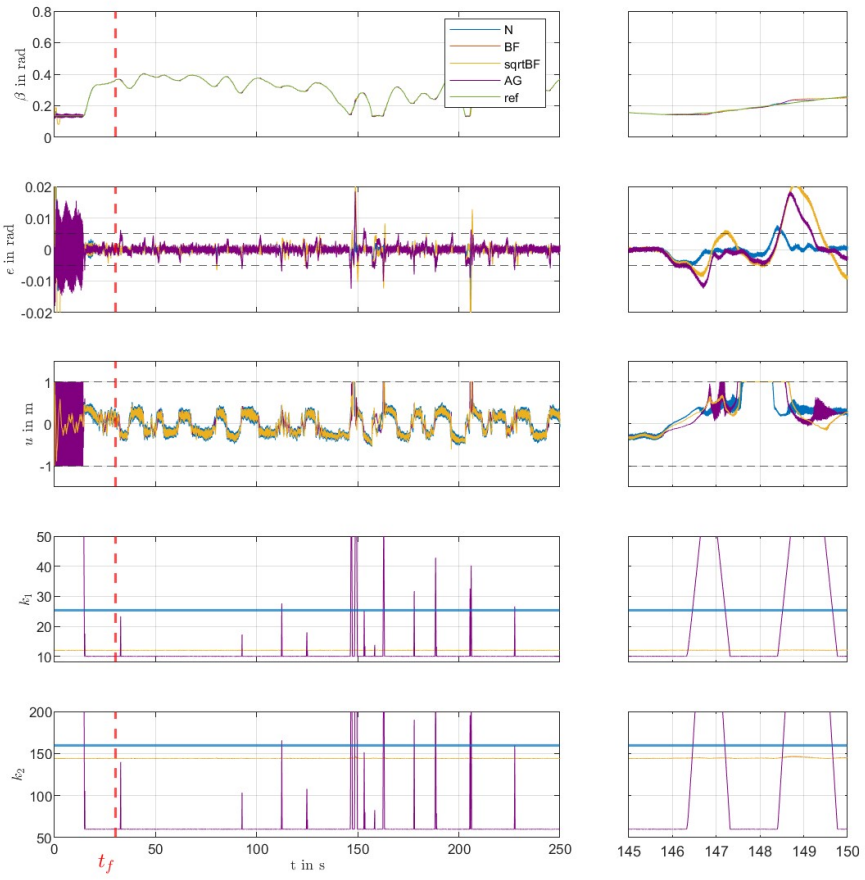

(A) Plot of the output β, error e, input u, and gains k_1, k_2. Simulation time $250s$, fault injection at $t_f = 30s$. On the right, a zoom from time instant $t = 145s$ to $t = 150s$.

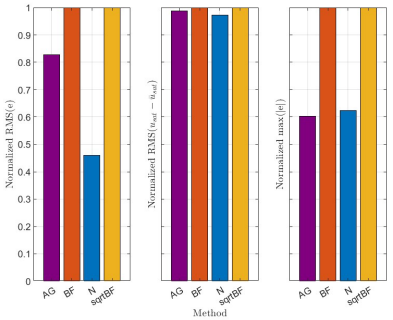

(B) Metrics in faulty case: Normalized RMS(e), normalized RMS($u_{sat} - \bar{u}_{sat}$) and normalized MAX($|e|$).

FIGURE 5.31: Fault 30 - Simulation results and metrics.

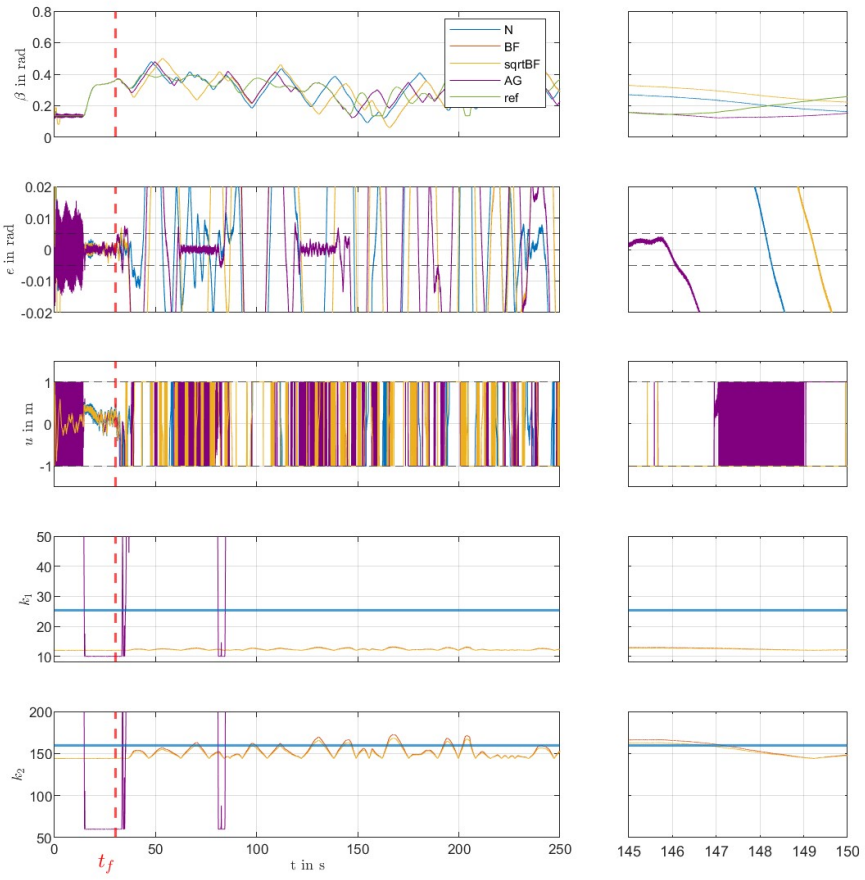

(A) Plot of the output β, error e, input u, and gains k_1, k_2. Simulation time $250s$, fault injection at $t_f = 30s$. On the right, a zoom from time instant $t = 145s$ to $t = 150s$.

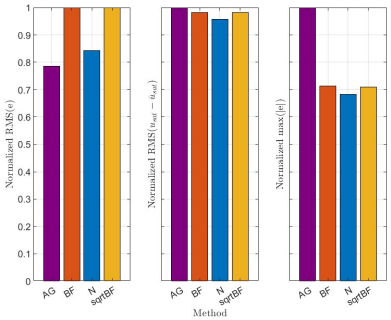

(B) Metrics in faulty case: Normalized RMS(e), normalized RMS($u_{sat} - \bar{u}_{sat}$) and normalized MAX($|e|$).

FIGURE 5.32: Fault 31 - Simulation results and metrics.

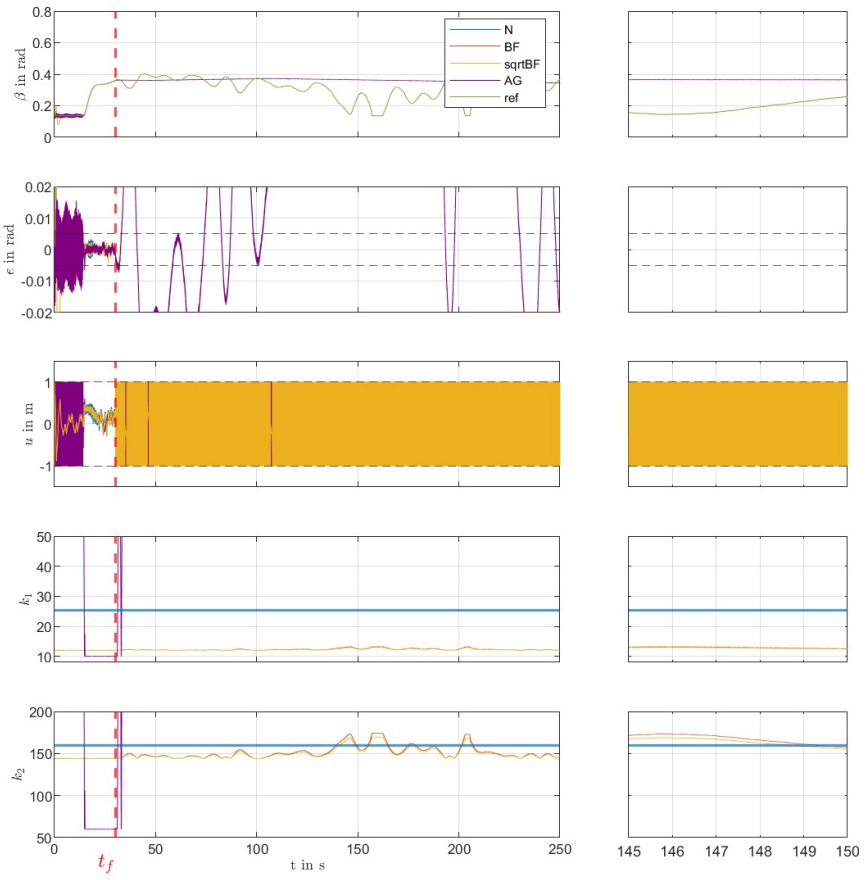

(A) Plot of the output β, error e, input u, and gains k_1, k_2. Simulation time $250s$, fault injection at $t_f = 30s$. On the right, a zoom from time instant $t = 145s$ to $t = 150s$.

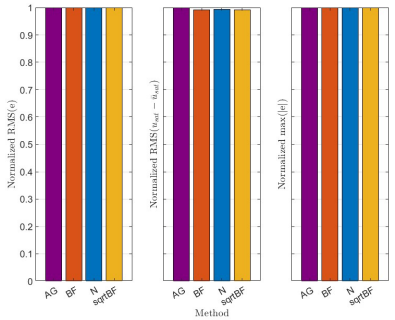

(B) Metrics in faulty case: Normalized RMS(e), normalized RMS($u_{sat} - \bar{u}_{sat}$) and normalized MAX($|e|$).

FIGURE 5.33: Fault 32 - Simulation results and metrics.

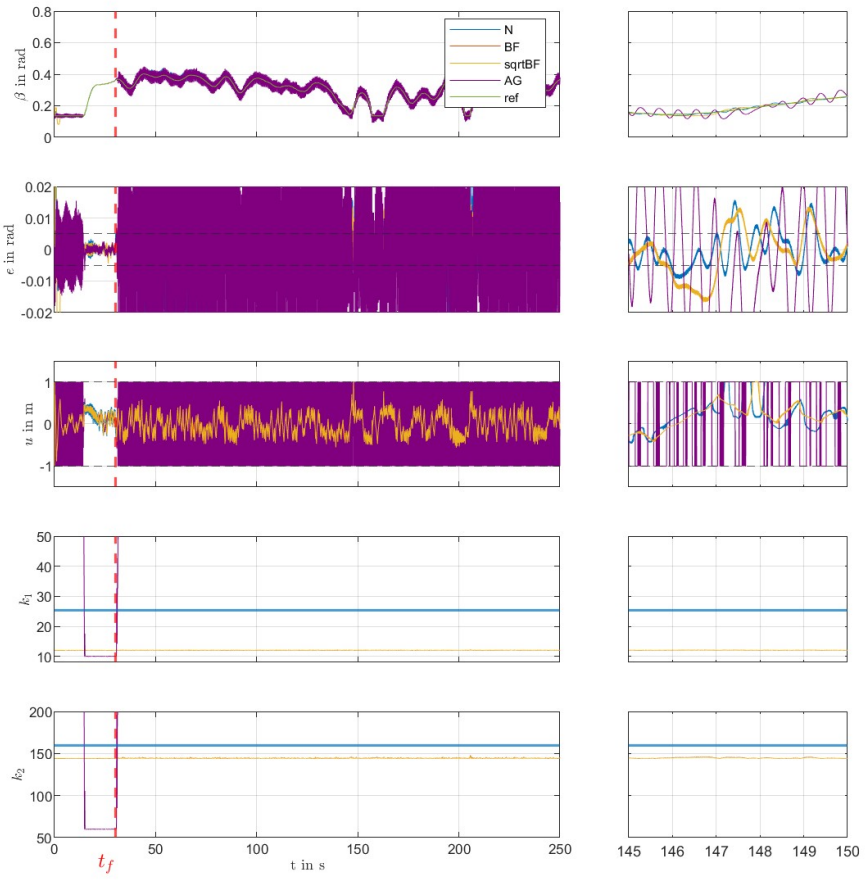

(A) Plot of the output β, error e, input u, and gains k_1, k_2. Simulation time $250s$, fault injection at $t_f = 30s$. On the right, a zoom from time instant $t = 145s$ to $t = 150s$.

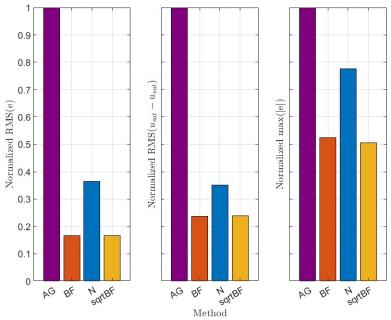

(B) Metrics in faulty case: Normalized RMS(e), normalized RMS($u_{sat} - \bar{u}_{sat}$) and normalized MAX($|e|$).

FIGURE 5.34: Fault 33 - Simulation results and metrics.

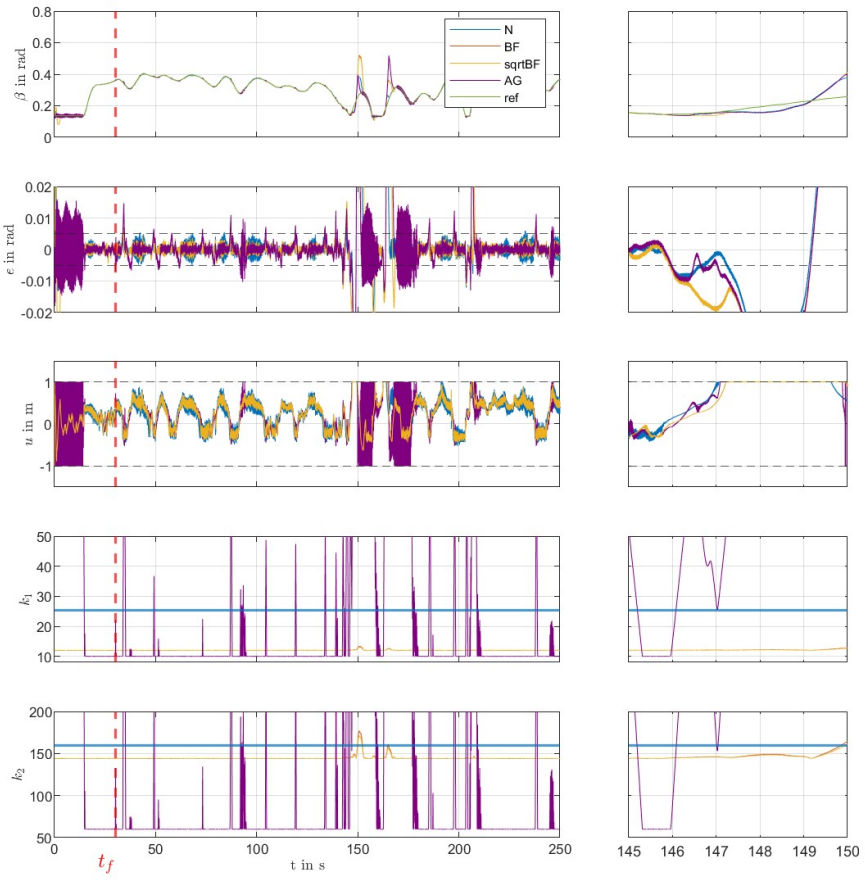

(A) Plot of the output β, error e, input u, and gains k_1, k_2. Simulation time $250s$, fault injection at $t_f = 30s$. On the right, a zoom from time instant $t = 145s$ to $t = 150s$.

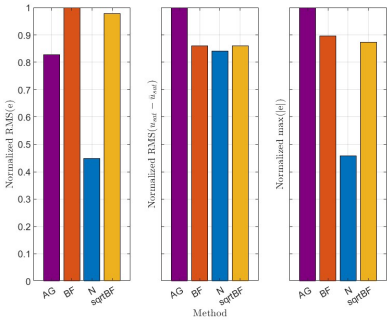

(B) Metrics in faulty case: Normalized RMS(e), normalized RMS($u_{sat} - \bar{u}_{sat}$) and normalized MAX($|e|$).

FIGURE 5.35: Fault 34 - Simulation results and metrics.

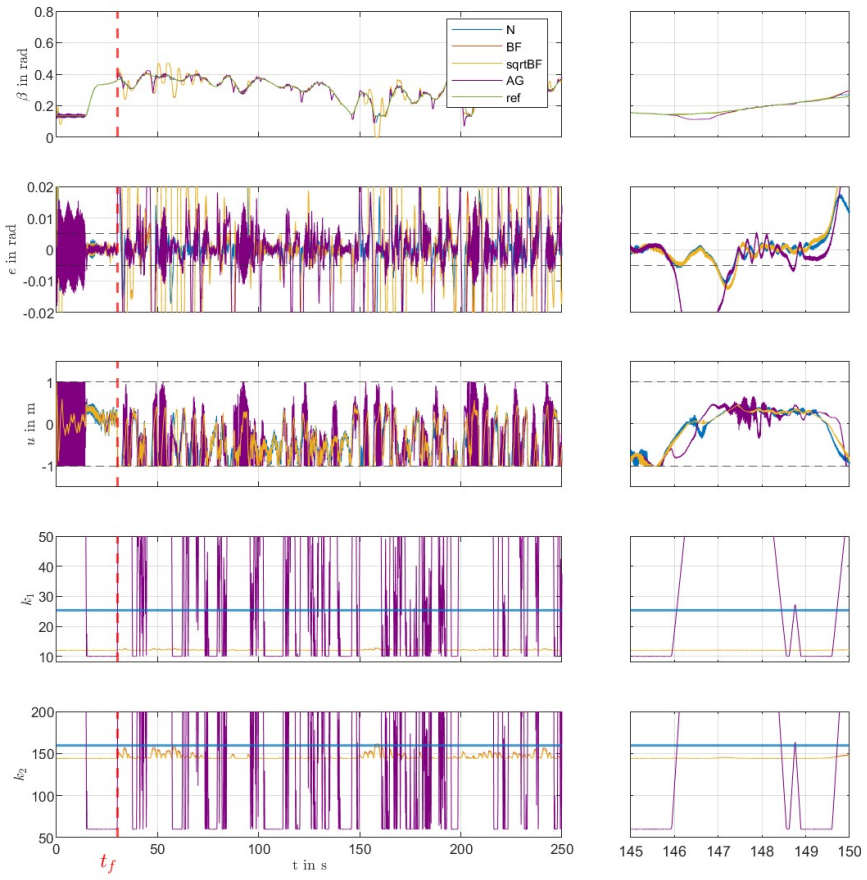

(A) Plot of the output β, error e, input u, and gains k_1, k_2. Simulation time $250s$, fault injection at $t_f = 30s$. On the right, a zoom from time instant $t = 145s$ to $t = 150s$.

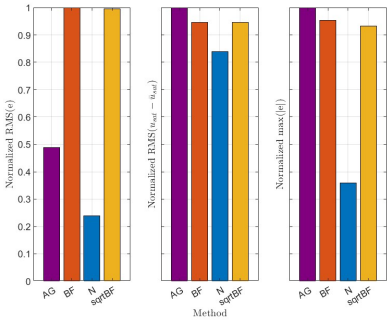

(B) Metrics in faulty case: Normalized RMS(e), normalized RMS($u_{sat} - \bar{u}_{sat}$) and normalized MAX($|e|$).

FIGURE 5.36: Fault 35 - Simulation results and metrics.

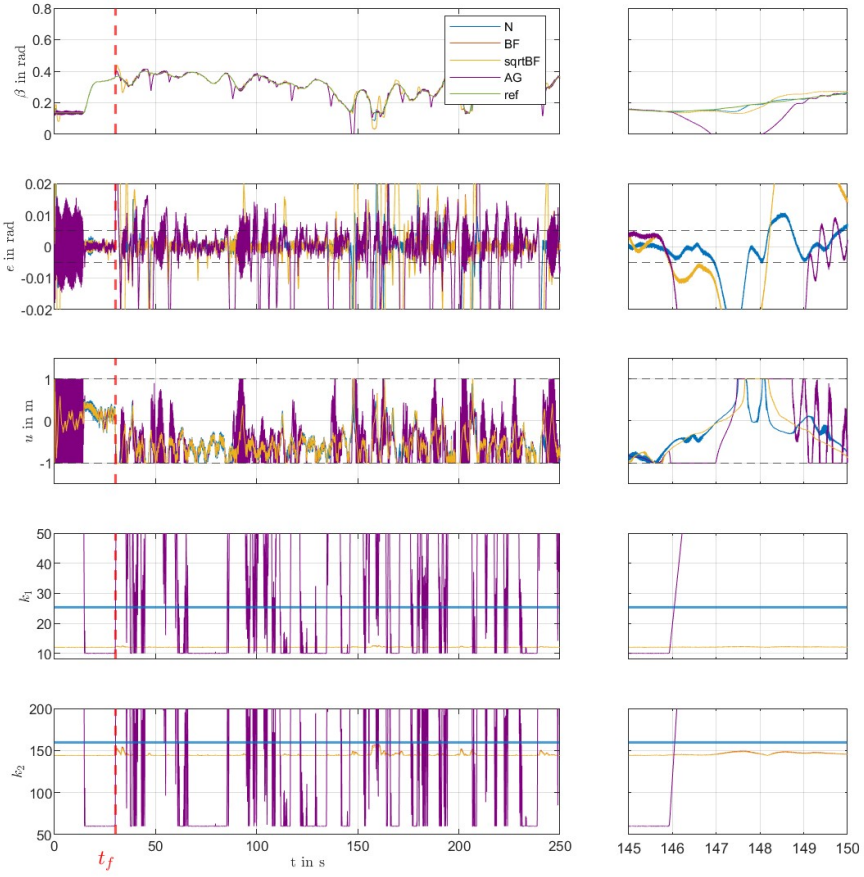

(A) Plot of the output β, error e, input u, and gains k_1, k_2. Simulation time $250s$, fault injection at $t_f = 30s$. On the right, a zoom from time instant $t = 145s$ to $t = 150s$.

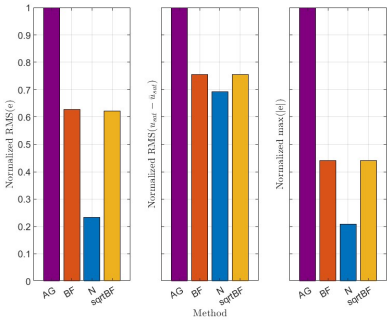

(B) Metrics in faulty case: Normalized RMS(e), normalized RMS($u_{sat} - \bar{u}_{sat}$) and normalized MAX($|e|$).

FIGURE 5.37: Fault 36 - Simulation results and metrics.

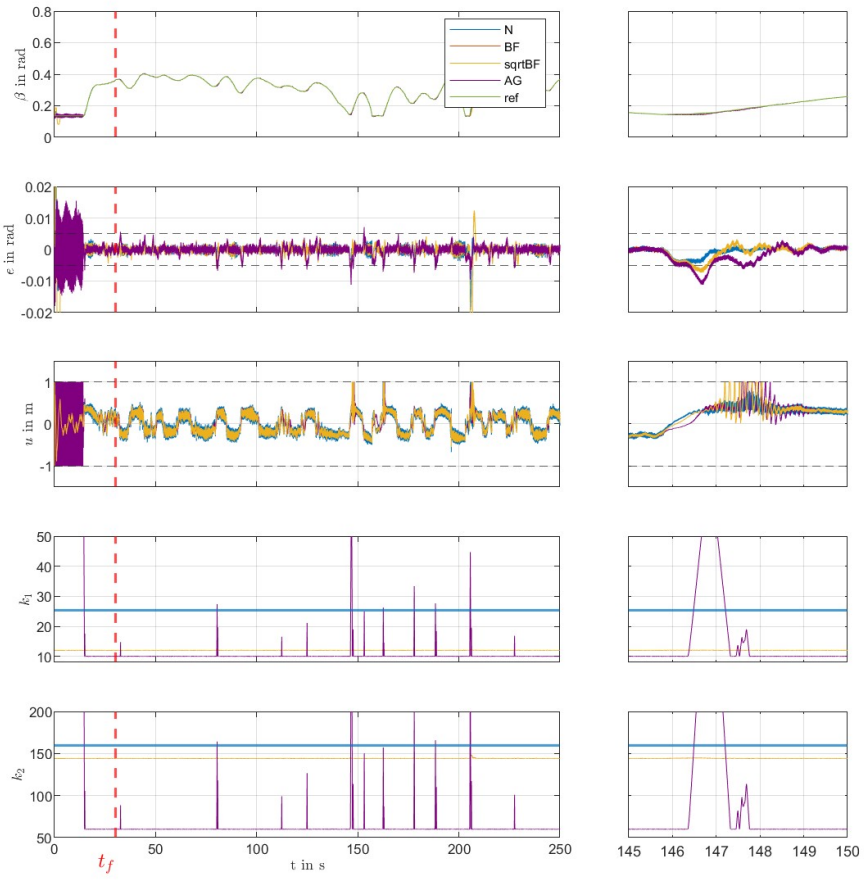

(A) Plot of the output β, error e, input u, and gains k_1, k_2. Simulation time $250s$, fault injection at $t_f = 30s$. On the right, a zoom from time instant $t = 145s$ to $t = 150s$.

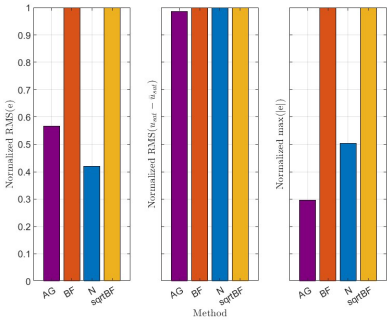

(B) Metrics in faulty case: Normalized RMS(e), normalized RMS($u_{sat} - \bar{u}_{sat}$) and normalized MAX($|e|$).

FIGURE 5.38: Fault 37 - Simulation results and metrics.

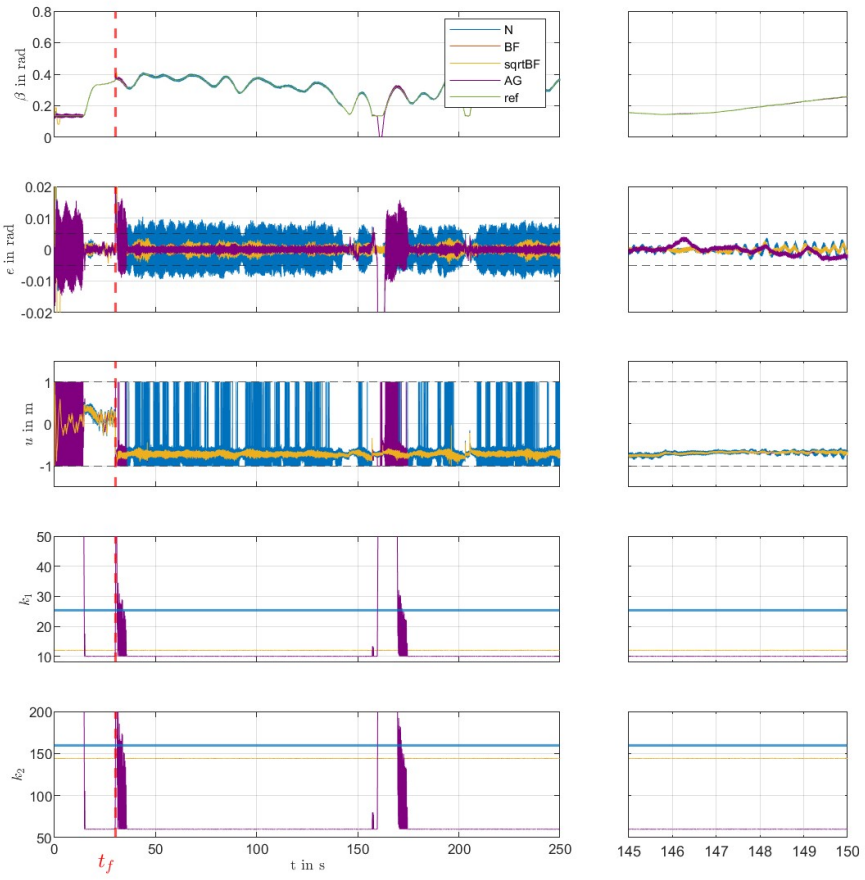

(A) Plot of the output β, error e, input u, and gains k_1, k_2. Simulation time $250s$, fault injection at $t_f = 30s$. On the right, a zoom from time instant $t = 145s$ to $t = 150s$.

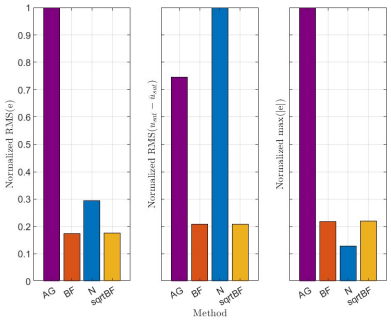

(B) Metrics in faulty case: Normalized RMS(e), normalized RMS($u_{sat} - \bar{u}_{sat}$) and normalized MAX($|e|$).

FIGURE 5.39: Fault 38 - Simulation results and metrics.

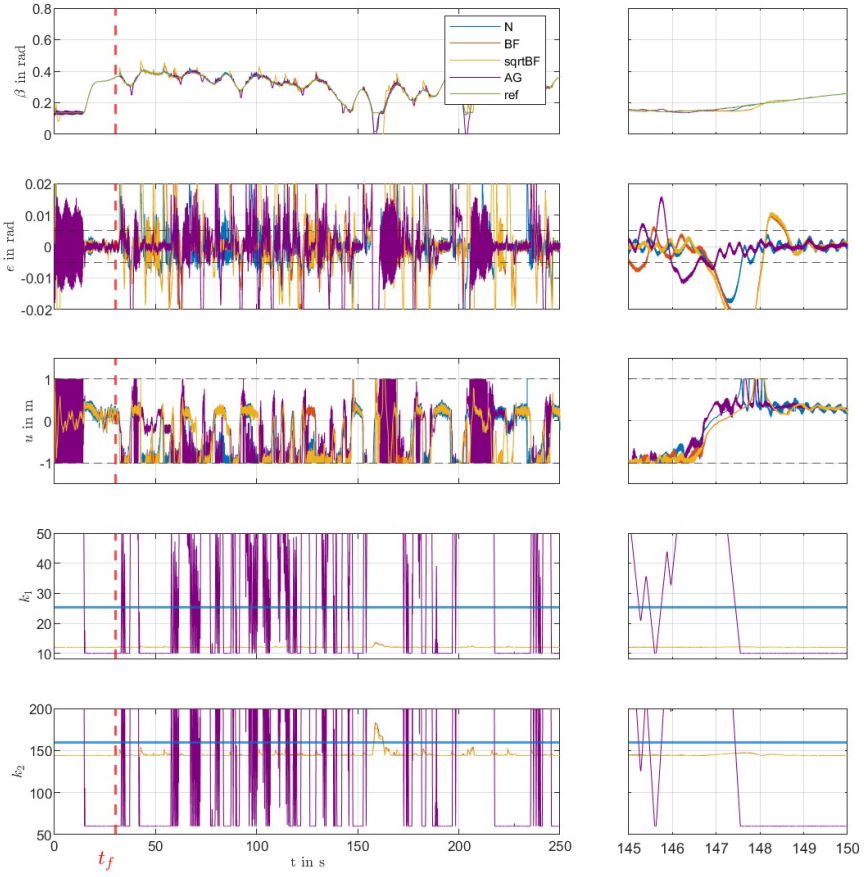

(A) Plot of the output β, error e, input u, and gains k_1, k_2. Simulation time $250s$, fault injection at $t_f = 30s$. On the right, a zoom from time instant $t = 145s$ to $t = 150s$.

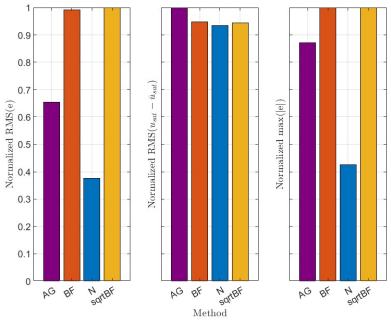

(B) Metrics in faulty case: Normalized RMS(e), normalized RMS($u_{sat} - \bar{u}_{sat}$) and normalized MAX($|e|$).

FIGURE 5.40: Fault 39 - Simulation results and metrics.

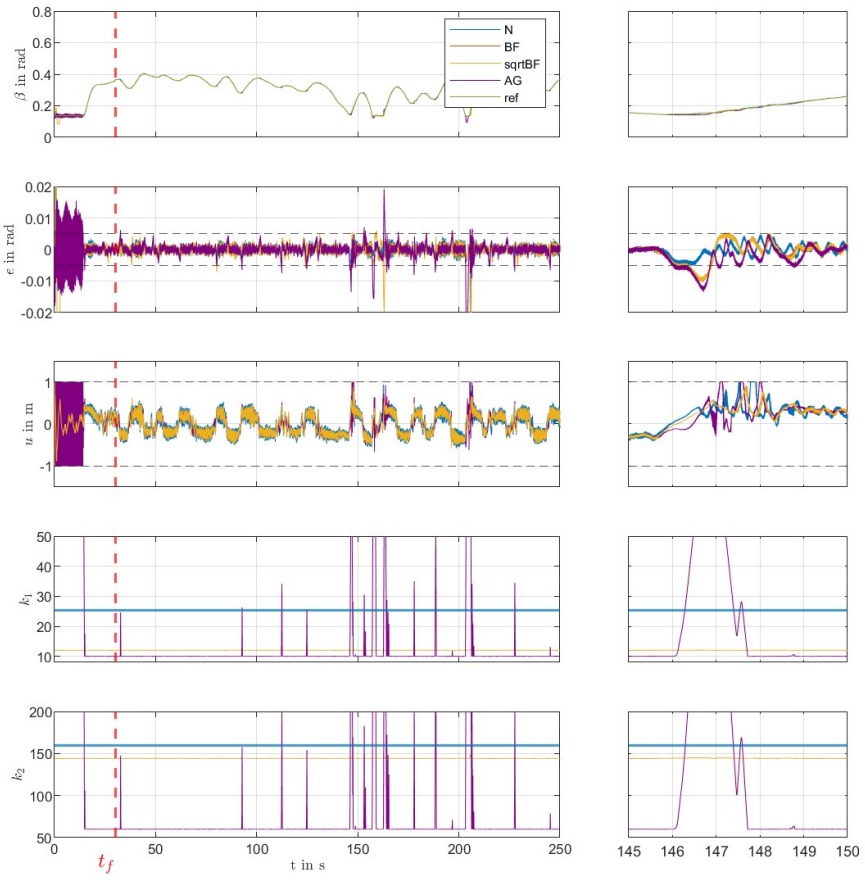

(A) Plot of the output β, error e, input u, and gains k_1, k_2. Simulation time $250s$, fault injection at $t_f = 30s$. On the right, a zoom from time instant $t = 145s$ to $t = 150s$.

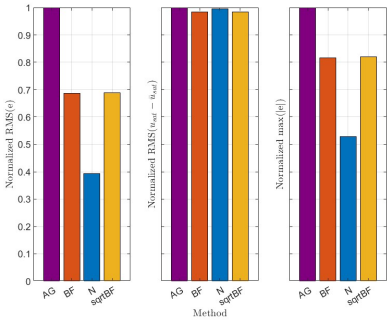

(B) Metrics in faulty case: Normalized RMS(e), normalized RMS($u_{sat} - \bar{u}_{sat}$) and normalized MAX($|e|$).

FIGURE 5.41: Fault 40 - Simulation results and metrics.

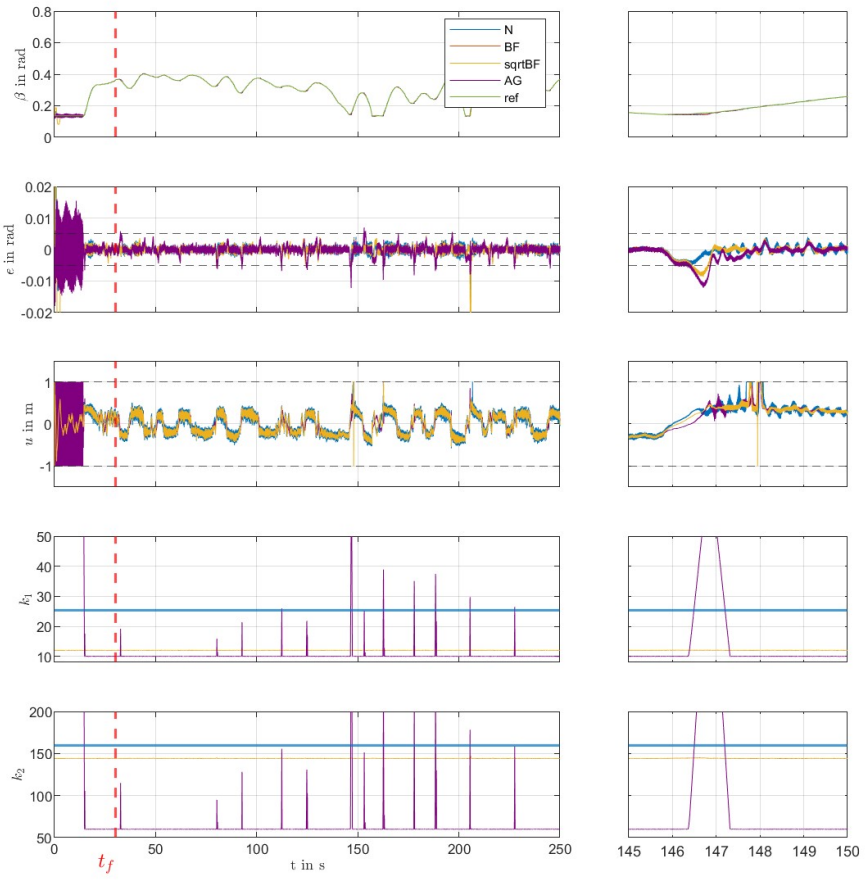

(A) Plot of the output β, error e, input u, and gains k_1, k_2. Simulation time $250s$, fault injection at $t_f = 30s$. On the right, a zoom from time instant $t = 145s$ to $t = 150s$.

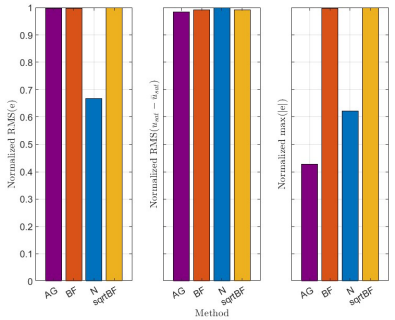

(B) Metrics in faulty case: Normalized RMS(e), normalized RMS($u_{sat} - \bar{u}_{sat}$) and normalized MAX($|e|$).

FIGURE 5.42: Fault 41 - Simulation results and metrics.

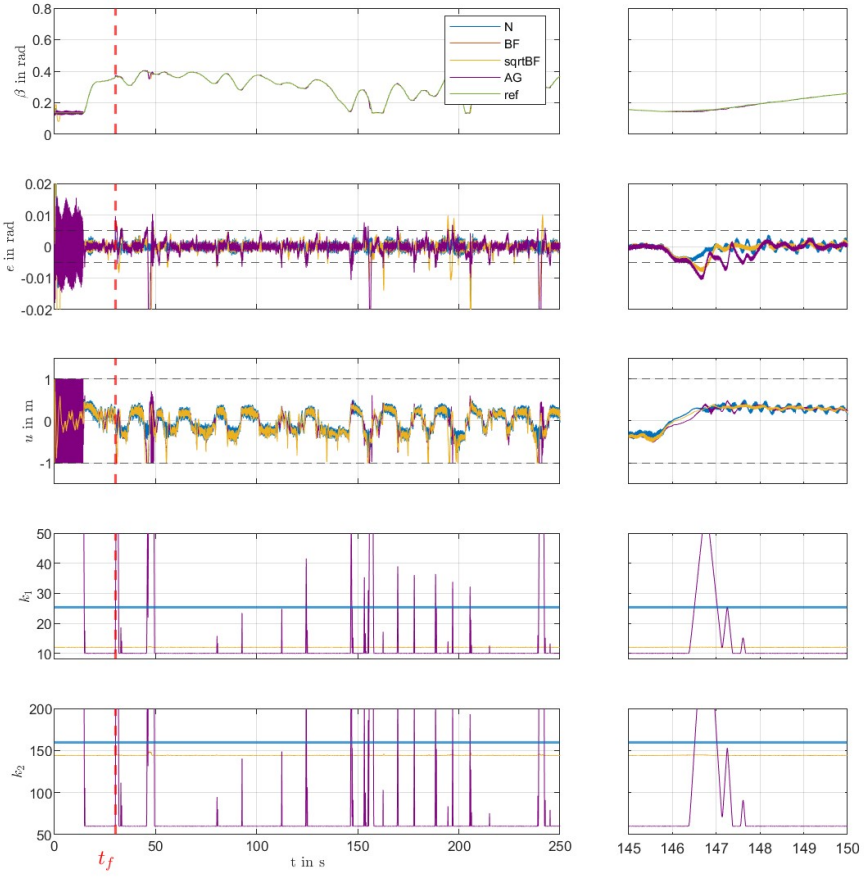

(A) Plot of the output β, error e, input u, and gains k_1, k_2. Simulation time $250s$, fault injection at $t_f = 30s$. On the right, a zoom from time instant $t = 145s$ to $t = 150s$.

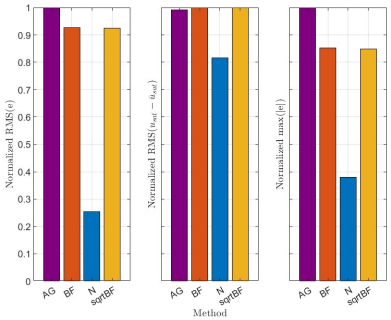

(B) Metrics in faulty case: Normalized RMS(e), normalized RMS($u_{sat} - \bar{u}_{sat}$) and normalized MAX($|e|$).

FIGURE 5.43: Fault 42 - Simulation results and metrics.

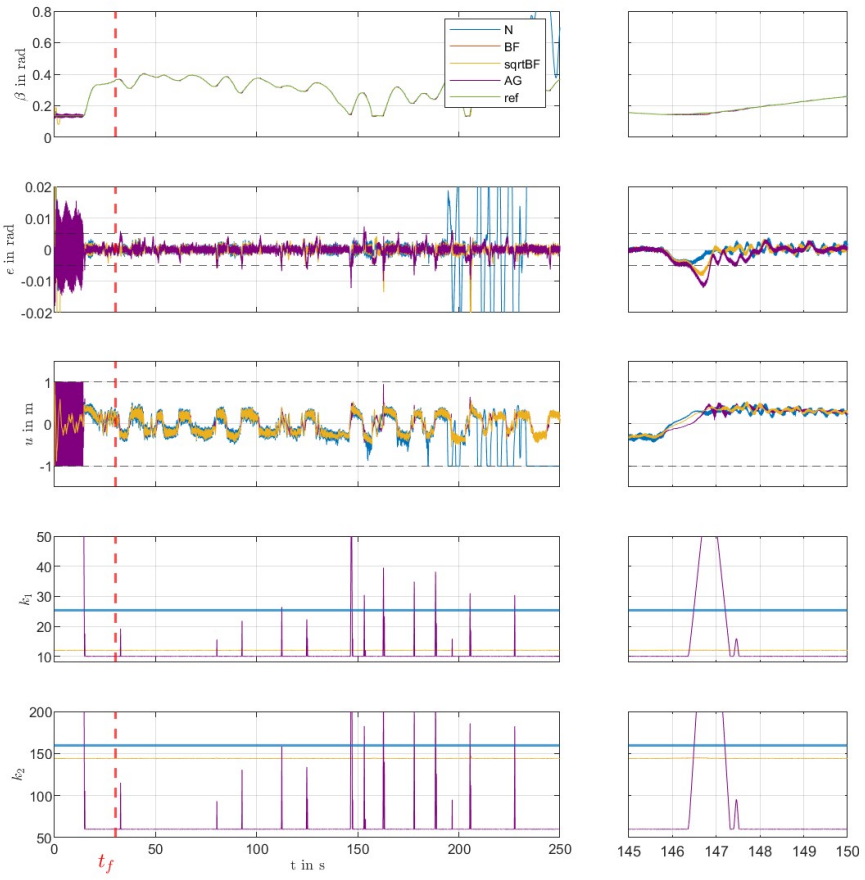

(A) Plot of the output β, error e, input u, and gains k_1, k_2. Simulation time $250s$, fault injection at $t_f = 30s$. On the right, a zoom from time instant $t = 145s$ to $t = 150s$.

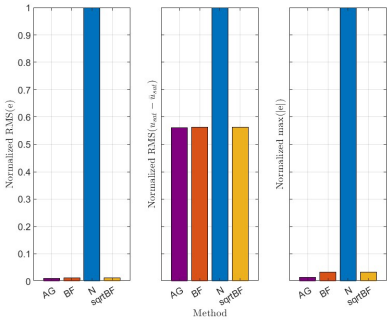

(B) Metrics in faulty case: Normalized RMS(e), normalized RMS($u_{sat} - \bar{u}_{sat}$) and normalized MAX($|e|$).

FIGURE 5.44: Fault 43 - Simulation results and metrics.

Scrolling through the figures, it is possible to notice behaviors that some categories have in common:

- no controller is able to handle the drift faults (Fault 3, 10, 17), except for the one of the β sensor (Fault 24) where the adaptive action performance is acceptable compared to the nominal one and in the case of the supply pressure drift (Fault 43) where the adaptive solutions manage the faults much better than the standard one;
- in all the gain faults (Fault 2, 9, 23), except for the case of position sensor gain fault (Fault 16), the adaptive controllers, that have similar performances, work in a superior way compared to the standard controller;
- the plots of the leakage faults (Faults 34, 35, 36) show that the standard controller is the best at managing the faults;
- in stuck faults (Fault 6, 13, 20), in general, AG controller seems to be the worst one to implement, while in Fault 27 no one has a satisfactory performance;
- the controllers action while the increased friction faults (Fault 29, 31, 32) are affecting the system, except for Fault 30, failed;
- the position and pitch angle sensor bias faults (Fault 15 and 22) are managed in the same way, where AG appears to be the worst choice, instead the other controllers have similar results. Pitch and rod pressure sensor bias faults (Fault 1 and 8) are handled in different ways: in the first one the AG solution appears to be better compared to the others, especially to the N one, instead in the second fault every controller fails;
- in the position and pitch angle sensor precision faults (Fault 18 and 25) there are similar performances, where no controller outperforms compared to the others, instead in pressure sensor precision faults (Fault 4 and 11), the nominal controller seems to be the best choice;

- in DC valve faults (fault 40 and 41) the baseline controller shows a better performance;
- in valve flows faults category (Fault 37, 38, 39) it was not individuated a common feature: in the first one AG and N perform better, in the second the sqrtBF and BF and finally in the third again N.

6

Conclusions and Future Research Directions

This thesis presents the design of some Adaptive Super Twisting Sliding Mode Controllers, namely robust and accurate controllers, that are necessary when dealing with systems subjected to disturbances, uncertainties and faults. It investigates some variations of A-ST-SMC already presented in literature to suggest which method could be a feasible solution to apply in real-world implementation compared to the baseline strategy.
In most of the fault cases, the adaptive solutions improved the reference tracking and reduced the gain values making the adaptive technique generally preferable to the nominal one. However, the chattering phenomenon was not sufficiently enhanced as expected.
Consequently, this thesis can not conclusively determine the best controller overall for a faulty situation since each scenario gave a different result. What can be noted is that in some categories similar behaviors have been identified and the simulations had led to confirm, in line with the literature, that the sqrtBF-ST-SMC and BF-ST-SMC providedin general better performances among the adaptive solutions.

The work of refining and perfecting the proposed control architecture does not end with this thesis. The presence of the chattering in the adaptive solution indicates a need for further meticulous design and implementation reviews.

This thesis gives some starting points for the developing of future works:

- discretization of the system: this could potentially improve the chattering issue;
- real system experiments: this thesis simulates the system with an high-fidelity simulator, but by implementing the controllers on a real architecture, the comparison between the controllers would lead to even more interesting findings. Moreover, it would allow to determine unforeseen limitations of each controller.

Bibliography

[1] Alessio Dallabona, Mogens Blanke, Henrik C Pedersen, and Dimitrios Papageorgiou. Fault diagnosis and prognosis capabilities for wind turbine hydraulic pitch systems: An overview. *arXiv preprint arXiv:2312.09018*, 2023.

[2] Henrik C Pedersen, Torben O Andersen, and Jesper Liniger. Investigation of load reduction possibilities in wind turbines using a fluid power pitch system. In *Fluid Power Systems Technology*, volume 57236, page V001T01A051. American Society of Mechanical Engineers, 2015.

[3] Jesper Liniger. Design of reliable fluid power pitch systems for wind turbines. 2018.

[4] JA Burton and Alan SI Zinober. Continuous approximation of variable structure control. *International journal of systems science*, 17(6):875–885, 1986.

[5] Arie Levant. Sliding order and sliding accuracy in sliding mode control. *International journal of control*, 58(6):1247–1263, 1993.

[6] Shyam Kamal, Asif Chalanga, Jaime A Moreno, Leonid Fridman, and Bijnan Bandyopadhyay. Higher order super-twisting algorithm. In *2014 13th International Workshop on Variable Structure Systems (VSS)*, pages 1–5. IEEE, 2014.

[7] Jaime A Moreno and Marisol Osorio. A lyapunov approach to second-order sliding mode controllers and observers. In *2008 47th IEEE conference on decision and control*, pages 2856–2861. IEEE, 2008.

[8] Yuri B Shtessel, Jaime A Moreno, Franck Plestan, Leonid M Fridman, and Alexander S Poznyak. Super-twisting adaptive sliding mode control: A lyapunov design.

In *49th IEEE conference on decision and control (CDC)*, pages 5109–5113. IEEE, 2010.

[9] Yuri Shtessel, Mohammed Taleb, and Franck Plestan. A novel adaptive-gain supertwisting sliding mode controller: Methodology and application. *Automatica*, 48(5):759–769, 2012.

[10] Christopher Edwards and Yuri B Shtessel. Adaptive continuous higher order sliding mode control. *Automatica*, 65:183–190, 2016.

[11] Xiaowei Yang, Jianyong Yao, and Wenxiang Deng. Output feedback adaptive supertwisting sliding mode control of hydraulic systems with disturbance compensation. *ISA transactions*, 109:175–185, 2021.

[12] Qi Dong, Qun Zong, Bailing Tian, and Fang Wang. Adaptive-gain multivariable super-twisting sliding mode control for reentry rlv with torque perturbation. *International Journal of Robust and Nonlinear Control*, 27(4):620–638, 2017.

[13] Mohammad J Mirzaei, Mohamed A Hamida, Franck Plestan, and Mohammed Taleb. Super-twisting sliding mode controller with self-tuning adaptive gains. *European Journal of Control*, 68:100690, 2022.

[14] Keng Peng Tee, Shuzhi Sam Ge, and Eng Hock Tay. Barrier lyapunov functions for the control of output-constrained nonlinear systems. *Automatica*, 45(4):918–927, 2009.

[15] Hussein Obeid, Leonid M Fridman, Salah Laghrouche, and Mohamed Harmouche. Barrier function-based adaptive sliding mode control. *Automatica*, 93:540–544, 2018.

[16] Hussein Obeid, Salah Laghrouche, Leonid Fridman, Yacine Chitour, and Mohamed Harmouche. Barrier function-based adaptive super-twisting controller. *IEEE Transactions on Automatic Control*, 65(11):4928–4933, 2020.

[17] Salah Laghrouche, Mohamed Harmouche, Yacine Chitour, Hussein Obeid, and Leonid M Fridman. Barrier function-based adaptive higher order sliding mode controllers. *Automatica*, 123:109355, 2021.

[18] Long Chen, Zhihui Jin, Ke Shao, Hai Wang, Guangyi Wang, Herbert Ho-Ching Iu, and Tyrone Fernando. Sensorless fixed-time sliding mode control of pmsm based on barrier function adaptive super-twisting observer. *IEEE Transactions on Power Electronics*, 2023.

[19] Hussein Obeid, Salah Laghrouche, and Leonid Fridman. Dual layer barrier functions based adaptive higher order sliding mode control. *International Journal of Robust and Nonlinear Control*, 31(9):3795–3808, 2021.

[20] Yukuan Liu, Guanglin He, Yanan Du, Yulong Zhang, and Zenghui Qiao. Multivariable adaptive super-twisting guidance law based on barrier function. *Applied Sciences*, 11(23):11178, 2021.

[21] Biel Roig. Adaptive sliding mode control for motion control systems, adaptiv sliding mode regulering af motion kontrol systemer, 2023.